

Final Design Report
CubeSat SADA (2) Team

Sponsored By
NASA/JPL

Version 2.0

Project Engineer – Scott Miller
Chief Engineer – Paul Chow

Prepared by:

Arnold Ahnood (EE/CSE)
Alexander Buchholz (EE/CSE)
Dylan Carberry (ME)
Brandon Chun (ME)
Niyati Desai (EE)
Kevin Doremus (EE/CSE)
WeiXuan Lai (ME)
Christine Marini (ME)



Rensselaer Polytechnic Institute



Executive Summary

The interest in space exploration has been steadily increasing over the past several decades. The high cost of researching and developing new devices and technologies to operate in space makes the field more challenging. Weight and power are the two critical design aspects that have led to the creation of miniature sized satellites. CubeSats are compact satellites used to execute a variety of missions and can contain various payloads such as GPS and communication systems. Their small size has benefits, with lower launch costs, cheaper and faster development. A Solar Array Drive Assembly (SADA) is a module that can maximize the power generated for the CubeSat by rotating the solar panels.

The CubeSat Solar Panel (2) team designed space-grade SADA that uses space-rated commercial-off the shelf (COTS) components that achieves Technology Readiness Level 3. The team also designed and built a mechanically and electrically-functional prototype. For the prototype, the team selected a motor-gearhead that drove a transmission system to rotate the solar panels and a mechanical system to support and deploy the panels. Also control algorithm was written to emulate solar panel sun tracking. This control algorithm was used along with an infrared sensor that was designed to emulate a panel mounted sun sensor. The final space grade design was then created based off of this prototype.

Contents

Executive Summary	2
List of Figures	5
List of Tables	8
Revision History	10
Glossary	11
1. Introduction	12
1.1 History of the Project	12
1.2 Problems to be Addressed	12
1.3 Justification for Project	12
2. Project Objectives & Scope	13
3. Assessment of Relevant Existing Technologies and Standards	13
4. Professional and Societal Considerations	13
5. System Requirements and Design Constraints	14
5.1 Chassis Subsystem	14
5.2 Hinge and Deployment Subsystem	16
5.3 Transmission Subsystem	17
5.4 Controls Subsystem	20
6. System Concept Development	22
6.1 Chassis Subsystem Concept Development	22
6.2 Hinge Subsystem Concept Development	26
6.3 Transmission Subsystem Concept Development	30
6.4 Control Subsystem Concept Development	37
6.4.1 Microcontrollers and Motor Drivers	37
6.4.2 Sensors	40
6.4.3 Motor Type Selection	42
7. Design Analysis	43
7.1 Chassis	43
7.2 Hinge Subsystem Analysis	44
7.3 Motor/Gearhead	54
7.4 Transmission System	56
7.5 Control System Analysis	59
7.5.1 Sensor Analysis	59
7.5.2 Control Algorithm Development	61
7.5.3 State Diagram Walkthrough	68
8. Final Design and Engineering Specifications	69
9. System Evaluation	71
9.1 Performance Requirements	71

9.2 Tolerance and Sensitivity.....	72
9.3 Failure Analysis	73
9.4 Simulation Step Responses.....	74
9.4 Simulation Control Systems	75
10. Significant Accomplishments and Open Issues.....	76
11. Conclusions and Recommendations	77
Bibliography	78
Appendix A: Customer Requirements	80
Appendix B: System Evaluation Plan.....	81
Appendix C: Assembly Instructions	83
Appendix D: Expense Report	98
Appendix E: Overshoot Calculations.....	101
Appendix F: Stepper Motor/Gearhead Analysis.....	104
Appendix G: Failure Analysis Example Calculations	107
Appendix H: Shaft Loadings and Minimum Shaft Diameter Calculation	117
Appendix I: Calculated Dynamic Load Rating.....	125
Appendix J: Software.....	127
Appendix K: Full Prototype Schematic	136
Appendix L: Prototype Block Diagram	137
Appendix M: Hinge and Deployment.....	138
Appendix N: Control Algorithm Flowchart.....	139

List of Figures

Figure 1: Image of Height Requirements.....	15
Figure 2: Image of Side Length Requirements	15
Figure 3: Panel Deployment Path	16
Figure 4: Hinge and Panel Physical Constraints [24]	16
Figure 5: Block Diagram that shows Transmission Subsystem functions.....	17
Figure 6: Panel Rotation Accuracy	17
Figure 7: Solar Panel Surface Area.....	18
Figure 8: Panel Axis of Rotation	19
Figure 9: Rotational Inertia Requirements for One Panel	19
Figure 10: SADA Solar Panel Axis of Rotation	21
Figure 11: Pointing Accuracy Diagram.....	21
Figure 12: Solar Panel Layout for Maximum Inertia.....	22
Figure 13: Isometric View of Final Chassis and Cover with Brackets.....	24
Figure 14: Top View of Final Chassis with Out Cover	25
Figure 15: Encoder Bracket Comparison.....	25
Figure 16: Slip Ring and Bearing Bracket Comparison	26
Figure 17: 2014 Hinge and Deployment Design [4].....	26
Figure 18: Burn Wire Deployed vs Stowed [25]	27
Figure 19: Shape Memory Alloy Hinge; Stowed (top) and Deployed (bottom) [x].....	28
Figure 20: SMA Material Demonstration [26]	28
Figure 21: Ball Detent (McMaster 84835A21) [27].....	29
Figure 22: Prototype Hinge and Deployment Design.....	30
Figure 23: Top-Down View of configuration: The motor and the gearhead are to the side of (coplanar to) the main drive shaft that the panels are connected to. Single Coplanar Motor Configuration	31
Figure 24: Single Coplanar Motor Configuration block diagram that displays basic functionality	31
Figure 25: The motor and gearhead are in the tuna can, on top of the drive shaft. Single Vertical Motor Configuration	32
Figure 26: Single Vertical Motor Configuration block diagram that displays basic functionality32	
Figure 27: Top-Down view of Configuration: Two independent motors. One panel attached to each drive shaft. Double Coplanar Motor Configuration	33
Figure 28- Capsule Type Slip Ring Device Layout.....	35
Figure 29- Thru Bore Type Slip Ring Device Layout	36
Figure 30- Prosper Mini Capsule Slip Ring [10]	36
Figure 31: Controller Taxonomy [11].....	38
Figure 32: UC1625sp Motor Controller	39
Figure 33: International Rectifier RH Motor Control Module [13].....	39
Figure 34: Thin-Slit Sensor Theory [15]	40
Figure 35: Phototransistor Sensor Implementation.....	41
Figure 36: Force Diagram of Chassis	43
Figure 37: Chassis FEA Analysis Displaying Displacement.....	44
Figure 38: Chassis FEA Analysis Displaying Stress	44
Figure 39: Folded Panel Dimensions (Top View)	45
Figure 40: Cross Sectional View of the Panel from Pumpkin	45

Figure 41: States of Deployment	46
Figure 42: Prototype Panel Attachment Dimensions.....	47
Figure 43: Cross Sectional Area of the Physical Panel Stop	48
Figure 44: Force from Spring (left), Free Body Diagram of Pin (center), Tear out Distance (right)	49
Figure 45: FEA Constraints on Hinge Assembly	52
Figure 46: FEA of Panel Mechanism Results.....	53
Figure 47: Forces Acting on Primary Shaft	56
Figure 48: Forces Acting on Secondary Shaft	57
Figure 49: Depiction of Bearing Loading	58
Figure 50: Light Sensor Schematic.....	59
Figure 51: LTR-4206E.....	59
Figure 52: LTR-4206E Sensitivity Response [16].....	60
Figure 53: Sensitivity Plotted with 20° Offset.....	60
Figure 54: Sensitivity Plotted with 15° Offset.....	61
Figure 55: Satellite Rotating Around Earth	63
Figure 56: Sun and Earth Geometries	65
Figure 57: Shadow Time Output Graphs	66
Figure 58: State Diagram Summary	67
Figure 59: Final CAD Assembly of SADA Prototype.....	69
Figure 60: Final Assembly of SADA Prototype	69
Figure 61: Interior SADA Chassis	70
Figure 62: Prototype Motor-Gearhead Speed Specifications	72
Figure 63: Mechanical Failure Analysis Flowchart.....	73
Figure 64: Stepper Motor Simulink Diagram	74
Figure 65: Stepper Motor Step Response	75
Figure 66: Control Simulation Parameters	75
Figure 67: Control Simulation Output	76
Figure 68: SADA on Test Apparatus.....	81
Figure 69: Starting Point	82
Figure 70: Right Angle Tweezer Used for Soldering Electronics	83
Figure 71: Threaded Inserts	83
Figure 72: Empty Hole (Left) and Hole with Insert (Right)	84
Figure 73: Chassis with All Inserts In.....	84
Figure 74: Two Holes on Mock Panel	85
Figure 75: One Hole on Hinge.....	85
Figure 76: Primary Shaft Setup.....	86
Figure 77: Secondary Drive Shafts	86
Figure 78: Slip Ring Connected to Secondary Shaft	86
Figure 79: Mounting Points for Controller/Motor Driver.....	87
Figure 80: Mounting the Secondary Shafts	88
Figure 81: Mounting the Primary Shaft.....	88
Figure 82: Bracket for Primary Shaft and Slip Ring.....	89
Figure 83: Spring Loaded Contact Pins	89
Figure 84: Motor in Cradle with Connector	90
Figure 85: Motor & Encoder Mounted in Cradles.....	91

Figure 86: Initial SADA Wiring	92
Figure 87: Circuit Schematic	93
Figure 88: Side View of Hinge Mechanism	94
Figure 89: PCB Holder on Mock Panel	95
Figure 90: Sensor Schematic	96
Figure 91: Sensor Result Using a Perfboard.....	96
Figure 92: Light Sensor on Mock Panel/Riser.....	96
Figure 93: Chassis with Hinge/Panels Connected	97
Figure 94: L Brackets for Slip Rings	97
Figure 95: Spring Compression	98
Figure 96: Folded Panel Dimensions (Top View)	138
Figure 97: Cross Sectional View of the Panel for Pumpkin	138

List of Tables

Table 1: Transmission System Related Specifications	18
Table 2: Customer Requirements and Specifications for Control System	20
Table 3: Control System CubeSat Standards	21
Table 4: Mechanical Properties of Chassis Materials.....	23
Table 5: Hinge and Deployment Action Comparison Chart.....	29
Table 6: Transmission System Concept Comparison	34
Table 7: Slip Ring Selection Comparison.....	34
Table 8- Slip Ring Selection Comparison	37
Table 9: Microcontroller Comparison	38
Table 10: RH Motor Control Module Specifications [13].....	39
Table 11: Sun Sensing Comparison for Prototype.....	41
Table 12: Motor Type Selection	42
Table 13: Energy Equations for Each State of Deployment	46
Table 14: Springs Considered.....	46
Table 15: The Moment on the Panel due to the Spring	47
Table 16: Bending Stress on the Physical Panel Stop due to Space Grade Panel	48
Table 17: Physical Stop Bending Stress due to Impact of Prototype Panel Attachment.....	49
Table 18: Bending Stress and Tear out Distance of Springs on the Spring Stop Pin	50
Table 19: Spring Evaluation	51
Table 20: Constraints Applied to Hinge	52
Table 21: FEA Results	53
Table 22: Hinge Mechanism Components for Prototype and Space Grade	54
Table 23: Selection Process for Motor/Gearhead Combinations.....	54
Table 24: Final Selection of Prototype Gearhead	55
Table 25: Prototype and Space Grade Gearhead Specifications.....	56
Table 26: Material Properties Needed for Shaft Diameter Calculation	58
Table 27: Control Selection Pugh Matrix	62
Table 28: Constants Used	64
Table 29: Variables	64
Table 30: Transmisson Component Material List for Prototype ad Sapce-Grade Designs	70
Table 31: Rotational Speed for Motor/Gearhead.....	71
Table 32: Prototype and Space Grade Comparison	77
Table 33: CubeSat Orbits [18].....	80
Table 34: TRL 3 Explanation [19].....	80
Table 35: Fabrication of mock chassis.....	98
Table 36: Initial Fabrication for Prototype Chassis	98
Table 37: Re-Printing Costs.....	99
Table 38: Initial Fabrication of Hinge	99
Table 39: Hinge Re-Printing Costs	99
Table 40: 3D Printed Parts for Testing Apparatus.....	99
Table 41: Purchased Parts.....	100
Table 42: Required Inputs for Calculations	118
Table 43: Forces Generated by Gears	119
Table 44: Calculated Reaction Forces on Bearings	120
Table 45: Calculated Moments and Minimum Diameter at Point A	121

Table 46: Calculated Moments and Minimum Shaft Diameters at Point C	122
Table 47: Calculated Moments and Minimum Shaft Diameter at Point E	123
Table 48: Calculated Basic Dynamic Load Rating for Primary Shaft.....	125
Table 49: Calculated Basic Dynamic Load Rating for Secondary Shaft.....	126

Revision History

Version	Date	Name	Reason for Changes
1.0	5/9/2016	Brandon Chun	Initial document.
1.2	5/17/16	Christine Marini	Integrated Sections and Started Formatting
1.3	5/17/16	Christine Marini	Numbering Tables and Figures
1.4	5/17/16	Dylan Carberry	Initial Formatting
1.5	5/17/16	Brandon Chun	Finished Section 8
1.6	5/17/16	Alexander Buchholz	Proofreading and References
1.7	5/17/16	Christine Marini	Grammatical Changes
1.8	5/17/16	Brandon Chun	Proofreading
2.0	5/17/16	Dylan Carberry	Finalized Document

Glossary

- IPSPT – Iodine Propelled Science and Payload Transporter
- COTS – Commercial off-the-shelf
- NASA – National Aeronautics and Space Administration
- JPL – Jet Propulsion Laboratory (Part of California Institute of Technology)
- EPS – Electrical Power System
- LEO – Low Earth Orbit
- GEO – Geosynchronous Earth Orbit
- GTO – Geosynchronous Transfer Orbit
- FOS – Factor of Safety
- TRL – Technology Readiness Level (Defined by NASA and used in industry)
- ISS – International Space Station
- RPI – Rensselaer Polytechnic Institute
- GPS – Global Positioning System
- SADA – Solar Array Drive Assembly
- CubeSat – Cube Satellite
- MSDS – Material Safety Data Sheet
- TID – Total Ionizing Dose
- BOM – Bill of Materials
- FEA – Finite Element Analysis

1. Introduction

1.1 History of the Project

A CubeSat is a standard for small, modular satellites. This standard provides an inexpensive alternative to creating large custom-built satellites. The base module of a CubeSat is a “1 U” chassis, a cube with length, width, and height of 10 centimeters. This concept was developed by Prof. Twiggs of Stanford University. CubeSats were created with the goal to be “a vehicle to support hands-on university-level space education and opportunities for low-cost space access” [1]. To achieve this goal of low cost, CubeSats are built primarily using COTS components. The modules can be designed to perform various tasks. For example, it can act as a communications satellite or take images of the Earth from space. Modules can also be connected together into groups of up to 6U to make a multi-functional satellite. CubeSats are often launched into orbit as payload in large satellite launches. The CubeSat and SADA module assembly is deployed from a spring loaded package from a launch vehicle.

In 2014, a capstone team designed the Iodine Propelled Science and Payload Transporter (IPSPT), a 6U CubeSat. The goal of this design was to test the functionality of COTS components in orbits higher than low earth orbit. This design was only a paper design that gave an overview of the various modules that would make up the entire system. Further development would be needed before this system could be launched into space, and that is the goal of the CubeSat Solar Panel (2) team.

1.2 Problems to be Addressed

The goal of the current team is to further develop and create a functioning prototype of one of the modules of the IPSPT system. The module to be created is the Solar Array Drive Assembly (SADA). This module will control the deployment and rotation of solar panels that generate power for the entire CubeSat. In space, it is a challenge to get the required amount of energy. Most satellites use some form of solar panels. To ensure that the greatest amount of energy is gathered, the SADA must be capable of positioning the panels to face the sun.

The current team is responsible for creating a mechanically and electrically functioning prototype of the device. This prototype is not intended to be created using space grade components; it is only meant to demonstrate how the device will function. The team is also responsible for creating a paper design that uses space grade COTS components to NASA Technology Readiness Level 3. This final module will be able to connect to CubeSats of various sizes. The final space grade device will be able to operate in both Low Earth Orbit (LEO) and Geosynchronous Orbit (GEO).

1.3 Justification for Project

The cost for a larger satellite can fall between \$100 -\$400 million dollars. The cost of launching those large satellites can be between \$50 - \$400 million dollars [2]. On the other hand, a typical 1U CubeSat costs close to \$8000 and the cost of putting it on a shuttle is \$40,000 [3]. While the price may increase as size and internal complexity of the CubeSat increase above 1U, large satellites cost millions compared to thousands of dollars for a CubeSat.

1.4 Summary of Report Sections

This report gives an overview of the design process done to create the SADA device. Section 2 of the report details the objectives that the team had to accomplish in developing the

device. Other similar technologies as well as work from the previous capstone team are given in section 3. The professional and societal considerations are given in section 4. System requirements and design constraints for all subsystems are given in section 5. In section 6 concept selections for every subsystem is detailed. All analysis on the subsystems is given in section 7. Description of the overall final design is given in section 8. Lastly, in section 9 evaluation of the overall device is given. Additional information is given in the following appendices.

2. Project Objectives & Scope

The team's semester objectives are:

- Design, develop and construct a mechanically and electrically functional prototype
 - Demonstrate continuous panel rotation about a single axis
 - Demonstrate rotational speeds as defined by JPL: $3.6 * 10^{-5} \frac{\text{rad}}{\text{s}}$ (GEO) to $2.4 * 10^{-5} \frac{\text{rad}}{\text{s}}$ (LEO)
 - Implement sun/light tracking to ensure that panels can orient towards the Sun and maximize power generation to CubeSat
- Meet mass and size requirements
- Be able to attach to CubeSats of sizes ranging from 3U to 6U.

The team's long-term objectives are to contribute to creating a fully functional space-ready SADA system. The final system will be able to adapt to any orbit between LEO and GEO and provide power to the attached CubeSat. The solar panels will be able to freely rotate about a single axis to absorb the greatest amount of sunlight possible.

3. Assessment of Relevant Existing Technologies and Standards

The design for the SADA module is a continuation of the 2014 IPSPT team's design [4], which detailed not just a SADA module, but a full CubeSat. The purpose of the project was to reduce the cost of satellites by designing a relatively inexpensive CubeSat using entirely COTS components. Typical satellite launches can cost over 200 million dollars, but by using COTS components and deploying several satellites per mission, the average cost per satellite can be significantly reduced for all stakeholders involved. The CubeSat SADA Module (2) team aims to further the SADA design of the IPSPT team and demonstrate that the design is feasible with a prototype.

Commercial options already exist for CubeSat SADA modules, but they have problems that need to be addressed. For example, the Honeybee Robotics SADA is a working space-grade product, but only offers $\pm 180^\circ$ of rotation without a slip ring, and the Honeybee SADA must be mounted on top of a CubeSat [5]. The CubeSat SADA Module (2) team aims to build a device that is similar to the Honeybee SADA, but more modular in functionality, so that SADA products can be used across different CubeSat missions.

4. Professional and Societal Considerations

The SADA design outlined in this report will massively improve the power generation of a CubeSat as is its purpose. Although this feat may not seem to affect the everyday lives of common people all across the world, it does have indirect ramifications that will allow for more

ambitious space design decisions that can push the boundaries of the human understanding of the universe. With the use of SADAs, CubeSats will be able to distribute more power to components included within them. This maximized power distribution will allow a larger variety of powerful components to be included increasing the variability of missions for which a CubeSat can be commissioned for. Scientists and sponsors that were initially deterred from using CubeSats due to their small size and absence of efficient power generation will now welcome the low-cost devices to handle missions that were previously impossible. As CubeSats become more powerful as well as more mainstream in the science community their usage and funding will both increase. The ability to perform space missions at a lower cost and size will allow ambitious missions to become feasible, leading to the results for these missions aiding in the improved understanding of space and the universe as a whole.

5. System Requirements and Design Constraints

5.1 Chassis Subsystem

Geometric requirements are based on CubeSat and NanoRacks standards. Both set limits on the maximum size allowable. In the specifications given by Tom DiSarro from NASA at the start of the project, it was stated that the chassis should occupy 1/4 of the volume of a typical CubeSat unit. In the NanoRacks deployer, there is extra volume available in the “tuna can” space. This extra volume is an option to use but there is the possibility of damage from compaction of the spring. There will be no difference in these geometric values from the paper design and the prototype design.

Figure 1 depicts the front view of the chassis that represents the maximum amount of usable space. This gives the maximum allowable height of the base that will sit within the CubeSat as well as the maximum height allowed for the “tuna can” volume. Figure 2 depicts the top view of this same representative chassis. This shows the maximum allowable tuna can diameter. The side lengths of 10 centimeters by 10 centimeters is a standard for CubeSats. Rails are present on the CubeSat for deployment. The 0.85 centimeter by 0.85 centimeter cutouts in the base corners are to allow the SADA unit to fit within and attach to these rails.

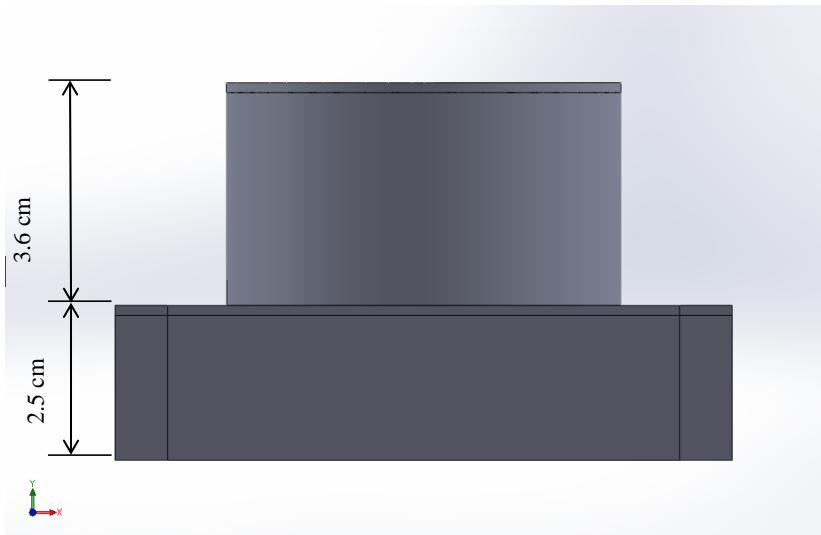


Figure 1: Image of Height Requirements

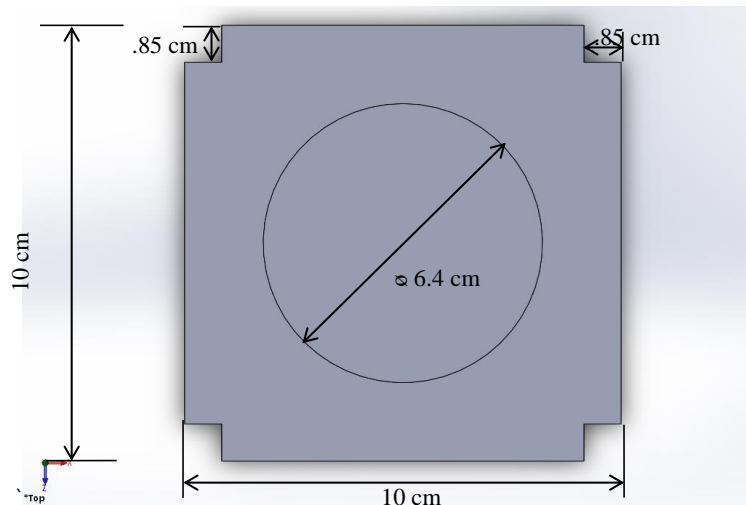


Figure 2: Image of Side Length Requirements

As with any device operating in space, mass of the device is the greatest concern. From the NASA specifications given at the start of the project, the maximum allowable mass for the chassis is 1 kg. The solar panels that will attach to the chassis must have a total maximum mass of 3 kg. Therefore, the mass of the entire system will be no greater than 4 kg. This is a strict requirement

for the space grade paper design. The prototype design may go over this mass requirement due to the use of non-space grade components.

The hinges that will deploy the solar panels are included in this subsystem. The deployment of the solar panels will happen at a minimum of 30 minutes after the CubeSat has been launched out of the NanoRacks Deployer. This is to prevent early deployment which could damage the solar panels.

5.2 Hinge and Deployment Subsystem

Once the CubeSat is deployed out of the NanoRacks Deployer, the panels must deploy from the stowed position to 90 degrees from the CubeSat Body. Figure 3 shows the path of deployment.

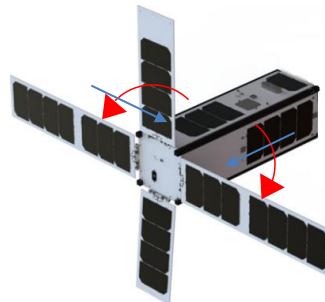


Figure 3: Panel Deployment Path

The deployment of the solar panels will happen at a minimum of 30 minutes after the CubeSat has been launched out of the NanoRacks Deployer. This is to prevent early deployment which could damage the solar panels. In the stowed position, the solar panel and hinge assembly must be able to fit within the NanoRacks Deployer. Figure 4 shows the constraints for the hinges in the NanoRacks Deployer.

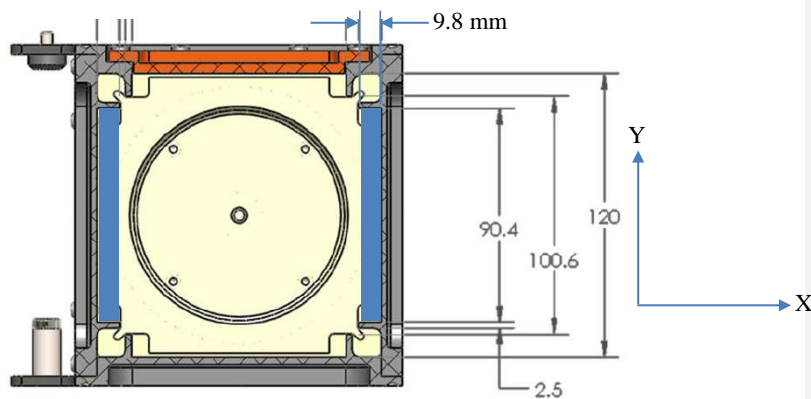


Figure 4: Hinge and Panel Physical Constraints [24]

The hinge and panel must fit within the constraints of 9.8 mm in the X axis, 90 mm in the Y axis, and 250 mm in the Z axis. The 250 mm in the Z axis is the maximum height that the SADA is able to occupy in the CubeSat. In addition to size constraints, the hinge must be able to allow the panels to rotate 360 degrees without obstruction, and allow power and data wires to pass out of the chassis to the solar panels. Another constraint for the hinge is that the deployment of the solar panels must happen at a minimum of 30 minutes after the CubeSat has been launched out of the NanoRacks Deployer. This is to prevent early deployment which could damage the solar panels.

5.3 Transmission Subsystem

The main function of the transmission subsystem is to allow the SADA motor to rotate the solar panels about a single axis. The panels will be capable of continuous rotation. For the space-ready design, the transmission subsystem must ensure that the panels rotate within the required rotational speed requirements. The prototype will be built to function similarly to the space-ready design, so the prototype will also demonstrate these required panel rotational speeds. For both the prototype and the space-ready design, the transmission subsystem must also ensure that the panels meet a required pointing accuracy. The pointing accuracy means that the panels must be within a certain angular distance of its intended angular position when tracking the sun.

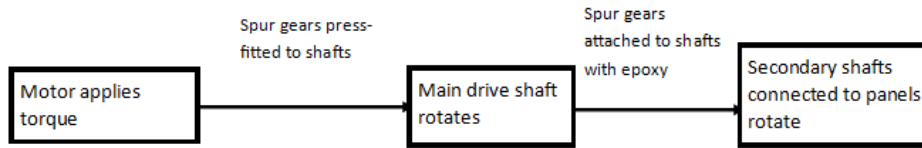


Figure 5: Block Diagram that shows Transmission Subsystem functions

The ideal angular position would have the panels be perpendicular to the light to expose as much of the panel surface area to the sun as possible:

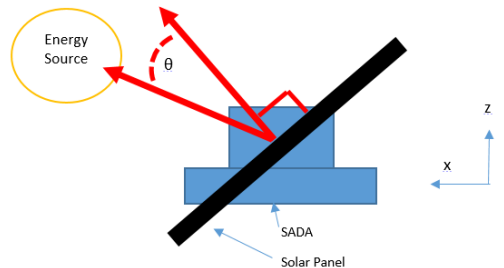


Figure 6: Panel Rotation Accuracy

Here are the engineering design specifications applicable to the Transmission subsystem:

Table 1: Transmission System Related Specifications

Engineering Specification	Space-ready design	Prototype
Panel rotational speed	$3.6 * 10^{-5} \frac{\text{rad}}{\text{s}}$ to $2.4 * 10^{-3} \frac{\text{rad}}{\text{s}}$	(same as space-ready design)
Sun tracking accuracy	$\leq 1 \text{ degree}$	$\leq 10 \text{ degrees}$
Range of panel rotation	$> 360 \text{ degrees}$	(same as space-ready design)
Total Mass of SADA	$< 1 \text{ kg}$	n/a
Dimensions of SADA base, excluding the Tuna Can	10 cm x 10 cm x 2.5 cm	(same as space-ready design)
Solar panel mass	$\leq 3 \text{ kg total}$	(same as space-ready design)

The solar panels have inertia that applies in space, but they do not have gravitational forces acting on them. The motor-gearhead must be able to apply enough torque to overcome the inertia of the panels and rotate them. To determine the panel inertia that the motor must overcome, the panel geometric dimensions, the panel mass, and the panel axis of rotation must be analyzed.

The power that the solar panels must provide the SADA and CubeSat are not specifications that the team was responsible for. However, the panel power requirements factored into the required geometric dimensions of the panel. JPL intends to use panels that can provide a total of 96 Watts of power to the SADA and CubeSat. These panels require a surface area of 60 cm x 30 cm, and the panel thickness (for analysis purposes) is 3 mm:

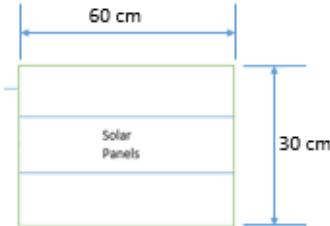


Figure 7: Solar Panel Surface Area

The solar panels have a total allowable mass of 3 kg, so each panel will be at most 1.5 kg. Lastly, the panel axis of rotation is located a 1/3 of the width from the center:

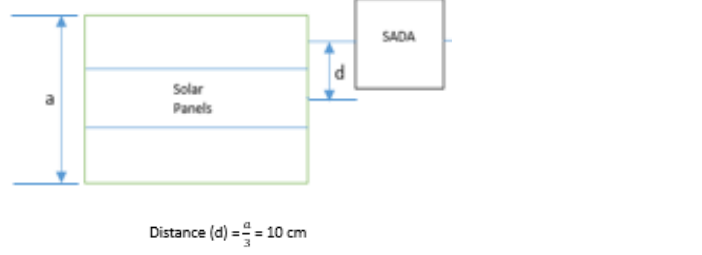


Figure 8: Panel Axis of Rotation

With those three parameters taken into account, this is the rotational inertia for one panel:

$$I_p = \frac{m}{12} (a^2 + b^2) + m \left(\frac{a}{3}\right)^2 = 0.053 \text{ kg-m}^2$$

Mass (m) = 1.5 kg

$$\text{Distance (d)} = \frac{a}{3} = 10 \text{ cm}$$

Thickness (b) = 3 mm

Figure 9: Rotational Inertia Requirements for One Panel

The transmission subsystem also needs to be able to provide a wiring solution that connects wires to sensors that are on rotating solar panels to a stationary controller inside the SADA (in the prototype) or a stationary controller inside the CubeSat (for the space-grade design). Slip rings provide this wiring solution. Slip rings allow wires attached to one end to rotate and wires attached to the other end to remain stationary, and provide electrical connection between both sets of wires. This is the exact function that is required for the SADA; wires from a rotating solar panel must be electrically connected to a stationary controller.

The main technical difficulty with meeting the engineering specifications is selecting a COTS motor, gearhead, slip rings, gears and shafts small enough to fit within the $\frac{1}{4}$ " U CubeSat SADA and Tuna Can dimensions and low weight enough to meet the overall 1 kg SADA module weight requirement. In particular, the gearhead must provide the correct reduction ratio that takes in the motor torque a produces an output torque that is sufficient to rotate the panels. The reduction ratio must also allow the motor speed to meet the specified rotational speeds, as well as reduce the output rotation of the motor so that any control-related rotational inaccuracy will not exceed the panel rotational accuracy specification. Lastly, the transmission system used for the space-ready design must consist of space-grade COTS components that meet the previous requirements. One space-grade specification given by JPL is a radiation rating of 100 krad TID.

Another technical difficulty is calculating torque requirements for panel rotation in space and during the demonstration. For space conditions, the panels do not experience gravitational forces, but they have inertia. For demonstration conditions, the panels do have gravitational forces acting on them. The different conditions for the prototype and the space-ready design require different torques to rotate the panels. A third technical difficulty is ensuring mechanical connection between the motor, gearhead, drive shaft and connecting gears. If any of the mechanical

connections fail, the entire prototype and space-grade design will be unable to perform their intended functions, making this a critical aspect of the entire project.

From the standpoint of the customer, the most important specifications would be the space-grade design mass requirement. The mass plays a significant role in the CubeSat's functioning in space. Most of the weight must be devoted to the CubeSat payload, so meeting the one-kilogram mass requirement would be the most important specification from the standpoint of the customer, JPL. From the standpoint of the design engineer, the most important specification would be geometric dimensions of the SADA and tuna can. The dimensions will determine the component options available for use in both the prototype and the space-grade design.

The components used in both the prototype and the space-grade designs will meet industry standards. The transmission subsystem will make use of Micromo-manufactured gearheads, which is an ISO 9001 and 13485 certified manufacturer [6]. The space-grade design will incorporate the use of Space Foundation-certified COTS materials and components.

5.4 Controls Subsystem

The requirements of the control system closely align with the other system requirements as the system sits within the chassis and interacts with the mechanical system. Below in table 2 is a summary of the requirements and specifications for the control system.

Table 2: Customer Requirements and Specifications for Control System

Customer Requirement	Specification	Prototype Value	Space-Design Value	Units
Must be able to continuously rotate solar panels in both directions	Degrees of rotation	+/-360+	+/-360+	Degrees
Panels must consistently maximize energy absorption	Pointing Angle Accuracy	+/-10	+/- 1	Degrees
Minimize the SADA mass	Mass	1	1	kg
Minimize SADA power consumption	Peak Power	5	5	W
Minimize SADA power consumption	Continuous Power	50	50	mW
Reduce the size of the SADA module	Volume	2.5x10x10	2.5x10x10	cm
Complete full solar panel rotation per LEO orbit	Solar Panel Minimum Rotational Speed	.0024	.0024	rad/s
Must rotate up to 3kg solar panels	Maximum Solar Panel Inertia*	.1156	.1156	kg-m ²
Transfer power from solar panel to CubeSat	Continuous Power Transfer	96	96	W

* Calculated using a 128W solar panel configuration (See Figure 12)

Table 3: Control System CubeSat Standards

Customer Requirement	Type of Standard	CubeSat Standard
SADA must communicate data to CubeSat CPU	Digital Communication	I2C, RS-232
SADA must use voltages regulated by CubeSat power system or must regulate its own voltage	CubeSat Regulated Voltages	3.3V, 5V, 12V

In accordance with Table 3 above, the SADA module shown in Figure 10 must be able to rotate indefinitely about the Y-axis.

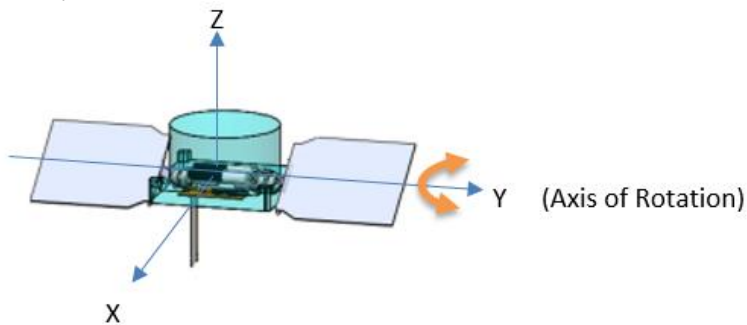


Figure 10: SADA Solar Panel Axis of Rotation

The maximum absorption of energy is when the face of the solar panels is perpendicular to the energy source. The SADA rotates the solar panels to face the energy source but it is acceptable to have an error (θ) of 1° in the space-ready design and 10° in the prototype.

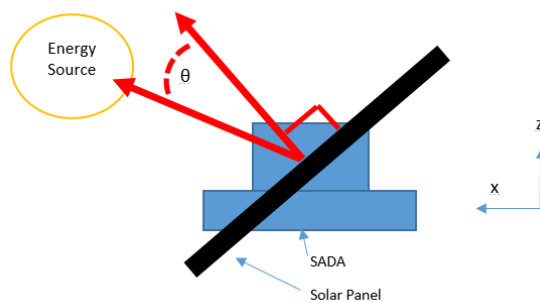


Figure 11: Pointing Accuracy Diagram

The calculation for the solar panel inertia comes from a 128W solar panel configuration from the 2014 team. This configuration has 16 panels. Each panel produces 8W. The thickness of each panel (z-direction: into/out of the page, in figure below) is approximately 2mm following the Clyde-space solar panels. The total mass of the panels together is 3kg based upon the JPL objectives.

This configuration was chosen because the SADA should be able to handle around 96W or more. An array that produces this power is limited in size based upon the NanoRacks deployer which only has 9.4 mm between the wall of the deployer and the CubeSat. The thickness of the panels is about 2 mm each as based upon the Clyde-Space design. This means only 4 panels can be stacked into that space assuming they can be pressed up against each other. Like other Clyde-Space designs, those solar panels would then unfold after deployment. Since each solar panel is approximately 8.5cm wide (y direction), the total width of the unfolded array would be 34cm. In order to find the maximum rotational inertia requirements, the axis of rotation is at the edge of the solar panel array.

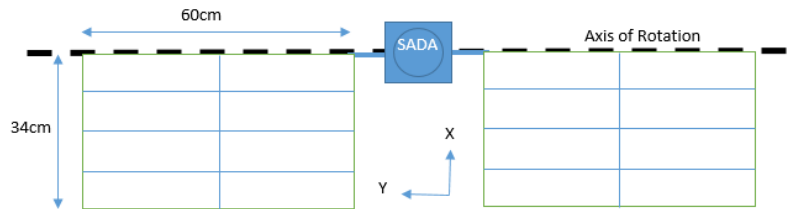


Figure 12: Solar Panel Layout for Maximum Inertia

The formula for the rotational inertia is:

$$\text{Rotational Inertia } (I) = \left[\frac{1}{12} m(B^2 + t^2) \right] + md^2$$

Equation 1: Rotational Inertia

Translating from equation 1, B is equal to 34cm and t refers to the thickness, which is 2mm. The variable ‘d’ is the distance from center of mass to the axis of rotation. The variable “m” refers to mass, which is 3 kilograms in total. Setting d to 17cm (1/2 the distance on the 34cm side) calculates the maximum rotational inertia of the solar panel array.

$$I_{max} = \frac{3}{12} (.002^2 + .34^2) + 3 * .17^2 = .1156 \text{ kg-m}^2$$

6. System Concept Development

6.1 Chassis Subsystem Concept Development

The chassis body is a standard structure that houses the electronics and mechanical system. The physical design of the chassis body is only limited by the volume that we are allowed to use.

This maximum volume can be seen in Figure 1 and Figure 2 and is detailed in Section 5. The material for the chassis body was one thing that needed to be selected. The CubeSat standards (revision 12) state that the CubeSat must be made from Aluminum 7075 or 6061 [24]. These aluminum alloys are commonly used in space. A comparison of these two alloys can be seen in table x. Because of the strict weight requirement, the 6061 alloy would be best for the final space design. Out of the two alloys 6061 had the lower density which would allow for a lower overall mass for the final chassis.

The prototype was created via rapid prototyping due to time constraints and cost. The options for material for this were either ABS plastic or SLA. The properties of each alloy are tabulated in Table 4 in comparison to ABS plastic and SLA. It was decided that the prototype chassis was to be made from the ABS plastic due to the higher yield strength of the material compared to SLA.

Table 4: Mechanical Properties of Chassis Materials

	Density	Yield Strength	Young's Modulus	Poisson's Ratio	Coefficient of Thermal Expansion
<i>ABS plastic</i>	1 g/cm ³	44.4 MPa	1.98 GPa	0.35	103 µm/m·°C
<i>SLA</i>	1.16 g/cm ³	36 MPa	2.02 GPa	0.43	167.9 µm/m·°C
<i>Aluminum 6061</i>	2.7 g/cm ³	276 MPa	68.9 GPa	0.33	23.6 µm/m·°C
<i>Aluminum 7075</i>	2.81 g/cm ³	503 MPa	77.7 GPa	0.33	23.6 µm/m·°C

For the chassis design it was decided that the extra “tuna can volume” was not going to be used. This was because of the risk of damage to the device by using this area. Also this extra space is not available for all types of deployers. By not using this space the SADA could be used in many other deployers, making it a more versatile product. As a result, the SADA device will only occupy a ¼ U of space on any CubeSat. Figures 13 and 14 depict the final design for the chassis. This design is essentially a box that takes up the ¼ U volume, with integrated mountings for the shafts and components of the transmission subsystem. There are also brackets that will be attached via screws to fully secure all internal components. These brackets were designed to best fit the specific components used. Due to the small scale of the device, screws of size 0-80 were used for all parts. This will be applicable for both the space grade design and prototype.

There are key differences between the space and prototype designs, other than choice of material. These differences are due the properties of the material used as well as making the function of the device easy to demonstrate. The “tabs” on either side of the chassis that can be seen in Figure 13 are used to mount the chassis onto the demonstration platform so that it can be tested on its side. Also there is an extra hole in the base of the chassis for cables to connect to an external power source. Instead for the space grade design there would be a connection point for the electronics to connect to the rest of the CubeSat.

Some considerations had to be made with working with ABS. Like many other plastics, it is much softer than many metals. Because of this the material itself can't be threaded and threaded inserts would have to be used along with the screws. With the screw size chosen, there were only two options. From these options brass screw to expand inserts were chosen because

they did not require a special insertions tool. These inserts were permanently pressed into their holes.

The cover will be a flat plate that just screws into the base, it will not have to support any loading caused by the transmission system. It was decided to take advantage of this and have the chassis made out of clear acrylic. This will allow viewers to see into the device as it runs. It can be seen in Figure 13 that there is an opening in the cover. This was a result of the headers of the microcontroller extending above the allowable space in the SADA device. This will not be in the space grade device, as no microcontroller will be used for the SADA.

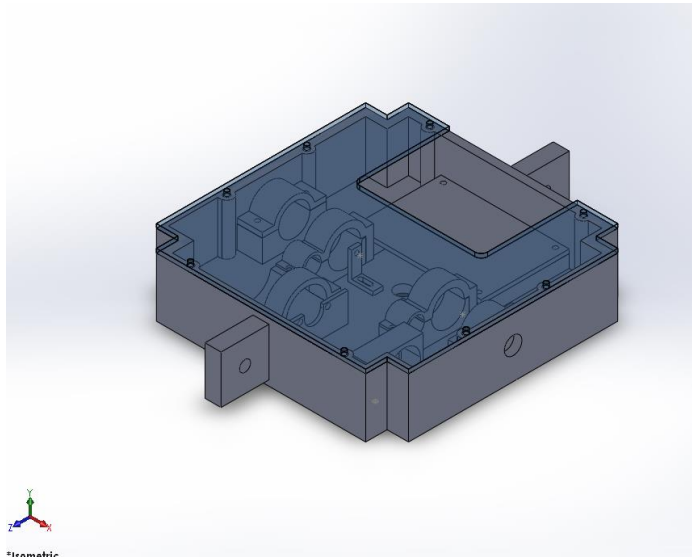


Figure 13: Isometric View of Final Chassis and Cover with Brackets

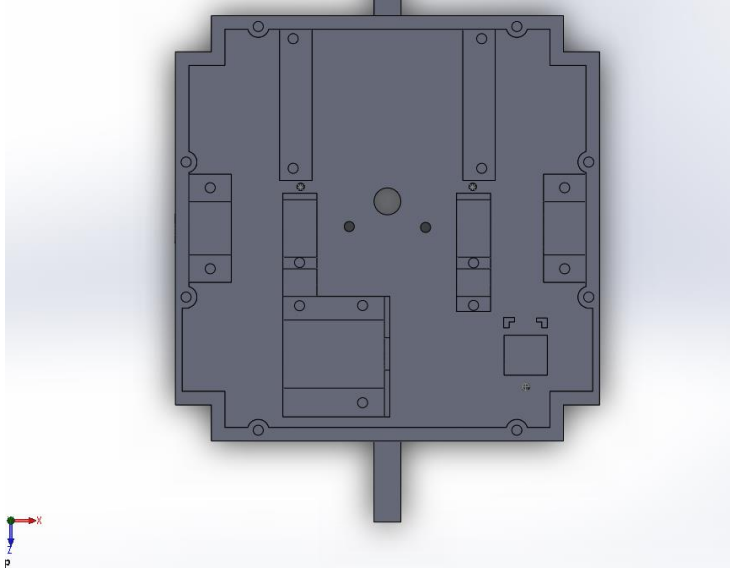


Figure 14: Top View of Final Chassis with Out Cover

During assembly it was determined that not all brackets held down components securely. Also some of the parts were warped from the 3D printing process. As a result, some brackets had to be redesigned and reprinted. One of the brackets that had to be redesigned was the encoder bracket. This bracket was intended to have a hole for one of the threaded inserts to be placed in. From the 3D printing process, the hole for the insert was too warped to allow for insertion. The walls of the bracket were too thin to allow for the original hole to be just drilled larger. Figure 15 below shows a comparison of the two designs. Another bracket that had to be redesigned was the primary bearing bracket. This was due to concerns with securing the slip rings. The L-brackets originally created would not be enough to hold them in place when the device is being demonstrated on its side. Due to the closeness of the slip rings and the primary shaft bearings, a single bracket enclosing both was created. A comparison of the two designs can be seen in Figure 16.



Figure 15: Encoder Bracket Comparison

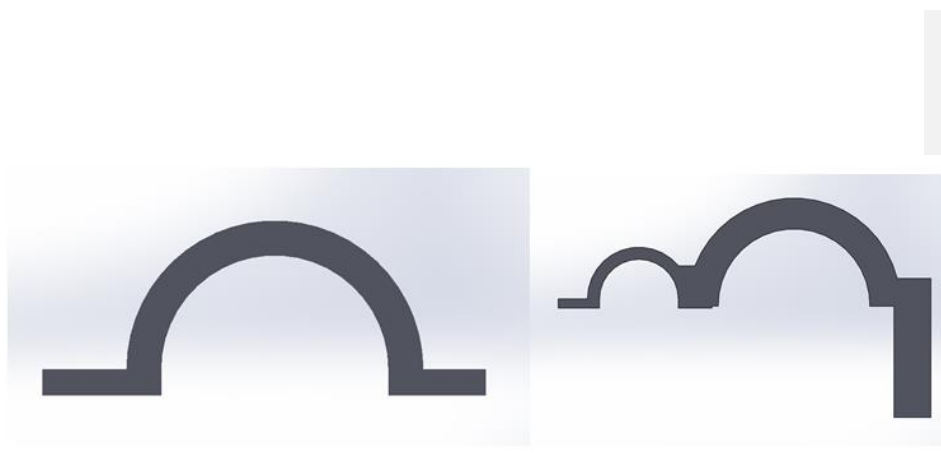


Figure 16: Slip Ring and Bearing Bracket Comparison

6.2 Hinge Subsystem Concept Development

The hinge and deployment subsystem for the device evolved from that of the 2014 design. The hinge design used for the 2014 report use spring hinges that lock into place and travel along a channel bracket. The design is show in Figure 17.

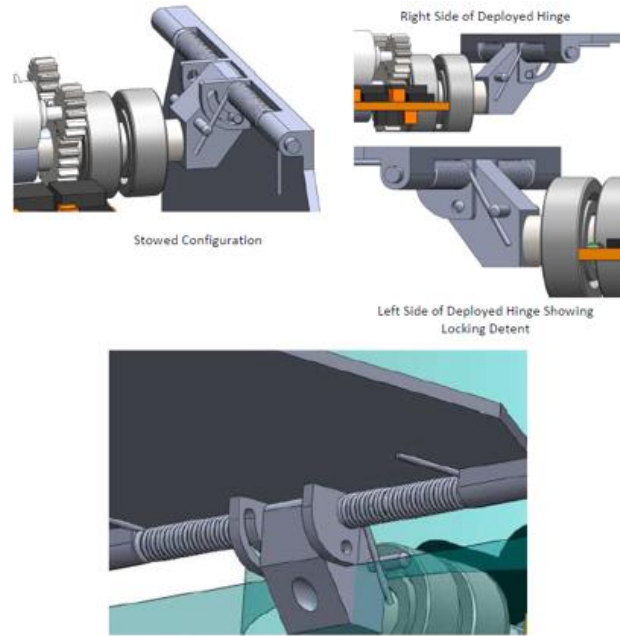


Figure 17: 2014 Hinge and Deployment Design [4]

This design uses semi-custom brackets with ball/pin detent to lock it into place. This design utilizes torsional springs which would apply the force to deploy the panels when activated. In this design, a burn wire would be needed allow the panels to deploy. The burn wire can be seen below in Figure 18.

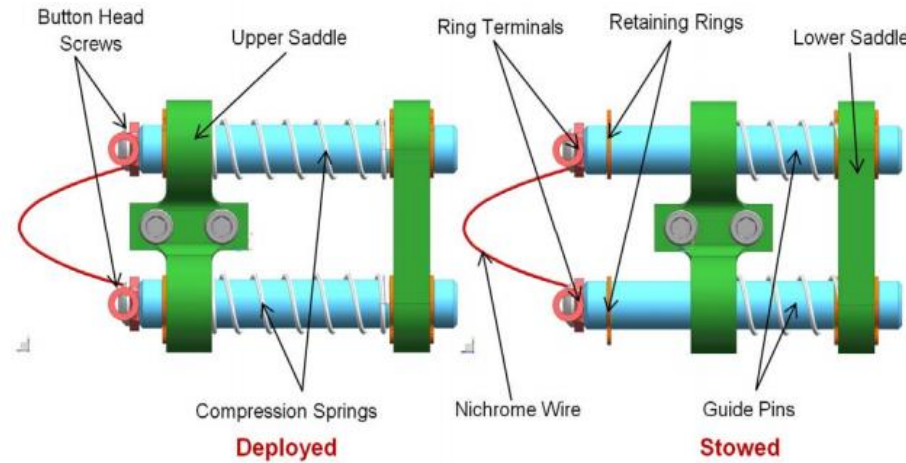


Figure 18: Burn Wire Deployed vs Stowed [25]

The burn wire inputs current into the Nichrome wire to heat it up. The heat of the wire cuts through a chord that is holding the panels in place. Once the burn wire completely cuts through the chord, the panels will be released by the torsional springs that push against the panels. The burn wire can stop drawing current once the chord is cut. This design was too large for the allowable space in the NanoRacks Launcher. This hinge design exceeds the 9.8 mm width of the available space.

In order to develop a design for the hinge and deployment mechanism, there are two aspects that are vital in the design. The first is the action. The action is the part of the hinge that provides a torsional force to move the panels from the stowed position to the deployed position. The 2014 design used springs and they are still a viable option for providing torque to the panel. Another option for the action of the hinge would be to use Shape Memory Alloys (SMA) for the hinges. An example of an SMA used for solar panel deployment is shown in figure 19 below.

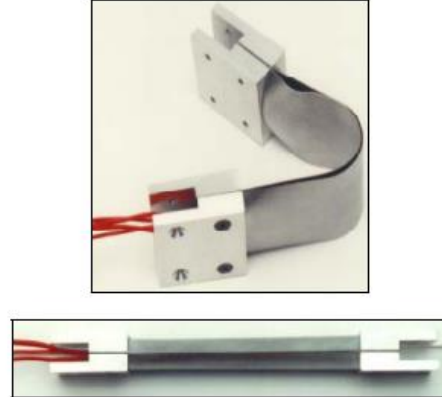


Figure 19: Shape Memory Alloy Hinge; Stowed (top) and Deployed (bottom) [x]

These hinges would be created by SMA ribbons that are charged electrically. Once charged electrically, the temperature of the ribbon begins to increase. As the temperature increases, the ribbon begins to contract into a preset position. An example of this mechanism is shown in figure 20.

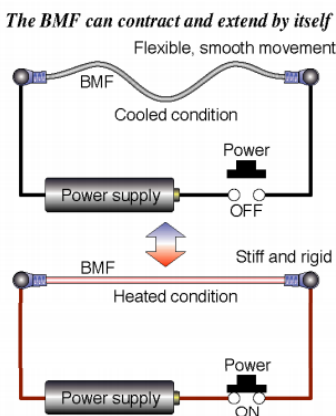


Figure 20: SMA Material Demonstration [26]

The change of shape of the ribbon causes the hinge to move and deploy the solar panels. This would be attached at one end to the solar panels and the other to the chassis. The SMA hinge would allow for deployment and retraction of the panels, if necessary. A negative aspect of the SMA hinge would be the constant current is needed to hold the panels in a specific positon.

This could however be solved by using pins that lock into place when the panels are fully deployed. To evaluate these two options, the power consumption of a spring hinge with a burn wire and the power consumption of SMA materials were compared. In addition to power consumption, the deploy time of each type of action was compared. The power consumption and the deployment time of the burn wire, springs, and SMA material is tabulated in table 5 below.

Table 5: Hinge and Deployment Action Comparison Chart

Component	Type	Power Consumption	Deployment Time
Burn Wire	NA	0.9 W	8 seconds
McMaster 9271K88	Music Wire Spring	NA	5.01 seconds
McMaster 9271K603	Music Wire Spring	NA	1.87 seconds
McMaster 971K98	Music Wire Spring	NA	2.61 seconds
McMaster 9271K94	Music Wire Spring	NA	3.06 seconds
Flexinol Actuator Ribbon	SMA	37.12 W/m to 88.8 W/m	1.5 seconds
Flexinol Actuator Springs	SMA	14.27 W/m to 58.05 W/m	15 seconds
BioMetal Fiber	SMA	3.37 W/m to 7.05 W/m	Not found
BioMetal Spring	SMA	7.84 W/m to 36 W/m	Not found

The analysis of the options of the actions showed that the power consumption of the burn wire and spring combination would be the least. The power consumption is the 0.9 Watts of power for the 8 seconds, at most, that the burn wire takes to cut through the nylon cord that holds down the panels. In addition to power consumption and deployment time, springs are a better option because of they are readily available. SMA materials are also much harder to work with.

The second aspect is the mechanism that will bring the panels to a stop at the deployed position. After researching different mechanisms to do so, two options arose. The first option is to use a physical stop that will stop the panels at the deployed position. The action would push the panels until the panels hit the physical stop. This is the simplest option. However, the panels could move out of the fully deployed position if it were pushed by a force. The second option is a ball/pin detent. This was used in the 2014 design. This ball/pin detent would push into a hole on the hinge bracket that would lock the panel in the deployed position. An example of a ball detent is shown in Figure 21.



Figure 21: Ball Detent (McMaster 84835A21) [27]

After the analysis done on some springs, the residual force of the springs would hold the panel in place. Therefore, there is no need for a detent however it could be used to provide redundancy.

After evaluating the aspects of the design that would accomplish the requirements for the hinge and deployment subsystem, a design was developed. Figure 22 shows the prototype design for the hinge and deployment that will be used in the demonstration.

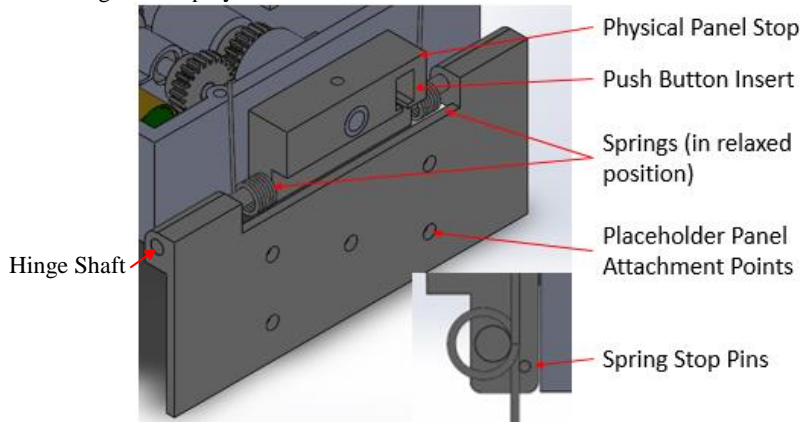


Figure 22: Prototype Hinge and Deployment Design

The hinge and deployment design consists of a physical panel stop; push button insert, springs, placeholder panel attachment, and spring stop pins. The physical panel stop was designed to be able to sustain the impact of the panels during deployment. The panel stop also has a hole to house the hollow shaft from the transmission subsystem to allow wires to pass through. The push button insert is used to house a push button that would be used in the control algorithm to confirm mechanical deployment of the panels. The placeholder panel attachment is used to simulate panels on our prototype. For the space grade option, the panels' attachment would be replaced with panels that are chosen for that specific mission. The spring stop pin holds the spring in place as the panel is moved to the stow position. This creates torque that is stored in the spring until the panels are released. These pins are made from 316 stainless steel to be able to handle the bending and shearing forces that the spring would put on the pin. The hinge mechanism is held together by a hinge shaft that runs through the physical stop, springs, and the panel attachments.

6.3 Transmission Subsystem Concept Development

The SADA motor will be attached to a gearbox. The gearbox will be used to provide a reduction ratio that takes the motor torque and reduces it to a torque value that acts on the panels and produces required panel rotational speeds. The panels will be attached to a drive shaft that runs the length of the SADA. The drive shaft will have a gear on it that the gearbox will mesh with, thus allowing the motor to rotate it. The drive shaft will be mounted to the SADA base with sleeve bearings.

There are numerous ways of implementing this gearbox within the SADA. One way is to mount the motor and gearbox next to the drive-shaft inside the SADA base:

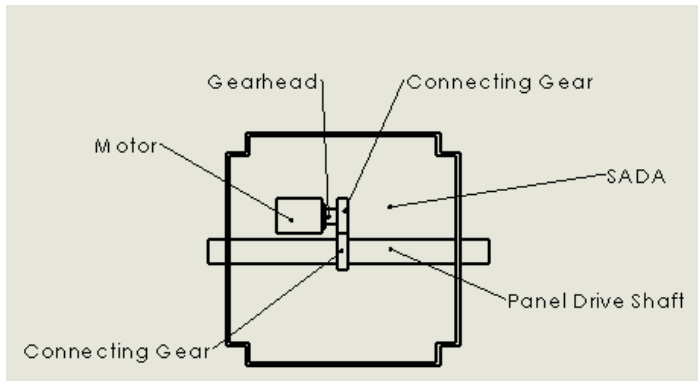


Figure 23: Top-Down View of configuration: The motor and the gearhead are to the side of (coplanar to) the main drive shaft that the panels are connected to. Single Coplanar Motor Configuration

The controller is placed on the other side of the drive shaft. Figure 24 displays the functionality of this configuration:

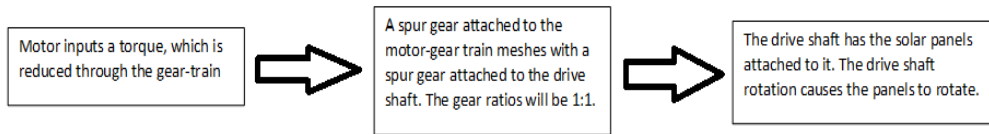


Figure 24: Single Coplanar Motor Configuration block diagram that displays basic functionality

Benefits:

- This configuration removes the need for the tuna can.

Drawbacks:

- The configuration also necessitates that the motor-gearhead, gearhead and the gears connecting them have geometric dimensions that can fit within the 2.5 cm height of the SADA base.
 - This creates a significant geometric dimension requirement that will greatly limit the selection of valid components, both for the prototype and the COTS components for the space-grade design.

Another way of implementing the gearhead within the SADA is to store the motor and gearhead inside the SADA, have the gearhead come down onto the drive shaft and rotate through a bevel gear.

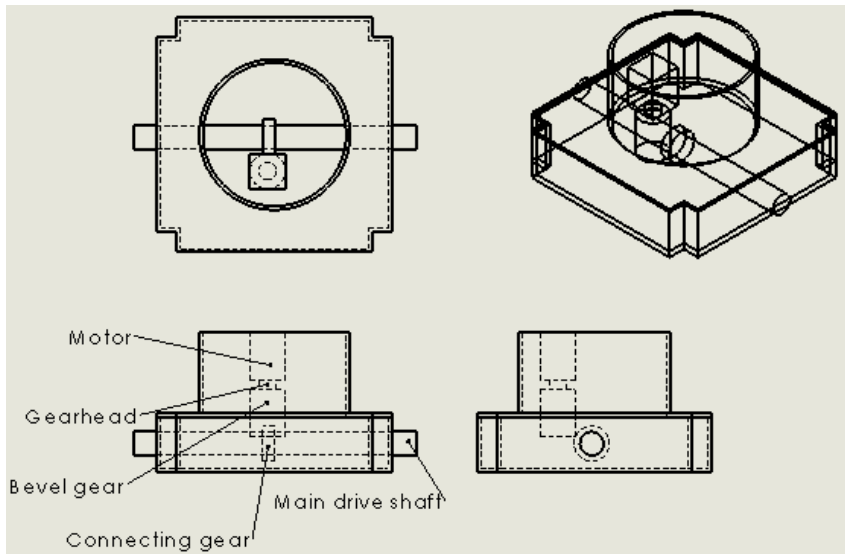


Figure 25: The motor and gearhead are in the tuna can, on top of the drive shaft. Single Vertical Motor Configuration

The controller is located inside the SADA base. Figure 26 displays the functionality of the Single Vertical Motor Configuration:

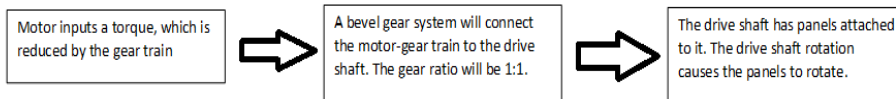


Figure 26: Single Vertical Motor Configuration block diagram that displays basic functionality

Benefits:

- This configuration takes advantage of the Tuna Can space. This configuration creates more space in the SADA base and allows for more lenient geometric dimensions for the motor and gearbox.
 - More available space inside the SADA base allows for a second backup motor that interfaces with the drive shaft.
- If a backup motor is not implemented, the configuration allows the space-grade SADA base to be completely solid, while having crevices created for the drive shaft, the bevel

gear attached to the gearbox, and the controller. A solid SADA base will have greater mechanical strength than a hollow SADA base.

Drawbacks:

- The only downside of this setup is that the SADA will have more weight at the tuna can, and make it top-heavy. But, the SADA will be attached to the much heavier CubeSat, so the weight distribution will balance out overall when implemented.

A third concept is having two motors, two gearheads each interfaced with a motor, and two separate drive shafts each with one panel attached. The motors will be inside the SADA base, coplanar to the drive shafts:

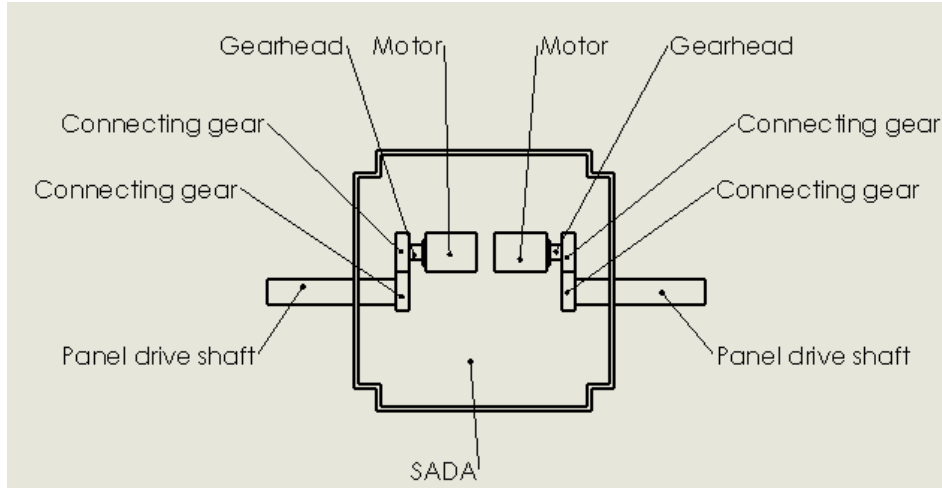


Figure 27: Top-Down view of Configuration: Two independent motors. One panel attached to each drive shaft. Double Coplanar Motor Configuration

The space taken up by both motors will mean that the tuna can is the only place in the SADA that the controller can be put in. The basic functionality is identical to the Single Coplanar Motor Configuration.

Benefits:

- Each motor only has to rotate a single 1.5 kg panel, making motor torque requirements less.
- The mechanical stress on the drive shafts will be less since they are each attached to only one panel, not two.

Drawbacks:

- Two motors indicate more weight and more SADA base space taken up. This will limit the selection of motors and gearheads that can meet still meet the 1 kg weight requirement and be able to fit within the SADA base.

- The controls subsystem will have to coordinate two separate motors.
- Two motors and two separate drive shafts means there are more moving components inside the SADA. This lowers the available space in the SADA. The wiring from the panels that are responsible for power generation have a greater chance of being tangled up on one or both of the drive shafts and motors.

This is a summary of the concept selection process for the configuration within the SADA:

Table 6: Transmission System Concept Comparison

Selection Criteria	Concept 1: Single Coplanar	Concept 2: Single Vertical	Concept 3: Double Coplanar
<i>Need of Tuna Can</i>	+1	-1	+1
<i>Minimizes Size</i>	+1	-1	0
<i>Minimizes Weight</i>	+1	+1	-1
<i>Expected Reliability</i>	0	0	+1
<i>Power Needed</i>	+1	+1	-1
Sum	4	2	2

The three most important selection criteria are the need of a tuna can, the weight, and the power needed. The use of the tuna can would limit the CubeSat sizes that the SADA module could interface with to 3U or larger, and eliminating the need for it would be ideal (insert citation). NASA space launches have stringent mass requirements, and it is ideal to minimize the weight of the SADA as much as possible. Lastly, the SADA is intended to provide power for CubeSat, therefore, it is ideal to minimize the power required to operate it. The Single Coplanar configuration meets all three of the criteria and is the finalized design of the transmission subsystem configuration.

Slip rings come in three different types: mini capsule, mini capsule thru-shaft, and thru-bore. Table 7 is an example table of the three types:

Table 7: Slip Ring Selection Comparison

Criteria	Mini Capsule Type	Mini Capsule Thru-Shaft Type	Thru Bore Type
Outer Shell Diameter	~6-18 mm	~6-10 mm	~17-22 mm

Rated Voltage	150-250 V	75-250V	240-250V
Rated Current per Ring	1-2 A	1-2 A	1-2 A
Number of Rings (circuits)	6-12	6-12	6-12
Picture of Example	[7]	[8]	[9]

Mini Capsule and Mini Capsule Thru-Shaft slip rings require secondary shafts for the panels to connect to, as shown in Figure 28.

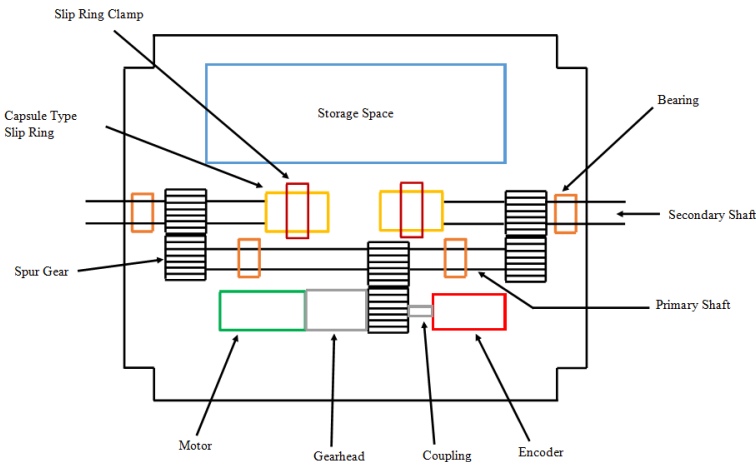


Figure 28- Capsule Type Slip Ring Device Layout

The thru-bore slip ring does not require secondary shafts, and can be used in the configuration shown in Figure 29.

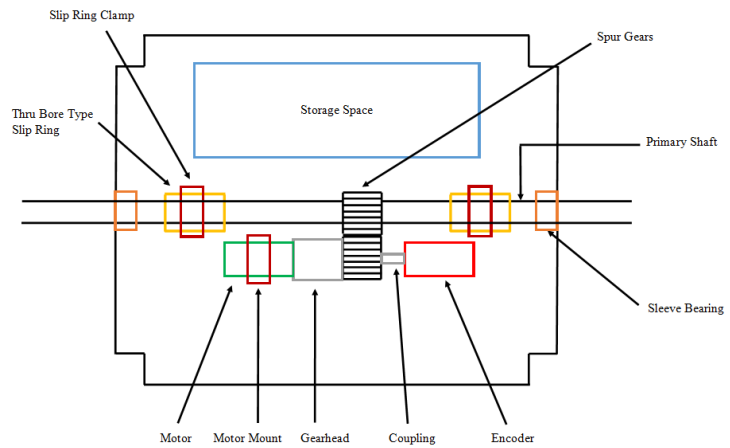


Figure 29- Thru Bore Type Slip Ring Device Layout

While the design shown in Figure 29 is ideal due to the lack of a secondary shaft, the long lead times on thru-bore slip rings invalidated this design for the SADA prototype. As a result, the capsule slip ring layout was used. The Adafruit Prosper Mini Capsule Slip Ring, shown in Figure 30, was selected as the prototype slip ring, due to its low cost, low size, and quick delivery time.

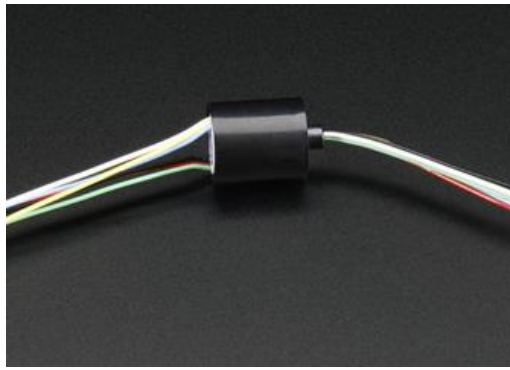


Figure 30- Prosper Mini Capsule Slip Ring [10]

The other slip ring types are still viable for the space-grade design, as they all meet the requirements needed for the project. Table 8 shows the specifications on each of the space-grade examples. A slip ring should be selected based on the lead times required for the project.

Table 8- Slip Ring Selection Comparison

Criteria	Prototype Design	Space Grade Design		
<i>Manufacturer</i>	Adafruit (Prosper)	Electro-Miniatures		Cobham Aeroflex
<i>Model</i>	SRC012C-6 [10]	2040 [7]	2321 [8]	CAY-1398 [9]
<i>Type</i>	Capsule	Capsule	Capsule - Through Shaft	Capsule - Through Shaft
<i>Max Number of Circuits</i>	6	10	12	12
<i>Rated Voltage</i>	240 VAC/VDC	250 VAC/VDC	250 VAC/VDC	150 VAC/VDC
<i>Rated Current per Circuit</i>	2.00 AM	1.00 AM	1.00 AM	1.00 AM
<i>Max Speed</i>	300 RPM	225 RPM	400 RPM	1000 RPM
<i>Stator Diameter</i>	12.4 mm	5.7 mm	9.5 mm	9.4 mm
<i>Body Length</i>	17 mm	19.9 mm	25.0 mm	26.2 mm
<i>Contact Type</i>	Precious Metals	Gold on Gold	Gold on Gold	Gold on Gold
<i>Max Noise</i>	10 mΩ	5 mΩ	5 mΩ	10 mΩ

6.4 Control Subsystem Concept Development

6.4.1 Microcontrollers and Motor Drivers

Many different technologies can be used to satisfy the needs of the SADA control system, but some implementations are both more complicated and more expensive for this purpose. Figure 31 shows taxonomy of available processing technologies.

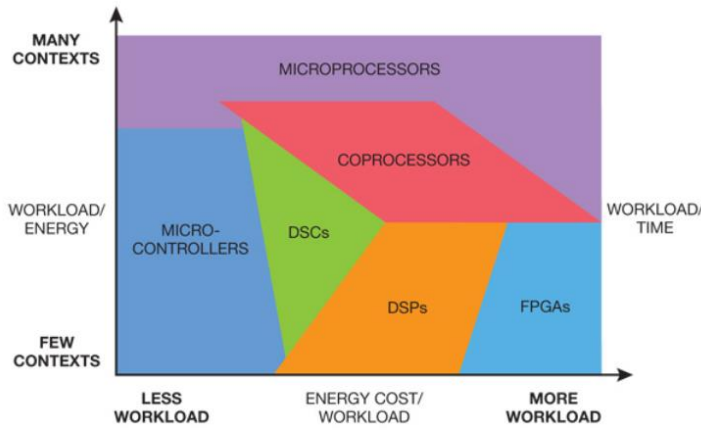


Figure 31: Controller Taxonomy [11]

Since the prototype needs to be designed quickly and needs to account for unexpected design flaws, a low workload and many context option Figure 31 is desirable. Therefore, microcontrollers are a good option for prototyping, since many cheap options exist that can satisfy the needs of the SADA prototype. Table 9 compares some of the best microcontroller options.

Table 9: Microcontroller Comparison

Criteria	Requirement	Arduino Mini [20]	Pololu B-328 [21]
Size	$\leq 4 \times 3 \times 2 \text{ cm}$	$3.3 \times 1.8 \times 1.05 \text{ cm}$	$3.1 \times 1.8 \times 1.10 \text{ cm}$
Digital I/O	2	14	16
Analog Inputs	4	8	8
Motor Drivers	2	0 (Need Driver)	2 (1A Continuous)
Image of Controller	-		

All of the controllers listed are inexpensive, and have available libraries that make them easy to use for building a prototype quickly. Because the SADA control system will be responsible for motor control, the Pololu Baby Orangutan B-328 was selected as the strongest option, due to its two onboard motor drivers, numerous analog/digital pins, and simple interface.

While these microcontrollers are suitable for the prototype, none of the controllers listed are space rated. The IPSPT team recommended use of the UC1625sp motor controller, shown in

Figure 32. The UC1625sp may have been a suitable option, but it has since been declared obsolete and cannot be used for the SADA module [12].



Figure 32: UC1625sp Motor Controller

Rather than select a space-rated microcontroller, the SADA can instead rely on a given CubeSat's computer. This would reduce the price and size of the SADA, and would also allow for increased flexibility in the SADA algorithm. However, even if the SADA uses the CubeSat computer, it must still contain motor drivers that the computer can use to drive the SADA motor. Figure 33 shows a suitable space-rated motor driver—the International Rectifier RH Motor Control Module. This motor driver's ratings, shown in Table 10, meets all of the specifications required to withstand the conditions of space, but also meets the voltage and current ratings of the selected SADA motor.

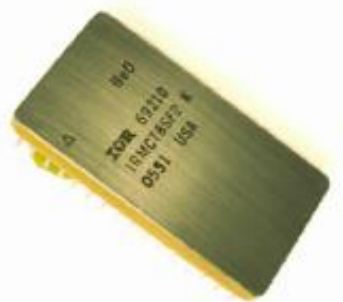


Figure 33: International Rectifier RH Motor Control Module [13]

Table 10: RH Motor Control Module Specifications [13]

TID Radiation Hardness	100 krad
Pressure	Atmospheric to space vacuum
Operating Temperatures	-55°C to 125°C
Operating Voltage	Up to 400 VDC
Operating Current	0 to 2 A

6.4.2 Sensors

Sun sensing is not part of the requirements set for the SADA, and should not be included in the final space-grade design. However, CubeSats that use the SADA may likely use some form of sun sensing that the SADA must interact with. Therefore, it is essential that the prototype emulates such functions, and that the SADA is designed with sun sensing in mind. Some common attitude determination systems used for satellite navigation are [14]:

- Star Trackers
- Horizon Scanners
- Magnetometers
- Gyros
- Digital Sun Sensors
- Analog Sun Sensors

Of these sensors, Star Trackers, Digital Sun Sensors, and Analog Sun Sensors can be used for sun sensing; Horizon Scanners, Magnetometers, and Gyros are best used for finding an attitude relative to Earth. Star Trackers capture an image of the sky, and compares the image to a known star map.

Digital Sun Sensors, such as the thin-slit sensor shown in Figure 34, refract sunlight onto an array of photodetectors, and use the distance from the centerline, d , to calculate the angle θ given the equation $d = h \tan \theta$ [15].

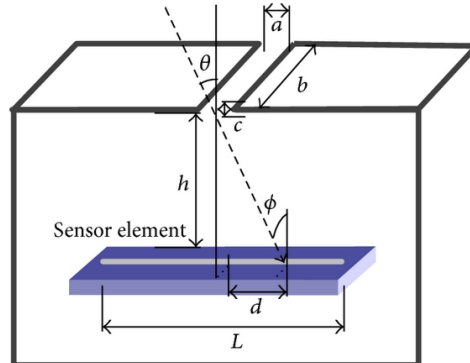


Figure 34: Thin-Slit Sensor Theory [15]

While these sensors provide accuracy within 1° error, dedicated sensors like these often cost thousands of dollars, and cannot be used for prototyping. This makes dedicated sun sensors a good option for the space-grade design, but a poor choice for prototyping, where inexpensive options are necessary.

Analog Sun Sensors can be mounted on three sides of the CubeSat, each returning a value proportional to the intensity of sunlight. These currents can be used to find the sun vector through the equation:

$$v = \begin{bmatrix} X & 0 & 0 \\ 0 & Y & 0 \\ 0 & 0 & Z \end{bmatrix} \cdot \begin{bmatrix} I_{left} \\ I_{front} \\ I_{top} \end{bmatrix} \cdot \frac{1}{I_{max}}$$

Where X, Y and Z equal 1 or -1, depending if the sensor is placed on the positive or negative side of the satellite [14]. This type of design can be cheaply implemented with phototransistors as sensors, but may have inaccuracies up to 20° errors.

As an alternative, Analog Sun Sensors can be selected to cover different fields of vision, and the relative difference in measured intensity can be used to orient the panels. A concept of such a design is shown in Figure 35, using phototransistors as light sensors.

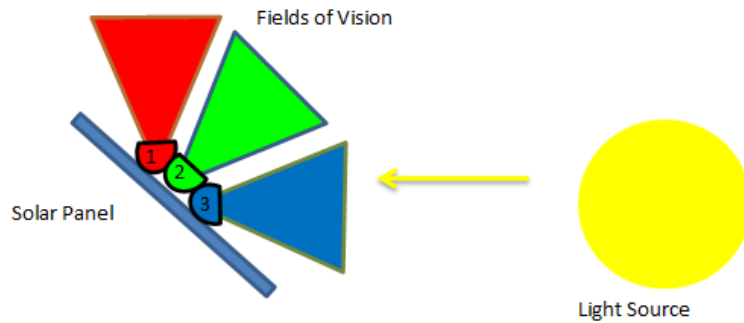


Figure 35: Phototransistor Sensor Implementation

By mounting phototransistors directly on the solar panels, error can be reduced to within 10°.

All three of these options have similar size and mass constraints, but offer different price ranges and accuracies. Given these three options, a selection matrix was formed for the prototype using cost and accuracy as the main criteria, shown in Table 11.

Table 11: Sun Sensing Comparison for Prototype

Selection Criteria	Solar Panel Mounting	SADA Base Mounting	Thin-Slit Sensors
Cost	< \$20	< \$20	> \$1000
Accuracy	< 10°	< 20°	< 1°
Total	+2	0	0

Since the prototype requires lower costs but allows for less accuracy, using phototransistors with solar panel mountings is an appropriate approach. The space-rated design should not include built-in sun sensors, as they may come packaged with the solar panels or other CubeSat components, but Thin-Slit sensors would be an appropriate choice if necessary. Other options,

like Star Trackers and Magnetometers, are too bulky and expensive for both the prototype and space-rated design, and will not be considered further.

6.4.3 Motor Type Selection

The SADA requires a device that will allow controlled rotation of the solar panels. With access to electrical power, the team chose to use an electric motor which provides a straightforward way to control rotation by applying an electric signal.

Due to the time constrained project, the motor vendors were restricted to RPI approved vendors. The two common sources were Micromo and Maxon Motors. These vendors were able to supply prototype motors and could also make small modifications to support space-qualified motors. From these sources there were three types of motors under consideration due to their availability and development ease: brushless, brushed, and stepper motors. Servo motors were not included because they were difficult to find in the correct sizes for the space-qualified design. The brushed motor was included in the selection process in order to compare all the possible motors from the vendors but was not highly considered and was quickly discarded because brushed motors are not often used in space. A main reason for this is that brushed motors can cause electrical arcing and stray electromagnetic noise.

The following chart compares the three types of motors from Micromo. In order to keep them in the same scale, these numbers come from motors with a diameter of 1-2cm. The purpose of the SADA is to orient the solar panels to a particular position. This is built in to the requirements as the motor must have the torque to move the panels and the position/speed accuracy required by JPL while optimizing the remaining specifications.

Table 12: Motor Type Selection

Criteria	Brushed	Brushless	Stepper
Torque (mN*m)	2.5	3.5	4.0
Mass (g)	16	10	12
Speed (RPM)	>5k	>5k	<1k
Position Accuracy (Overshoot) ¹	Up to 50%	Up to 50%	1/2 Step Size
Lifespan (Hrs) ²	3k	10k	10k
Max Efficiency (%)	50-70	60-80	~60-80 ³
Cost (\$)	\$50-150	\$150-300	\$150-350
Total Rank (Green-Yellow)	-3	-1	3

- 1) The overshoot comes from simulations located in Appendix E using simple PID controllers
- 2) The lifespan is estimated from non-space-qualified motors [Anaheim motors citation]
- 3) The efficiency of the stepper motor is not given since stepper motors output the same power regardless of the load. It is estimated to have the same efficiency as a brushless motor since they have similar internal construction

As mentioned and revealed from the chart, the brushless motor was the worst choice. The brushless and the stepper motor were comparable in their physical characteristics. The choice to use the stepper is entirely based upon the required mission. The stepper motor has a slightly higher torque which means a smaller gear ratio and thus less weight. The stepper motor also has controllable speed and accuracy that works from a digital signal. The high speed of the brushless motor means the position accuracy of the brushless motor is decreased.

7. Design Analysis

7.1 Chassis

As part of the analysis of the chassis, a mock prototype chassis was created early in the design phase. The purpose of this was to give the team a better sense of the scale of the project. Also this mock chassis was used to test fit any internal components being considered. The mock chassis itself was created to represent the maximum possible exterior volume, these dimensions can be seen in Figures 1 and 2. The walls of the mock chassis were 1/16th of an inch and the interior was hollow. This mock chassis was instrumental in deciding how the internal components would fit within the final chassis.

Finite Element Analysis (FEA) was used to determine how the expected loadings will affect the chassis as well as the hinge. The software used for this analysis was NX NASTRAN. This allowed for the areas of high stress concentration, and the related values, to be determined. Maximum stress values were compared against the yield strength of the material to determine if there will be failure at that point. Maximum displacement under the same loading conditions was determined as well to see if it would greatly affect the performance of the chassis.

Figure 36 is a free body diagram showing the loading expected to be experienced by the chassis. In detail, a 0.0342 N load was applied to the mountings of the bearings for the primary shaft and a 0.00511 N load was applied to the mountings of the bearings for the secondary shafts. These values are representative of the load caused by the shaft rotating in the bearings. The calculation for these values is detailed in section 7.3. Also a 0.1765 N force was applied to the motor cradle and a 0.127 N load was applied to the encoder cradle. Both are representative of the weight of their respective parts. The last load applied was a 2g acceleration load that was applied to the entire chassis. This is representative of the maximum acceleration experienced during deployment. All of these forces are applied in the vertical direction, into the page. Lastly the chassis was held fixed in the corners of the cutouts to simulate the SADA being held to the rails of the CubeSat.

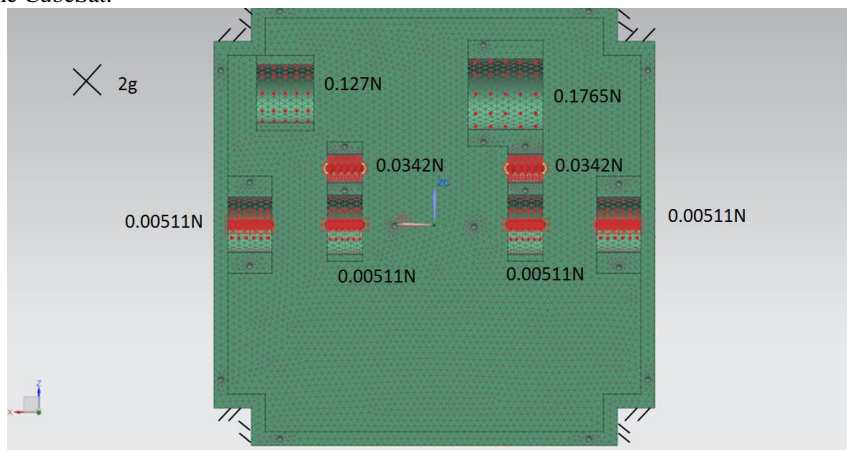


Figure 36: Force Diagram of Chassis

Images of the results of this analysis can be seen in Figures 37 and 38. The maximum stress determined from this analysis is 0.0683 MPa, its location can be seen in Figure 38 circled in red.

As it can be seen in table 4, the yield strength of ABS is 44.4 MPa, much greater than the stress experienced by the chassis. This indicates that the chassis is overdesigned. The location of maximum displacement can be seen in Figure 37, its value is 1.625×10^{-3} mm. This value is negligibly small, further indicating that the chassis is overdesigned.

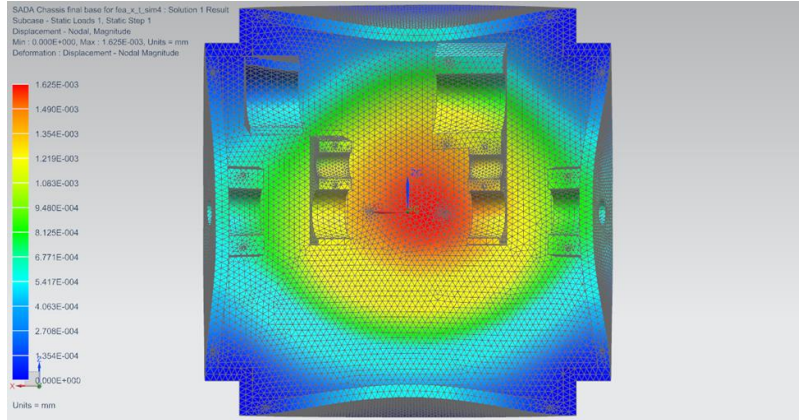


Figure 37: Chassis FEA Analysis Displaying Displacement

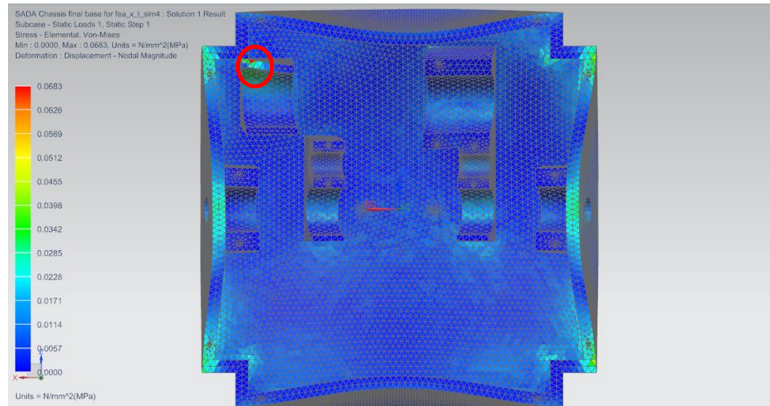


Figure 38: Chassis FEA Analysis Displaying Stress

7.2 Hinge Subsystem Analysis

The hinge and deployment design was analyzed at three points. The panel bending failure, the panel stop failure, and the spring pin failure. The failure analysis at these points was used to determine the spring that would be used. The failure analysis of the panels is done assuming that the panels folded up can be represented by a 6 mm thick block of copper. This is

because when analyzing the failure of one panel, the copper is the part of the panel which will dictate the deflection of the panel.

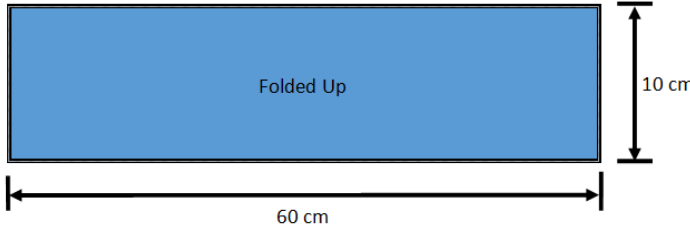


Figure 39: Folded Panel Dimensions (Top View)

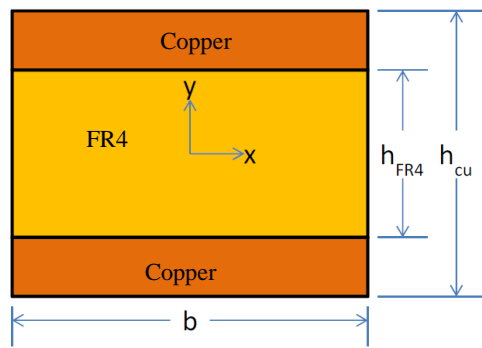


Figure 40: Cross Sectional View of the Panel from Pumpkin

The stiffness of the panel is found by applying an arbitrary distributed load on the panel. This Maple Code can be seen in Appendix M. The panel is modeled as a cantilever beam. Using the simulation, the slope of the end of the panel is found. The stiffness is found using the equation below.

$$k_{stiffness} = \frac{M_{Max}}{Slope_{ave}}$$

It was found that the stiffness of the full size panels and the prototype panel attachment are 1440 Nm/rad and 14 Nm/rad, respectively. The bending of the panel is analyzed through energy analysis of each state of deployment. The energies at each state are shown in figure 41.

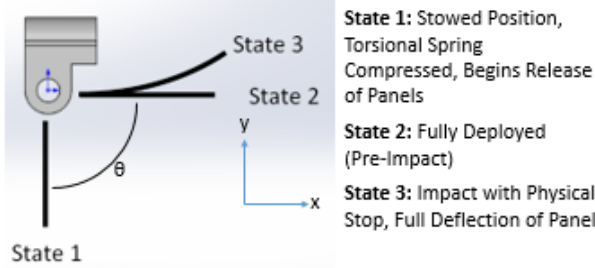


Figure 41: States of Deployment

The energies at each state are shown in Table 13.

Table 13: Energy Equations for Each State of Deployment

State 1	State 2	State 3
$PE_1 = \frac{1}{2}k_{spring}(\Delta\theta_1)^2$	$PE_2 = \frac{1}{2}k_{spring}(\Delta\theta_2)^2$	$M = k_{stiffness}\Delta\theta_3$
$KE = 0$	$KE_2 = \frac{1}{2}I_{rotation}\omega_2^2$	$\frac{1}{2}I_{rotation}\omega_2^2 = \frac{1}{2}k_{stiffness}(\Delta\theta_3)^2$

At state 1, the spring in the stowed position will store all of the potential energy because there is no kinetic energy of the state. At state 2, the spring still has residual energy stored and the panel is at its maximum kinetic energy. At state 3, the panel deflects to its maximum point due to the impact with the physical stop. The kinetic energy of the panel at state 2 is converted to a deflection in the panel. The moment on the panel is proportional to the deflection angle and the stiffness of the panel. This moment is used to evaluate if the failure of the panel. The moments on the panel from the different spring options are tabulated in table 14.

Table 14: Springs Considered

Spring	Stow Torque	State 1	State 2	State 3
McMaster 9271K88	0.0169 N-m	$PE_1 = 0.027 J$ $KE_1 = 0$	$PE_2 = 0.0066 J$ $KE_2 = 0.020 J$	$M = 7.5 Nm$
McMaster 9271K603	0.121 N-m	$PE_1 = 0.19 J$ $KE_1 = 0$	$PE_2 = 0.047 J$ $KE_2 = 0.14 J$	$M = 20 Nm$
McMaster 9271K98	0.0624 N-m	$PE_1 = 0.098 J$ $KE_1 = 0$	$PE_2 = 0.024 J$ $KE_2 = 0.074 J$	$M = 15 Nm$
McMaster 9271K94	0.0454 N-m	$PE_1 = 0.071 J$ $KE_1 = 0$	$PE_2 = 0.018 J$ $KE_2 = 0.053 J$	$M = 12 Nm$

This same calculation was done for the prototype panel attachment. The prototype panel attachment is printed out of ABS plastic. The dimensions of the panel attachment can be seen in Figure 42.

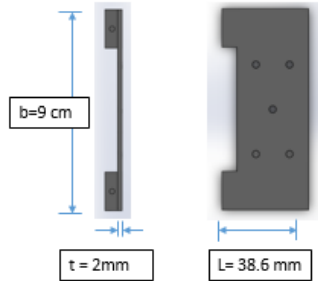


Figure 42: Prototype Panel Attachment Dimensions

The ABS printed panel attachment yielded at a maximum moment of 2.5 Nm and had a stiffness of 14 Nm/rad. The moment on the panel attachment with each of the springs is tabulated in table 15.

Table 15: The Moment on the Panel due to the Spring

Spring	Stow Torque	State 1	State 2	State 3
McMaster 9271K88	0.0169 N-m	$PE_1 = 0.027 J$ $KE_1 = 0$	$PE_2 = 0.0066 J$ $KE_2 = 0.020 J$	$M = 0.75 Nm$
McMaster 9271K603	0.121 N-m	$PE_1 = 0.19 J$ $KE_1 = 0$	$PE_2 = 0.047 J$ $KE_2 = 0.14 J$	$M = 2 Nm$
McMaster 9271K98	0.0624 N-m	$PE_1 = 0.098 J$ $KE_1 = 0$	$PE_2 = 0.024 J$ $KE_2 = 0.074 J$	$M = 1.4 Nm$
McMaster 9271K94	0.0454 N-m	$PE_1 = 0.071 J$ $KE_1 = 0$	$PE_2 = 0.018 J$ $KE_2 = 0.053 J$	$M = 1.2 Nm$

All the springs selected were able to provide enough torque without causing the space grade panel or prototype panel attachment to fail.

After analyzing the panel bending, the panel stop that provided a barrier for the panel movement was analyzed. The cross sectional area of the physical panel stop is shown in Figure 43.

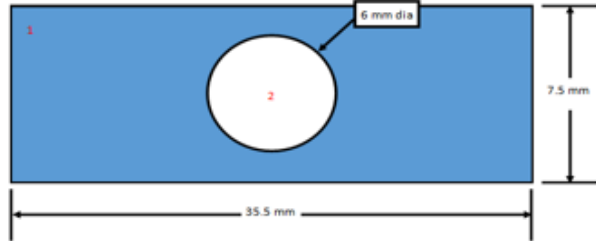


Figure 43: Cross Sectional Area of the Physical Panel Stop

In order to calculate the moment of inertia of the cross sectional area, the inertia of area 1 and area 2 were calculated individually. After the inertias of each area were calculated, inertia of area 2 was subtracted from the inertia of area 1 to find the inertia of the unique cross sectional area. The process can be seen below.

$$\begin{aligned}
 I_{stop} &= I_1 - I_2 \\
 I_1 &= \frac{1}{3}bh^3 = 4.99 * 10^{-9} m^4 \\
 I_2 &= \frac{\pi}{4}r^4 = 6.36 * 10^{-11} m^4 \\
 I_{stop} &= 4.929 * 10^{-9} m^4
 \end{aligned}$$

After calculating the inertia of the cross sectional area, the bending stress on the physical panel stop was calculated. The equation to find the bending stress is shown below.

$$\sigma_{bending} = \frac{M_{state3} c}{I_{stop}} ; c = 3.75 \text{ mm}$$

This bending stress moment was then compared to the yield stress of ABS plastic, 40 MPa. The bending stress on the physical panel stop due to the different spring options is tabulated in Table 16. These moments are from the moment of the space grade panel at state 3 of deployment. That moment is then used in the equation above as input to find bending stress.

Table 16: Bending Stress on the Physical Panel Stop due to Space Grade Panel

Spring	State 3	Bending Stress on Stop
McMaster 9271K88	$M = 7.5 \text{ Nm}$	$\sigma_{bending} = 5.76 \text{ MPa}$
McMaster 9271K603	$M = 20 \text{ Nm}$	$\sigma_{bending} = 15.4 \text{ MPa}$
McMaster 9271K98	$M = 15 \text{ Nm}$	$\sigma_{bending} = 11.1 \text{ MPa}$
McMaster 9271K94	$M = 12 \text{ Nm}$	$\sigma_{bending} = 9.44 \text{ MPa}$

The same calculations were done for the prototype panel attachment. The results of that analysis can be seen in Table 17.

Table 17: Physical Stop Bending Stress due to Impact of Prototype Panel Attachment

Spring	State 3	Bending Stress on Stop
McMaster 9271K88	$M = 0.75 \text{ Nm}$	$\sigma_{bending} = 0.38 \text{ MPa}$
McMaster 9271K603	$M = 2 \text{ Nm}$	$\sigma_{bending} = 1.0 \text{ MPa}$
McMaster 9271K98	$M = 1.4 \text{ Nm}$	$\sigma_{bending} = 0.73 \text{ MPa}$
McMaster 9271K94	$M = 1.2 \text{ Nm}$	$\sigma_{bending} = 0.62 \text{ MPa}$

The results showed that the springs did not cause the physical panels top to fail due to bending when the panel attachment impacted the panel stop.

The use of springs resulted in the need for a pin to hold the spring in place in order to generate torque when the panel was in the stowed position. In order to do so, the torque of the spring in the stowed position was used to calculate the force applied to the pin. Figure 44 shows the force on the pin, the free body diagram of the pin, and the tear out distance of the pin.

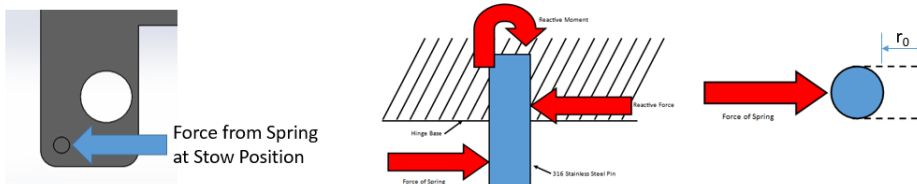


Figure 44: Force from Spring (left), Free Body Diagram of Pin (center), Tear out Distance (right)

The pin is made of 316 stainless steel with a yield stress of 290 MPa. The force from the spring was calculated by taking the torque at the stowed position of the spring and multiplying it by the distance on the spring leg that the pin was located, 2 mm. This resulted in the tangential force on the pin. This force was used to calculate the bending stress, shear stress on the pin, and the tear out distance of the pin. The process for which the calculations were carried out is shown below.

$$\begin{aligned}\sigma_{yield} &= 290 \text{ MPa} \\ \sigma_{ABS\ yield} &= 40 \text{ MPa} \\ F_{spring} &= \tau_{stow} * 2 \text{ mm} \\ \sigma_{pin\ bending} &= \frac{F_{spring} * L_{force}}{I_{pin}} \\ \sigma_{shear} &= \frac{F_{spring}}{A_{pin}}\end{aligned}$$

$$\sigma_{ABS\ Yield} = \frac{F_{spring}}{4(t(r_o - r_i))}$$

r_o = tear out distance, r_i = pin radius

After calculating the shear and bending stresses, the bending stress was much higher. The bending stress is the limiting factor to what spring to use. The results of the analysis are shown in Table 18.

Table 18: Bending Stress and Tear out Distance of Springs on the Spring Stop Pin

Spring	Stow Torque	Bending Stress on Pin	Tear Out Distance
McMaster 9271K88	0.0169 N-m	$\sigma_{bending} = 19.8 MPa$	0.55 mm
McMaster 9271K603	0.121 N-m	$\sigma_{bending} = 275 MPa$	0.88 mm
McMaster 9271K98	0.0624 N-m	$\sigma_{bending} = 114 MPa$	0.70 mm
McMaster 9271K94	0.0454 N-m	$\sigma_{bending} = 73.8 MPa$	0.64 mm

None of the pins would fail due to the force from the spring. However, the 9271K603 spring creates a bending stress that is very close to the yield stress.

After the failure analysis at each of the points, the springs were selected on the following criteria:

1. The springs must fit within a physical constraint between the panel and the hinge shaft.
2. The spring must not cause failure in the panel, panel stop, or the spring pin.
3. Fastest deployment time.

The evaluation of the springs is shown in Table 19.

Table 19: Spring Evaluation

Characteristics	Requirement	McMaster 9271K88	McMaster 9271K603	McMaster 9271K98	McMaster 9271K94
<i>Inner Diameter (mm)</i>	>3.175	3.56	4.75	3.56	3.56
<i>Outer Diameter (mm)</i>	<7.1	5.49	7.72	6.33	5.69
<i>Torque Rating (in-lbs/deg)</i>	-	0.00083	0.00594	0.00307	0.00223
<i>Stow Torque (N-m)</i>	-	0.0169	0.121	0.0624	0.0454
<i>Deployment Time (s)</i>	Lowest	5.01	1.87	2.61	3.06
<i>Bending Moment on Panel (N-m)</i>	<157.5	7.56	20.25	14.55	12.40
<i>Stress on Physical Stop (MPa)</i>	<40	3.83	10.26	7.38	6.29
<i>Stress on Spring Stop Pin (MPa)</i>	<290	19.8	275	114	73.8

From the evaluation matrix, the 9271K98 spring was able to fit within the required dimensions, and not cause failure in the panel, panel stop, or the spring pin, and deploy the fastest. 9271K603 was eliminated because it would be fit between the hinge shaft and the panel.

After spring selection, finite element analysis was performed on the hinge assembly. The constraints on the simulation are shown in figure 45.

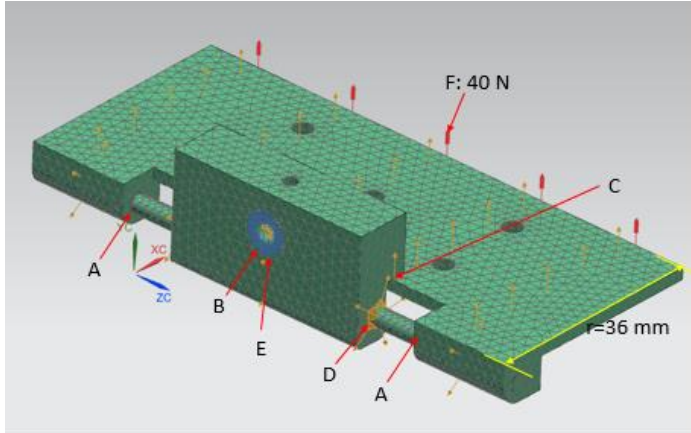


Figure 45: FEA Constraints on Hinge Assembly

The constraints on the hinge assembly are tabulated in Table 20 with the constraint corresponding to the letter in Figure 45.

Table 20: Constraints Applied to Hinge

Letter	Parts Involved	Constraint
A	Hinge Shaft and Panel Attachment	Surface to Surface Gluing
B	Hollow Shaft and Physical Stop	Surface to Surface Gluing
C	Panel Attachment and Physical Stop	Surface to Surface Gluing
D	Hinge Shaft and Physical Stop	Surface to Surface Contact
E	Hollow Shaft Face	Fixed

The force is applied to the end of the panel attachment in the Y direction to create the moment that the panel experiences at state 3 of deployment. The results of the finite element analysis are shown in Figure 46.

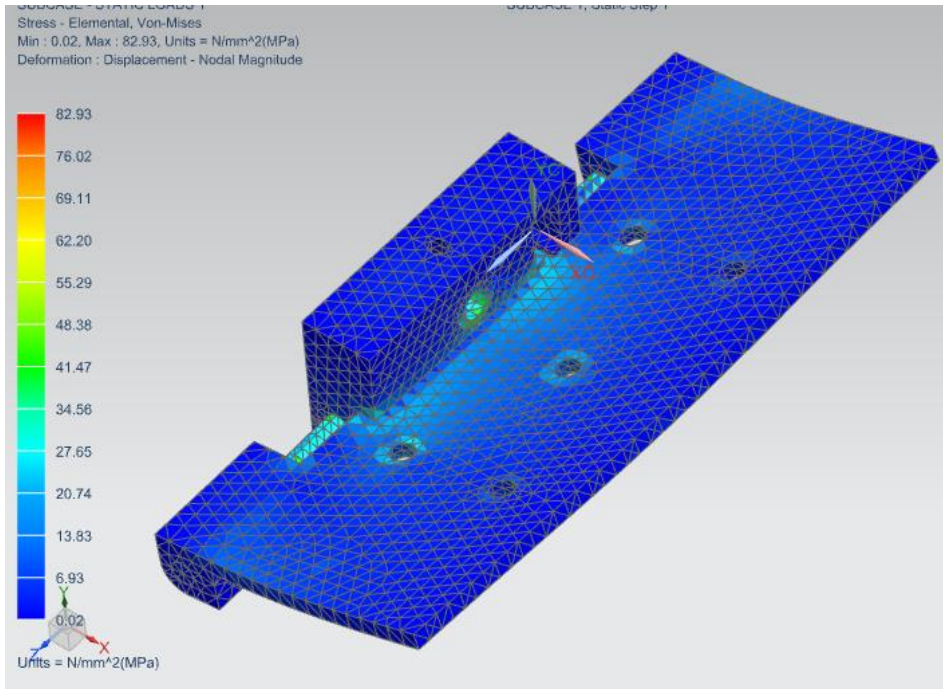


Figure 46: FEA of Panel Mechanism Results

The results of the finite element analysis are tabulated in Table 21. They show that the panel will not fail at impact. The prototype component list and space grade equivalent are shown in Table 22.

Table 21: FEA Results

Component	Material	Yield Stress	Max stress experienced
Physical Stop	ABS	40 MPa	35 MPa
Panel Attachment	ABS	40 MPa	25 MPa
Hinge Shaft	6061 Aluminum	276 MPa	63 MPa
Hollow Shaft	Stainless Steel	215 MPa	83 MPa

Table 22: Hinge Mechanism Components for Prototype and Space Grade

Component	Prototype	Space Grade Options
Stopping/Locking Mechanism	Physical Panel Stop	Physical Panel Stop or Detent Pin
Action	Springs	Springs
Panel	Prototype Panel (ABS)	Based on mission
Hinge Mechanism	ABS Plastic	6061 Aluminum
Hinge Shaft	6061 Aluminum	6061 Aluminum
Spring Stop Pin	316 Stainless	316 Stainless

The materials used for the prototype can be used for the space grade design. The only difference would be the use of ABS plastics. The physical panels top would be machined out of 6061 aluminums. The panel attachment would be replaced with space grade solar panels that are selected for that mission. For the space grade stopping/locking mechanism the use of a detent is an option to create a redundant system.

7.3 Motor/Gearhead

With a stepper motor chosen to be the best option to fulfill the requirements of this subsystem, the team proceeded to develop a mathematical model for stepper motors which could be ultimately used in the product selection process. In order to perform the analysis, the current and torque of the motor were approximated as a first order transient response.

With this analysis complete, the team proceeded to implement this model and ultimately use it to select a motor/gearhead combination for the prototype and space grade designs. Motors and gearheads from many manufacturers and distributors were benchmarked. Faulhaber motors (distributed by Micromo) were the only motors that had a small enough diameter to fit within the dimensions of the base of the SADA. Thus they became the only motors that went through the selection criteria depicted in Table 23. Micromo provided 20 different motor/gearhead combinations to be analyzed. First, it was checked whether the combination would fit the size requirement (diameter less than 2 cm) and be able to fit in the SADA. The next criteria involved the use of the model in Appendix F. With the use motor parameters (including mechanical time constant) within the model, the given motor holding torque was compared to the required maximum torque that the motor would feel. Third, it was checked whether a given gearhead could handle the continuous torque that it would output. This left seven combinations that could work within the team's design.

Table 23: Selection Process for Motor/Gearhead Combinations

Selection Criteria	Combinations Remaining
All Motor-Gearhead Combinations	20
1. Diameter (<2cm)	16
2. Holding Torque Requirement (Motor)	15
3. Maximum Continuous Torque Requirement (Gearhead)	7
4. Lowest Mass and Lowest Backlash Combinations (1 of each)	2

The major tradeoff with regard to this subsystem was mass vs. backlash in the system. As the team sought to minimize both of these characteristics, the remaining combination with the lowest mass was compared with that of the lowest backlash. The specifications for each of these combinations can be seen in Table 24. Both combinations featured the AM1524 Stepper Motor. The 15A planetary gearhead with sleeve bearings was chosen as the gearhead to be used in the prototype. This is due to it having lower cost, gear ratio, and mass due to it being made of plastic. The 15A also had a higher factor of safety in regards to the maximum continuous torque requirement. The only drawback of using this combination is that fact that it would introduce about 4 degrees of backlash into the system. This backlash could be mitigated by the use of a shaft position tracking device, such as an encoder, and will be discussed in the control subsystem section.

Table 24: Final Selection of Prototype Gearhead

Micromo AM1524 motor [9]	15A planetary gearhead w/sleeve bearings [10]	15/8 Zero-Backlash Spur Gearhead w/ ball bearings [11]
Total price	\$162	\$289.10
Mass of gearhead and motor	18 grams	38 grams
Max. expected backlash-no load	4 degrees	~0 degrees
Max. output shaft load: radial	0.5 N	6.0 N
Max. output shaft play: radial	15 μ m	12 μ m
Max. continuous torque for 100 hours	200 mN-m	100 mN-m
Gear ratio	249 / 1	485 / 1
Total score	3	-3

With the prototype motor/gearhead combination selected, the team sought to find a space-grade equivalent. The AM1524 motor is already vacuum ready, but the 15A gearhead is made of plastic and not self-lubricated and thus could not go into space. The 15/10 gearhead was selected due to it comprising of a housing of stainless steel and a Geartrain of steel gears. The specifications for both the prototype and space grade gearheads can be seen below in Table 25. Although the 15/10 gearhead is heavier, it shows a superior maximum continuous torque factor of safety as well as lower backlash, gear ratio, and shaft play.

Table 25: Prototype and Space Grade Gearhead Specifications

Micromo AM1524 Motor	15A Planetary Gearhead w/ sleeve bearings	15/10 Planetary Gearhead w/ sleeve bearings
Housing/Geartrain Material	Plastic/Plastic	Stainless-steel/steel
Mass of gearhead and motor	18 g	39 g
Max. expected backlash- no load	4 degrees	1.5 degrees
Max. output shaft load: radial	0.5 N	5 N
Max. output shaft play: radial	15 μm	5 μm
Max. Continuous Torque for 100 hours	200 mN-m	350 mN-m
Minimum Gear Ratio Available	249/1	123/1
Total Price	\$162	\$410.80

7.4 Transmission System

For the transmission system the minimum diameter of the shafts was calculated based on the torque of the motor and the resulting forces it generates. These calculations were performed after the decision on the layout of the transmission system was made, specifically the coplanar design with capsule style slip rings. Figure 47 depicts the forces acting on the primary shaft and Figure 48 depicts the forces acting on the secondary shaft. In both figures the y-axis runs along the shaft. In both images red force arrows are indicative of reaction forces on the bearings and blue force arrows are indicative of forces caused by the interaction of the gears. Yellow lines are representative of the pitch diameter of the gears used; the point of meshing for the gears is where the forces will be acting.

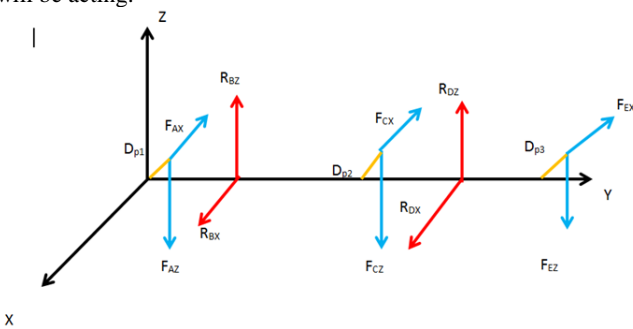


Figure 47: Forces Acting on Primary Shaft

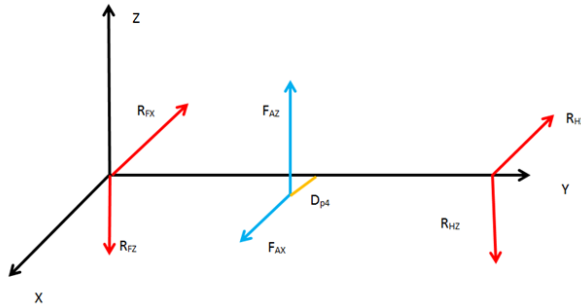


Figure 48: Forces Acting on Secondary Shaft

All gears used would be spur gears, and as a result both a radial and tangential force will be created when these gears interact. The first equation listed below is to determine the tangential force and the second equation listed below is to determine the radial force. These values along with material properties such as, the ultimate strength of the material are used in the third equation listed below to determine the minimum shaft diameter that will survive the forces. It is important to note that this equation is a simplified version of the equation to calculate the diameter at any point on a shaft. The assumptions for this equation are steady torque and reversed bending. Also the shaft must have a solid circular cross section and be made of a ductile material. These assumptions were applicable in this case. This calculation was performed at the locations of each gear on each shaft.

$$F_{zs} = \frac{T}{\left(\frac{D_p}{2}\right)}$$

$$F_{xs} = F_{zs} \tan(\varphi)$$

$$d = \left(\frac{16}{\pi} \left\{ 2K_{fb}(n_d) \frac{M_a}{S_N} + \sqrt{3} \frac{T_m}{S_u} \right\} \right)^{1/3}$$

An excel spreadsheet was used to perform this calculation multiple times so that the effect of varying shaft material as well as gear size can be seen. The specific shaft materials studied were 17-4 PH Stainless Steel, Aluminum alloys 6061 and 7075, and Stainless Steel alloys 303 and 304. The spread sheet giving the inputs, resulting forces, and diameters can be seen in tables 42 through 47 in Appendix H. The diameter values that resulted from this analysis were small, ranging from 0.04 to 0.006 inches. These values are much smaller than standard shaft or bar stock sizes. As a result, the shaft diameter or needed material was not limiting factor in shaft selection.

Table 26: Material Properties Needed for Shaft Diameter Calculation

Material	17-4 PH Stainless Steel	Al 6061	Al 7075	SST 303	SST 304
S _u (ksi)	200	45	83	90	75
S _f (ksi)	120	10.32	18	34	33
S _f (ksi)	61.236	5.27	9.19	17.35	16.84
k _{fb}	1.07	1.05	1.05	1.05	1.05
G (ksi)	11000	3770	3900	11200	12500
Density (lb/ft ³)	0.281	0.097	0.102	0.289	0.289

The final selection of shaft material was Aluminum 6061. This material had the lowest density as can be seen in table 26, as well as other properties needed for the calculation. The values of minimum shaft diameter calculated for this material were smaller than standard sizes available. As a result, the smallest standard size, 1/8th inch, was chosen for the primary shaft. This will be applicable for both the prototype and space grade designs. This same alloy is intended to be used for the secondary shaft as well. Due to material availability, a steel shaft was used for the prototype. As can be seen from the analysis, by choosing steel the secondary shaft is overdesigned and capable of supporting loads much greater than it will actually experience.

The same force analysis and excel spread sheet was used to determine the reaction forces experienced on the bearings of both shafts. Once again this is detailed in Appendix H. These calculated forces were then used to determine the dynamic load rating required. Equation x is the calculation for the dynamic load rating. In this equation P_e is representative of the dynamic equivalent load. Because spur gears are being used, all loads applied are radial. A depiction of this can be seen in Figure 49. The dynamic equivalent load would then be equivalent to the applied radial load. This calculation was done for every calculated reaction and completed in an excel spreadsheet. These are detailed in Appendix I. The calculated value was then compared with dynamic load ratings of commercially available bearings.

$$[C_d(R)]_{rec} = \left[\frac{L_d}{K_R(10^6)} \right]^{\frac{1}{\alpha}} (IF)P_e$$

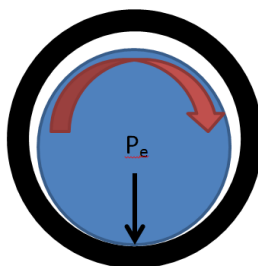


Figure 49: Depiction of Bearing Loading

As can be seen in the spread sheet the calculated dynamic load ratings were much lower than ratings for typical commercially available bearings. It was decided to take advantage of this and use Teflon (PTFE) for the bearing material. This has the additional advantage of having a very low

coefficient of friction, so the bearings are able to run without lubricant. This is also needed for the space grade design because lubricant can outgas in space.

7.5 Control System Analysis

7.5.1 Sensor Analysis

For the solar panel mounting, the IR phototransistors were mounted according to Figure 50. A full schematic of the design is shown in Appendix K.

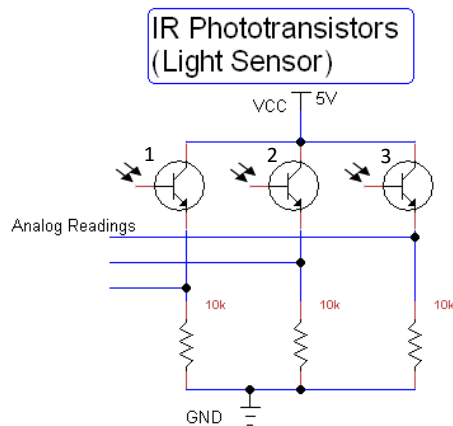


Figure 50: Light Sensor Schematic

With this design, the three analog readings could be put through an analog/digital converter and return a value between 0 and 1023, with 1023 being saturation at maximum brightness. This design was tested on a mock-setup with visible light phototransistors, but the ambient light of the room was creating interference, with readings up to 300 out of 1023 in the absence of an intended light source. To reduce the effects of interference, a phototransistor with a visible light block was used, in conjunction with a light source outside the visible light spectrum. The LTR-4206E, shown in Figure 51, was selected as the prototype sensor.



Figure 51: LTR-4206E

To ensure that the LTR-4206E could be used as depicted in Figure 35, the normalized angular sensitivity, shown in Figure 52, was taken off of the datasheet and plotted in MATLAB.

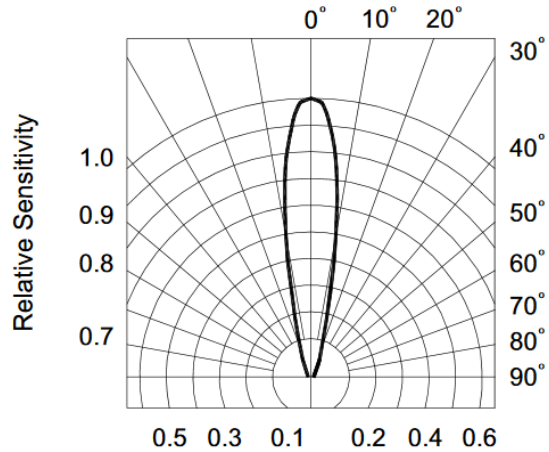


Figure 52: LTR-4206E Sensitivity Response [16]

With the prototype algorithm, panels will stop rotating when sensor 2 (in green) reads a higher value than the side sensors. It was found that, for 10° accuracy, a 20° offset was needed, due to the symmetry of the response. The three sensors were plotted at a 20° offset, shown in Figure 53.

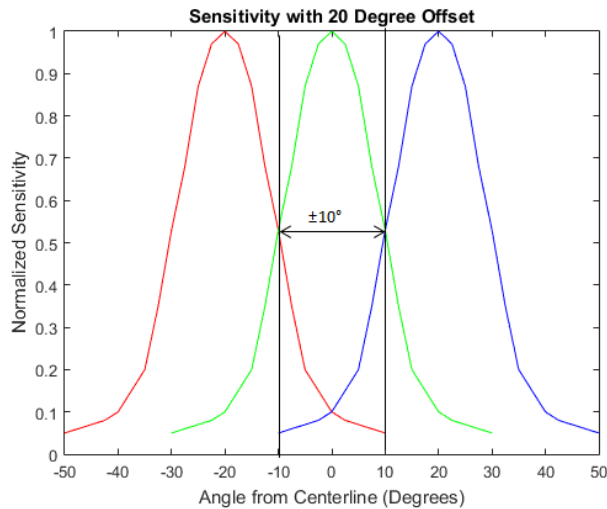


Figure 53: Sensitivity Plotted with 20° Offset

With a 20° offset, a 10°-degree error occurred when the normalized sensitivities of two sensors equaled 0.5. Offset was reduced until the sensitivities equaled 0.7, at a 15° offset, as

shown in Figure 54. This was done to accommodate for any errors present within the tracking mechanism, while still providing an appropriate field of vision.

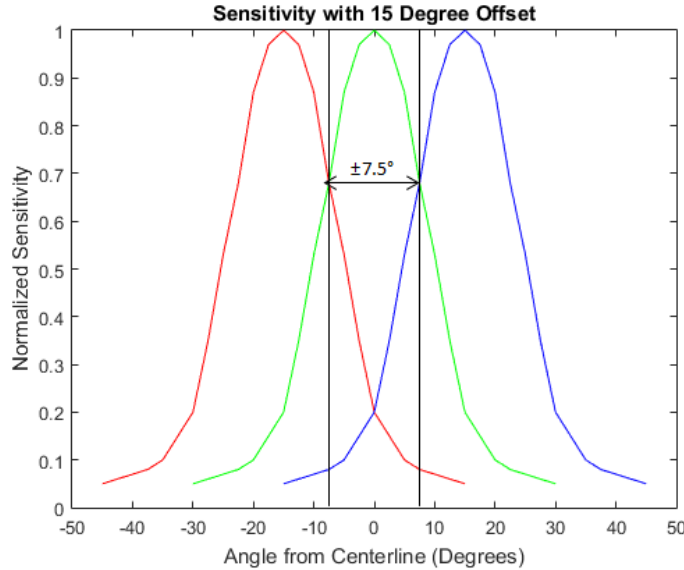


Figure 54: Sensitivity Plotted with 15° Offset

7.5.2 Control Algorithm Development

7.5.2.1 Background

The SADA module requires a control algorithm to perform the functionalities described by the system. The main functionalities of the SADA include solar panel deployment, sunlight sensing and tracking, and motor driving for solar panel rotation.

Any components selected must perform and cover all of the functionalities listed above. In addition, two control system designs are needed—one for a SADA prototype and one for a space grade design. The team developed an algorithm for prototype functioning that can be incorporated into an expanded space grade algorithm.

7.5.2.2 Assumptions and Corner Cases

Initial assumptions about the SADA include the fact that it is active and running and has received the signal from CubeSat control to deploy the solar panels, and are sending data back to the rest of the CubeSat. Power would be supplied to the SADA as the solar panels get oriented and begin generating power to sustain the SADA itself.

The control algorithm for the SADA operation shall:

- Perform mechanical checks
- Be prepared and account for sensor failures

- Provide a control scenario for when the SADA is in complete shade (behind the Earth, in its shadow)
- Allow for manual user takeover when necessary

7.5.2.3 Control Type Selection

Once the CubeSat has been deployed from the primary payload, there will be no external command aside from the CubeSat main control. Thus, the algorithm must operate autonomously from mission control, with minimal user input. This mitigates communication delays associated with other dependent control types. A Pugh matrix of basic control types was constructed, as shown below:

Table 27: Control Selection Pugh Matrix

Selection Criteria	Control Types		
	Open Loop	Closed Loop	Best case PID (proportional-integral-derivative)
Simplicity	+1	-1	0
Accuracy	-1	+1	+1
Stability	0	-1	+1
Feedback	-1	+1	+1
Error Correction/Adaptability	-1	+1	+1
Load on Motor	-1	0	0
Total	-3	+1	+4

The contents of the matrix above can be summarized as follows:

- Open Loop
 - Can use stepper motors.
 - Load on motors may vary, motor may not maintain goal speed.
- Closed Loop
 - It is possible to use relatively inaccurate and inexpensive components to obtain the accurate control of a given process or plant.
 - System stability may be a major problem, especially in badly designed systems.
- PID
 - There are 7 different combinations of PID control systems (combinations are formed of proportional, integral, and derivative algorithms). The +1 scores are assuming that the best case configuration is used.

According to the table above, a PID control type was the best option to move forward with. The team ultimately decided to use a combination of both open and closed loop systems,

as the algorithm needed to be simple for the prototype demonstration, but provide feedback for the more advanced control functions relating to scenarios occurring with in-flight operation. To incorporate this with the design chosen, the team used absolute (zero) encoders to record location. While stepper motors have good estimate for position, the encoder provides a level of redundancy to determine the position of the panel and light sensors. The position of the panel in rotation is crucial to calculations that the SADA control will need to carry out when responding to the case in which the SADA is in the Earth's shadow and is unable to receive any sunlight.

7.5.2.4 CubeSat in Earth's Shadow

A prominent corner case occurs when the SADA is deployed in the Earth's shadow. When the CubeSat rotates around the Earth, it has the possibility of entering Earth's shadow. At this time, the satellite would not be able to detect the sun using light intensity sensors found on most solar panels [1]. Only through more complex means of detection can the sun be detected. Assuming the CubeSat computer knows its position about the Earth, the SADA can ask the main computer for information. However, if this assumption is wrong, the SADA should have a way to know how to orient the panels. The largest concern is if the CubeSat is first launched from the deployer into the Earth's shadow, as the intensity sensors will have no sun source to immediately calibrate to.

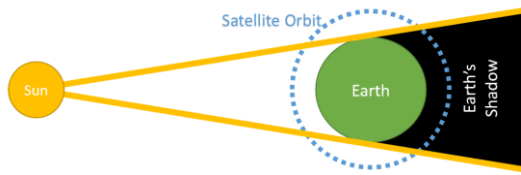


Figure 55: Satellite Rotating Around Earth

7.5.2.5 Control Response

Initial steps which would need to be taken include the following:

- 1) Ask the central CubeSat computer for direction and position and compute the angle that the solar panels will need to be at when the satellite leaves Earth's shadow
- 2) Ask the central computer for altitude (which will provide the speed of the satellite)
 - a. Perform a complete rotation every few minutes
 - i. Avoid continuous spinning as this wastes energy and the CubeSat can be in shade for >30 minutes
 - b. Rotate so often that the expected probability output is at a maximum
 - i. $E = \text{Probability of Sun} * \text{Power} - \text{Probability of Shadow} * \text{Power}$ for 1 rotation
- 3) Perform a rotation every few minutes using the worst case scenario for the time spent in the shadow to compute the probability of seeing the sun during the rotation

After the CubeSat has established its orbit in the shadow after completing a full rotation, control should:

- 1) Keep track of a few readings to find a pattern used to estimate direction desired when leaving the shadow.

7.5.2.6 Calculations

Formulas Used

Table 28: Constants Used

Symbol	Description	Value	Units
G	Gravitational Constant	6.67408×10^{-11}	$\text{m}^3 \text{ kg}^{-1} \text{ s}^{-2}$
r_e	Radius of Earth	6.371×10^6	m
d_s	Distance to the Sun	149.6×10^9	rad/s
m_e	Mass of Earth	5.972×10^{24}	kg

Table 29: Variables

r	Orbit radius of satellite	rad
T	Orbit period of satellite	rad

An important metric needed in order to find the maximum amount of time that the CubeSat would be in Earth's shadow is determined by using the time it takes the satellite to revolve around the Earth and the relative amount of time spent in the Earth's shadow.

The following assumptions are made in these calculations. Both assumptions overestimate the time spent in the Earth's shadow.

- 1) The light source acts like a point in space with negligible radius.
- 2) The satellite follows a Nadir orbit (shown below)

The time required for the satellite to complete one full revolution about the earth is given by the equation [17]:

$$T = 2 * \pi * \sqrt{\left(\frac{(r_e + r)^3}{G * m_e} \right)}$$

The angle spent in the Earth's shadow is equivalent to $2 * \theta_3$ based upon the following figure.

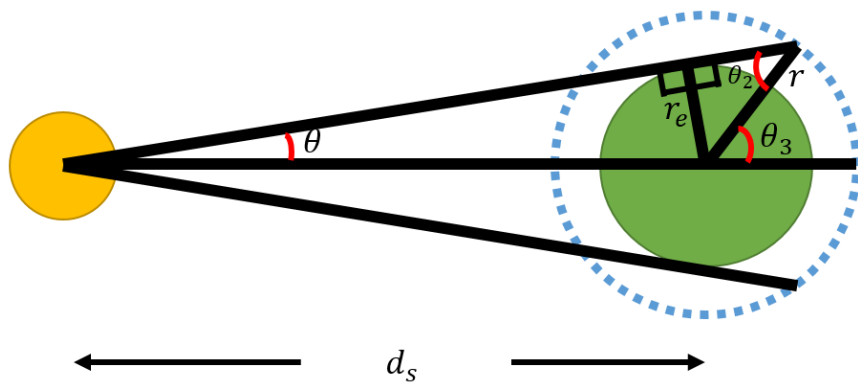


Figure 56: Sun and Earth Geometries

The angle θ_3 is equivalent to $\theta + \theta_2$. The first angle (θ) is calculated using the distance the Earth and the Earth's radius. The second angle uses the Earth's radius and the radius of the orbit.

$$\theta = \sin^{-1}\left(\frac{r_e}{d_s}\right) \quad \theta = \sin^{-1}\left(\frac{r_e}{r_e + r}\right)$$

Since the period calculated is for 360° , the ratio of the time spent in the shadow to the total orbit is given by $\theta/360^\circ$. The time spent in the shadow is given by

$$\text{Time in Shadow} = \frac{T * \theta}{360^\circ}$$

The two graphs below plot the orbit times and the time spent in the shadow for a range of orbit radii from Low Earth Orbit (200km) to Geosynchronous Orbit (36,000km).

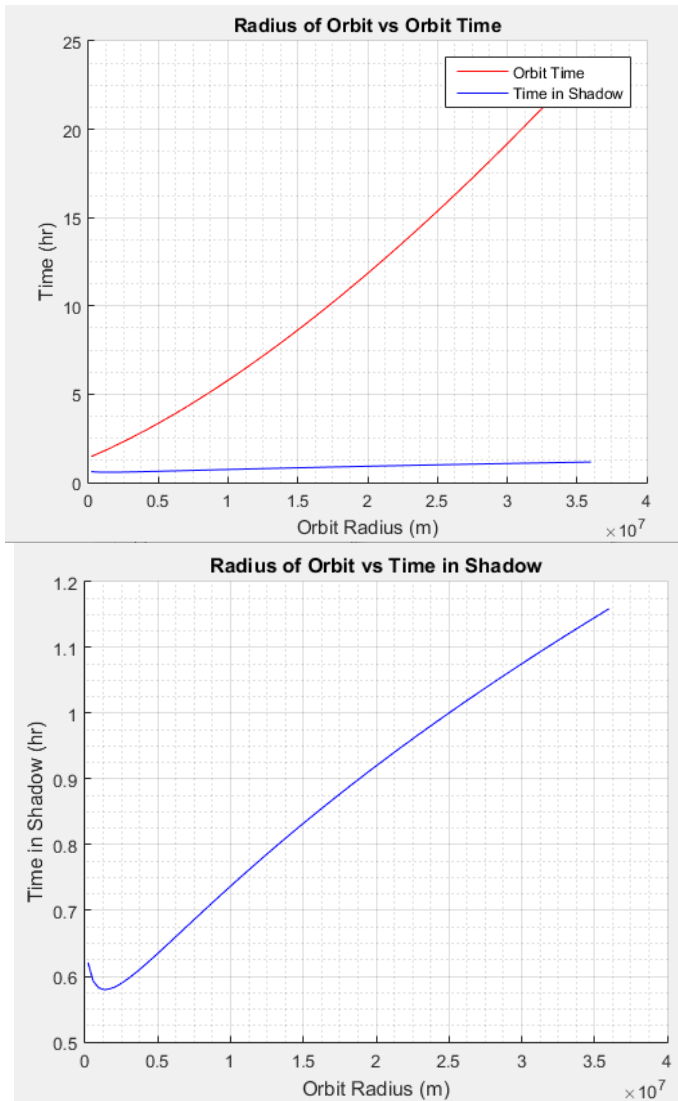


Figure 57: Shadow Time Output Graphs

7.5.2.7 Logic State Diagram

Aside from the mathematical logistics of the algorithm, the following diagram illustrates the flow of logic states and decisions that the control system must go through in order for the SADA to carry out all of its functions. An expanded and detailed flowchart of this state diagram can be found in Appendix N.

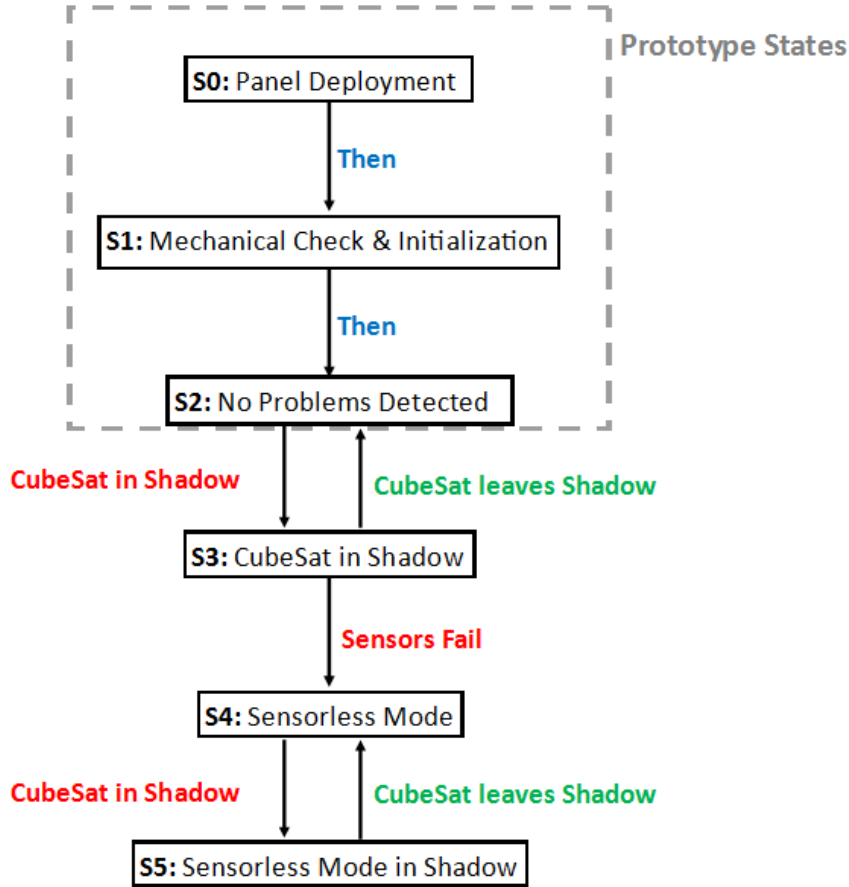


Figure 58: State Diagram Summary

7.5.3 State Diagram Walkthrough

Prototype states include the following:

S0) Panel Deployment

- The CubeSat and SADA have been ejected from the primary payload.
- The CubeSat control signal deploys solar panels.
- After indication of successful completion of this state, the algorithm moves on to State 1.

S1) Mechanical Check & Initialization

- If panels have not deployed successfully, mission control is notified and the motor and transmission are manually “wiggled.”
- If panels have successfully deployed, an initial 360° mechanical rotation check is carried out to find the position of the panels when a light source is detected.
- After successful completion of this state, the algorithm moves on to State 2.

S2) No Problems Detected

- For the prototype demonstration, this is the final state, as the demonstration is taking place with a reliable infrared diode source emitter, ensuring that the SADA is always sensing light.

For the Space Grade algorithm, the next state occurs if the CubeSat is in the Earth’s shadow (indicated by the absence of power being output by the solar panels) and the rotation has paused for the specified orbit pause time:

S3) CubeSat in Shadow

- Solar panels are rotated at orbit speed.
- Algorithm waits predicted time, and then a second sensor check is performed.
- If the CubeSat leaves the shadow, the algorithm returns to State 2.
- If it is determined that the CubeSat is in the shadow but the sensors have failed as well, the algorithm moves on to State 4.

S4) Sensorless Mode

- Panels are rotated until a maximum is found.
- If the panels are outputting power close to the maximum, panels continue rotating at orbit speed.
- If the panels are not outputting power close to the maximum, it is confirmed that the sensors have failed, the algorithm moves on to State 5.

S5) Sensorless Mode in Shadow

- Panels are rotated at orbit speed and control then waits the predicted time.
- If panels are outputting power close to the maximum, panels continue rotating at orbit speed and continue operation with the CubeSat operating out of the shadow without sensors, returning to state 4.
- If the CubeSat remains sensorless and in the shadow, SADA loops back through State 4 and comes back to State 5.

8. Final Design and Engineering Specifications

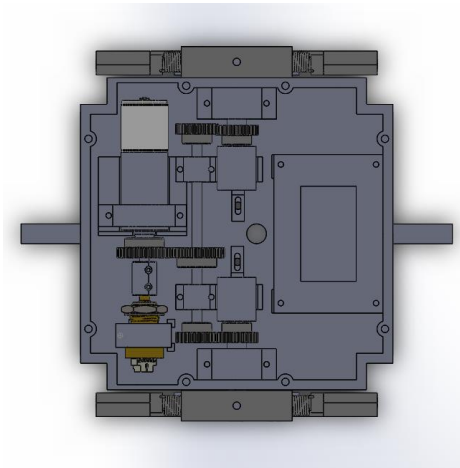


Figure 59: Final CAD Assembly of SADA Prototype

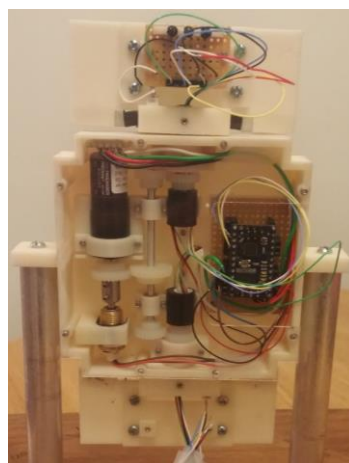


Figure 60: Final Assembly of SADA Prototype

Figure 59 and Figure 60 show the final design for the prototype. The space-grade design is similar to the prototype, excluding the attachment shafts on the sides.

The chassis and brackets used to hold components in place within the SADA are 3D printed ABS plastic. The cover for the prototype is acrylic. Acrylic was chosen because it allows the microcontroller, motor-gearhead, and transmission system inside the SADA to be seen, and

this facilitates prototype presentation and demonstration. The brackets are attached with 0-80 screws and threaded inserts are used within the SADA due to the softness of ABS plastic. Channels and grooves were printed inside the SADA chassis, which are meant to hold the motor-gearhead and transmission system in place, as shown in Figure 61.

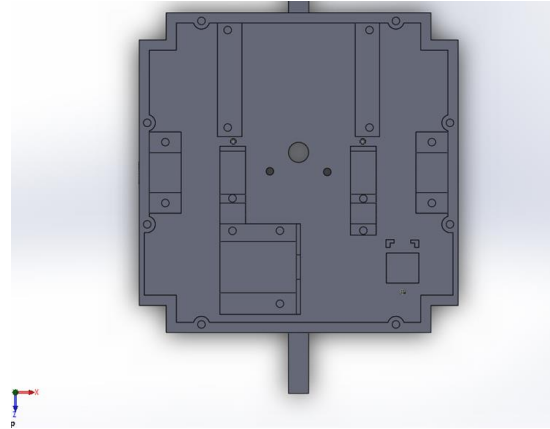


Figure 61: Interior SADA Chassis

The space-grade design will have these grooves and channels as well to hold the space-rated motor-gearhead and transmission system components. The space-grade design will be composed of Aluminum, and will not require threaded inserts for the bracket screws.

The prototype transmission system consists of nylon spur gears, a main drive shaft that runs the length of the SADA, and secondary shafts connected to the panels. The transmission system is based on the single coplanar configuration shown in Section 6.3, and does not require use of the tuna can. The spur gears are connected to the motor-gearhead, main drive shaft and secondary panel shafts, and they allow the motor to rotate the panels. The gearhead on the motor provides the necessary gear ratio for the motor to both output enough torque to rotate the panels and to reduce the motor output speed to meet GEO and LEO speed requirements. The connecting spur gears are not meant to perform either function, and they have an approximately 1:1 gear ratio. The space-grade design follows these parameters as well and utilizes components of identical geometric dimensions. Table 3 lists these differences in components.

Table 30: Transmission Component Material List for Prototype and Space-Grade Designs

Primary Shaft		Secondary Shaft		Gears		Bearings	
<i>Prototype</i>	<i>Space Grade</i>	<i>Prototype</i>	<i>Space Grade</i>	<i>Prototype</i>	<i>Space Grade</i>	<i>Prototype</i>	<i>Space Grade</i>
6061 Aluminum	6061 Aluminum	Steel	6061 Aluminum	Nylon	Bulk Metallic Glass	PTFE/Rulon J	PTFE

The control algorithm implemented in the prototype is meant for prototype demonstration of the sun/light tracking. It is meant to be a proof-of-concept for SADA sun tracking and allows for further iterations, in keeping with TRL 3. As such, there is no space-grade equivalent.

The prototype hinge deployment mechanism effectively demonstrates the functionality of the space-grade equivalent. The prototype hinge deployment mechanism includes the torsional springs and mechanical stop to allow for deployment visualization. The prototype mechanism lacks the burn wire included in the space-grade equivalent that stows and locks in the panels for 30 minutes after CubeSat deployment from the NanoRacks deployer. Lastly, the panels used in the final prototype do not have the required panel geometric dimensions or 3 kg total mass specification; the panels hold the IR light sensors for the sun/light tracking demonstration and emulate panel deployment.

The motor-gearhead for the prototype fits within the SADA. Faulhaber/Micromo is among the only vendors that provide motor-gearheads that can fit within the $\frac{1}{4}$ " U SADA, and they provide space-grade motor-gearheads. The space-grade motor-gearhead has a comparatively smaller gear ratio. This necessitates that the motor outputs a larger torque and a lower speed than the prototype motor. However, the space-grade gearhead has a larger maximum continuous torque rating, so this larger torque is mechanically viable.

9. System Evaluation

9.1 Performance Requirements

The motor-gearhead system is capable of meeting the panel rotational speed specification, but the team will not be implementing an algorithm to demonstrate them. Table 31 and Figure 62 summarize the calculations for achieving the rotational speeds with the prototype motor-gearhead:

Table 31: Rotational Speed for Motor/Gearhead

Gear ratio [R]	249 :1				
Steps per revolution [S]	24 (unitless)				
LEO speed [LEO]	0.0024 rad/s				
GEO speed [GEO]	0.000036 rad/s				
Required steps-per-second value from motor (GEO)	Required seconds-per-step value from motor (GEO)	Required steps-per-second value from motor (LEO)	Required seconds-per-step value from motor (LEO)	Motor speed to meet GEO (RPM)	Motor speed to meet LEO (RPM)
0.034239958	29.20564344	2.282663856	0.438084652	0.085599895	5.70665964

Stepper motor step-rate to meet GEO and LEO speeds

$$LEO \text{ speed} = 0.0024 \frac{\text{rad}}{\text{sec}} * \frac{1 \text{ revolution}}{2 * \pi \text{ rad}} * R * S$$

- Same idea with GEO speed

Required Motor Speed to Meet LEO panel rotational speed

$$0.0024 \frac{\text{rad}}{\text{sec}} * S * \frac{1 \text{ revolution}}{2 * \pi \text{ rad}} * \frac{60 \text{ seconds}}{1 \text{ minute}} = 5.7067 \text{ RPM}$$

- Same idea for GEO speed

Figure 62: Prototype Motor-Gearhead Speed Specifications

The LEO speed can be met with this line of code for the B-328 microcontroller used in the prototype:

```
myStepper.setSpeed(5); //set stepper motor speed to 5 RPM
```

The GEO speed cannot be met with a stepper function such as the one above. To meet the GEO speed, these lines of code are used:

```
for(i=0;i=60;i++)
{
    if(i=58)          //after 29 seconds have passed
    {
        myStepper.step(1); //step once
        i=0;      //restart timer
    }
    delay(500);
}
```

This function will run 60 times, with a half a second delay in between each run. After the 57th implementation, the stepper motor will make one step. After the 57th implementation, 29 seconds have elapsed. 29 seconds per step from the motor averages out to the GEO speed for the panels due to the reduction ratio provided by the gearhead attached to the motor. While the team will not be demonstrating the panel rotational speeds with the prototype, the prototype is capable of achieving both the GEO and LEO speeds.

The prototype is capable of demonstrating the sun/light tracking for the panels. The panels will use IR light sensors to track an IR light source. Refer to Appendix B for more information.

9.2 Tolerance and Sensitivity

The panel sun/light tracking uses IR light sensing for demonstration. One of the main concerns with this implementation is that ambient IR light in the demonstration environment would interfere with the panel light tracking. Thankfully, system evaluation tests revealed that the IR

light source threshold far exceeds the ambient IR lighting in typical expected demonstration environments, which are indoor environments with fluorescent lighting. Thus, the panel light tracking is able to operate reliably in indoor environments with fluorescent lighting.

The requirements state that the prototype must achieve panel rotational accuracy within 10 degrees. The system evaluation system can only demonstrate that this specification is met through qualitative observation of the panel rotation during light tracking; the user must look at the panels and qualitatively judge that they are facing the light source.

9.3 Failure Analysis

With the final design laid out, simulated, and tested the team had been thorough by evaluating the system in many ways. However, no matter how robust a given design is, such a design will always have a probability of failure. The team sought to develop a methodology for assigning a number to this probability of failure in order to assess the risk factors of using such a design. Thus, a failure analysis framework was created in order to further prepare the design for implementation. This failure analysis method only looks at the potential for mechanical failure and a similar electrical analysis should be carried out before the design is put into production.

In terms of failure, the design of the SADA can be represented by a series-parallel system, with everything on the motor and primary shafts being in series and with the secondary shafts being parallel to one another. The deployment mechanism is also in series. If one of the panels does not deploy, the power requirement on the device will not be fulfilled. The full flowchart for this mechanical analysis can be seen below in Figure 63.

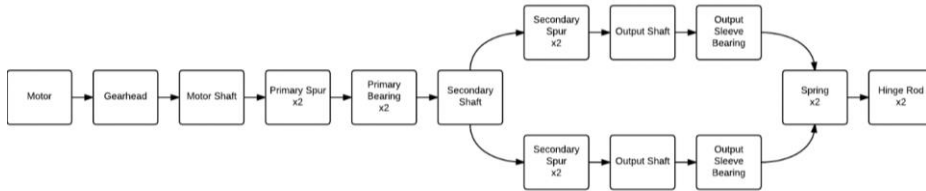


Figure 63: Mechanical Failure Analysis Flowchart

With the framework created through the use of a flowchart, the team sought to develop example reliability calculations for individual components of the system. The full calculations for the motor, motor shaft, primary gear, and primary bearings are carried out in Appendix G. The motor was the first of four components that were analyzed. During the team's correspondence with JPL a topic that needed to be addressed was whether a design with two motors would be a benefit and whether or not it should be considered. The hours to failure of the motor of the prototype motor was found by approximating its failure to be normally distributed about the MTBF (value provided by Micromo). After assuming a standard deviation and finding the amount of hours that the motor would actually be in use, the reliability of the motor was found to be 0.99994. Due to this extremely high reliability, the team concluded that that the additional weight added by the second motor would not be worth the slight added reliability and that a singular motor design was justified.

Example calculations were also performed for the shafts, gears, and bearings of the prototypes. For the shafts, a maximum shear stress calculation based on output holding torque was carried out. This produced a high prototype reliability of 1 due to the motor shaft being overdesigned as it is made of steel. This methodology could be used for the space grade design as

well because the shear forces would act in the same manner in a vacuum. The gears were evaluated with the use of the AGMA failure analysis approach that examined tooth bending stress when loaded cyclically. A reliability of 0.9999 was found for the primary shaft gears. This calculation would also hold true for the space grade design, but further calculations may be needed to examine other modes of failure for gears (especially wear). Finally, the bearings on the primary shaft were examined by calculating the wear depth that the bearings would have when under cyclical radial loading. Due to the low pressure and maximum velocity of the shaft on the bearings, a reliability of 1 was also found. This calculation would most likely not hold true in a vacuum. Tribology is a much more complicated phenomenon in space and the reliability of the bearings should be analyzed in the context of the vacuum by a more qualified mathematician.

9.4 Simulation Step Responses

The first step in motor simulations was to find the step response of the motor. This was done using MATLAB and Simulink/Simscape libraries. It required a controller, a model of the motor, and a model of the load. Basic measurements were also recorded at each stage. Further measurements were recorded in a more complex model of the system.

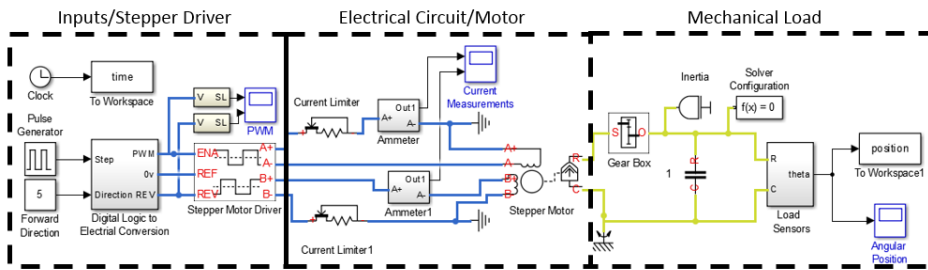


Figure 64: Stepper Motor Simulink Diagram

The diagram above simplifies the system to look at the electrical inputs and the position output. The system causes the stepper motor to move a single full step every time the voltage on the ENA pin of the Motor Driver changes from 0 to 5V.

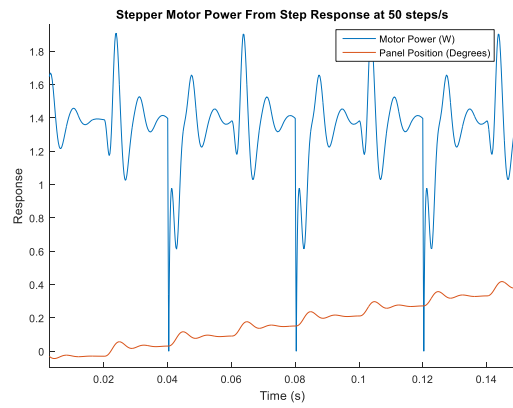


Figure 65: Stepper Motor Step Response

The simulation is able to plot the dynamic response of the stepper motor as shown above. The following data was extracted from the step response simulations:

- Max Speed = 630 step/s = 38 Degrees/s (after gear reduction)
- Maximum Position Overshoot = 0.03° (after gear reduction)
- Average Power While Rotating = 1.4W

9.4 Simulation Control Systems

Using the values from the step response tests, a simplified simulation reveals how the system would behave when on a satellite orbiting the sun. It simplifies the system in the following ways:

- Circular orbit. It is not an elliptical orbit
- Sun's rays are parallel [Insert citation]
- Satellite follows Nadir orbit

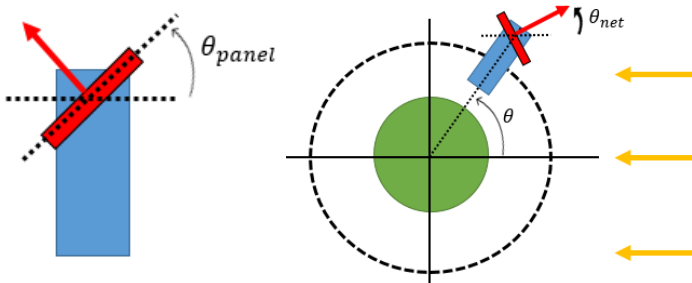


Figure 66: Control Simulation Parameters

A basic form of control chosen to test the power draw is outline as follows:

- Wait until sun is 1 degree off center

- Rotate the solar panel 2 degrees back (so it is 1 degree of center in other direction)
- If in shadow Earth's shadow,
 - Continue to pulse the motor at the same frequency and duty cycle that is currently being used

The source code for this simplified control system can be found in the Appendix J. An example of this control used for a satellite in LEO is found below:

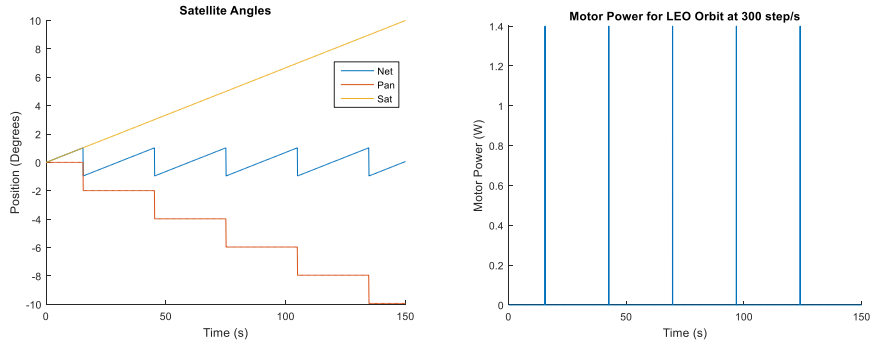


Figure 67: Control Simulation Output

In this system, each motor pulse is 0.2 seconds spaced apart by 30 seconds. This corresponds to a 0.6% duty cycle. Changing the angular accuracy of this algorithm does not affect the duty cycle, but varies the motor pulse width and the period.

These simulations are used to compute the motor power consumption in orbit. The motor will use 1.4W of power but is only on for 0.6% of the time for LEO orbit with motor speed of 300 step/s (panel speed of 18 degrees/s). This means that, on average, the motor consumes 8.4mW.

10. Significant Accomplishments and Open Issues

The SADA that the team built and designed is a functional and 1:1 scaled design for use in industry. One of the initial goals of achieving the desired pointing accuracy (10° for the prototype demo) was achieved and successfully demonstrated. Other design specifications, such as mass and size, were met, as the prototype SADA that the team built stayed within the $\frac{1}{4}$ U constraints while containing all required components.

Further development can be used for the hinge and deployment mechanism. As the project stands now, the panels are in the deployed state with the springs at equilibrium. In subsequent variations and improvements upon this project, the team should attempt to create a deployment mechanism (some options discussed in the initial stages included burn wires or shape-memory alloys (SMA)) to demonstrate panel deployment in real-time.

Another improvement which future teams may work on is accurately displaying the actual required rotation speeds for space grade operation (between $3.6E-5$ and $2.4E-3$ rad/s for GEO and LEO respectively, roughly corresponding to 1 day and 90 minute rotations). The current SADA demonstration shows the panel rotation at an accelerated speed for viewing and presentation purposes.

11. Conclusions and Recommendations

At the conclusion of this project, the team has successfully designed and built a Solar Array Drive Assembly (SADA) to track sunlight and maximize power generation to CubeSats, allowing the panels to rotate about one axis. Simulations and failure analyses have been carried out to ensure safe and reliable operation according to Technology Readiness Level 3, which includes a functioning prototype that operates mechanically and electrically according to solar panel rotational speed requirements and solar panel light tracking, as well as a complete paper design for a space grade equivalent. Commercial-off-the-shelf (COTS) components and concepts were selected for both the prototype and the space grade designs, as summarized in the Table 32 below.

Table 32: Prototype and Space Grade Comparison

	Prototype	Space Grade
Micromo AM124 Stepper Motor	15A Planetary Gearhead	15/10 Planetary Gearhead
Transmission Concept	Single Coplanar	Single Coplanar
Primary Shaft	6061 Al	6061 Al
Secondary Shaft	Steel	6061 Al
Gears	Nylon	Bulk Metallic Glass
Sleeve Bearings	PTFE/Rulon J	PTFE
Slip Ring	Adafruit (Prosper)	Electro-Miniatures or Cobham Aeroflex
Microcontroller/Motor Driver	Polulu B-328	International Rectifier RH Motor Control Module
Control Processor	**Same as microcontroller/motor driver**	On-Board CubeSat microcontroller (Pumpkin or Tyvak)
Encoder	US Digital Magnetic Shaft	**Not required for space grade design**
Light Sensors	LTR-4206E	**Not part of space grade design**
Hinge	Physical panel stop w/ hinge	Physical panel stop w/ hinge or Detent Pin

The designed SADA is compatible with CubeSats, and aligns with the goal of compact, cost-effective secondary payloads.

Bibliography

- [1] Clyde Space, "Some Useful Information about CubeSats," 2016. [Online]. Available: http://www.clyde-space.com/cubesat/som_useful_info_about_cubesats.
- [2] "GlobalCom," 2015. [Online]. Available: <http://www.globalcomsatphone.com/hughesnet/satellite/costs.html>. [Accessed 8 March 2016].
- [3] S. Antunes, "Makezine," 11 April 2014. [Online]. Available: <http://makezine.com/2014/04/11/your-own-satellite-7-things-to-know-before-you-go/>. [Accessed 8 March 2016].
- [4] C. C. T. D. D. H. N. H. S. R. C. S. Tristram Bone, "Final Report_SVD_IPSPT_Group5-1.pdf," 2014.
- [5] "CubeSat SADA," 11 2013. [Online]. Available: <http://www.honeybeerobotics.com/wp-content/uploads/2013/12/Honeybee-Robotics-CubeSat-SADA.pdf>. [Accessed 6 March 2016].
- [6] Micromo, "Corporate Overview," [Online]. Available: <http://www.micromo.com/company/about-micromo>. [Accessed 6 March 2016].
- [7] "Sub-Miniature All Purpose Slip Ring Capsule Model # 2040-00," [Online]. Available: http://www.electro-miniatures.com/mod2040_00.html. [Accessed 15 May 2016].
- [8] [Online]. Available: http://ams.aeroflex.com/motion/datasheets/SlipRings_1001398-008.pdf. [Accessed 15 May 2016].
- [9] "500 Series Hollow Shaft Slip Rings," 2016. [Online]. Available: <http://www.slipring.com/series-through-hole-slip-rings-0600-p-360-l-en.html>. [Accessed 15 May 2016].
- [10] "Miniature Slip Ring - 12mm diameter, 6 wires, max 240V @ 2A," [Online]. Available: <https://www.adafruit.com/products/775>. [Accessed 15 May 2016].
- [11] "RTA_Intro-1.pdf," [Online]. Available: http://www.rpi.edu/dept/ecse/rtas/RTA_Intro-1.pdf. [Accessed 5 February 2016].
- [12] "UC1625 Brushless DC Motor Controller," [Online]. Available: www.ti.com/product/uc1625/description. [Accessed 2 February 2016].
- [13] "HiRel Overview, International Rectifier," [Online]. Available: <http://www.irf.com/product-info/hi-rel/hirel-overview.pdf>. [Accessed 15 May 2016].
- [14] S. B. U. d. D. A. B. H. (Yonatan Winetraub (a), "Attitude Determination – Advanced Sun Sensors for Pico-satellites," [Online]. Available: <https://www.agi.com/downloads/corporate/partners/edu/advancedSunSensorProject.pdf>. [Accessed 3 March 2016].
- [15] J. L. R. L. Mark A. Post, "A Low-Cost Photodiode Sun Sensor for CubeSat and Planetary Microrover," 21 July 2013. [Online]. Available: <http://www.hindawi.com/journals/ijae/2013/549080/>. [Accessed 4 March 2016].
- [16] "LITE-ON ELECTRONICS, INC.," [Online]. Available: <http://www.mouser.com/ds/2/239/LTR-4206E-194892.pdf>. [Accessed 28 April 2016].

- [17] S. Holzner, "How to Calculate the Period and Orbiting Radius of a Geosynchronous Satellite," [Online]. Available: <http://www.dummies.com/how-to/content/how-to-calculate-the-period-and-orbiting-radius-of.html>. [Accessed 31 March 2016].
- [18] K. Ahmed, "Slideshare," 13 November 2013. [Online]. Available: <http://www.slideshare.net/kamranahmed7186/satellite-communication-a-tutorial-28226854>. [Accessed 8 March 2016].
- [19] NASA, "Technology Readiness Level," [Online]. Available: https://www.nasa.gov/directorates/heo/scan/engineering/technology/txt_accordion1.html.
- [20] Micromo, "How to Prevent Step Losses with Stepper Motors," [Online]. Available: http://static.micromo.com/media/wysiwyg/Technical-library/Stepper/Stepper_Why%20Steppers%20Loose%20Steps_WP.pdf. [Accessed 17 March 2016].
- [21] Engineers Edge, "Electric Motor Definitions and Terminology," [Online]. Available: http://www.engineersedge.com/motors/motors_definitions.htm. [Accessed 17 March 2016].
- [22] Minebea, "Stepper Motor Speed and Torque Relationship," [Online]. Available: <http://www.nmbtc.com/step-motors/engineering/torque-and-speed-relationship/>. [Accessed 16 March 2016].
- [23]. NanoRacks. (Dec 10, 2013). NanoRacks CubeSat Deployer (NRCSD) Interface Control Document. 5/16/16. From world wide web: http://nanoracks.com/wp-content/uploads/Current_edition_of_Interface_Document_for_CubeSat_Customers.pdf.
- [24]. Thurn, A., et al. (May 16, 2012). A Nichrome Burn Wire Release Mechanism for CubeSats. 5/16/16. From the world wide web: <http://www.nrl.navy.mil/PressReleases/2014/AMS%20Paper%20-%20A%20Nichrome%20Burn%20Wire%20Release%20Mechanism%20for%20CubeSats%20-%20Final%20-%20Adam%20Thurn.pdf>.
- [25]. Carpenter, B. , Lyons, J. Lightweight Flexible Solar Array Experiment Summary. 5/16/16. From world wide web: https://eo1.gsfc.nasa.gov/new/validationReport/Technology/Documents/Summaries/09-LFSA_Rev-0.pdf
- [26]. BioMetal Artificial Metal-Based Muscle BioMetal Fiber BMF Series. 5/16/16. From world wide web: http://www.toki.co.jp/biometal/download/downloadfiles/BMF_Catalog_140217.pdf
- [27]. McMaster. Press-Fit Steel Body Spring Plunger with Stainless Steel Ball. 5/16/16. From world wide web: <http://www.mcmaster.com/#84835a21/=12fyhl2>

Appendix A: Customer Requirements

The sponsor for the SADA design is the NASA Jet Propulsion Lab (JPL). JPL plans to use the team's design in future CubeSats. The SADA is specifically meant for CubeSats. Most CubeSats orbit the earth at LEO while some go as high as GEO [3]. Thus, the system must be able to rotate the panels at speeds that can allow the solar panels to face the sun while the satellite revolves around the Earth: The lower the orbit, the faster the revolution time.

Table 33: CubeSat Orbits [18]

Features	GEO	MEO	LEO
Height above the Earth surface (km)	36,000	6,000-12,000	200-3000
Time Per Orbit (hrs)	24	5-12	1.5
Speed (km/hr)	11,000	19,000	27,000

A key element of this SADA design is the ability for it to work independently without the need for much accommodation by the CubeSat. It would benefit JPL and other end users to have a simple device that is mostly self-sufficient such that it decreases the required inputs and simply produces the desired energy output. An additional benefit is if the solar panels have continuous rotation in a single direction. This would prevent the wasted time and energy to unravel the wires connecting the solar panel to the CubeSat.

Technology Readiness Level 3

Due to high costs and risks of space missions, the development of the CubeSat SADA module must happen in incremental steps that ensure the system will operate as planned. These steps are referred to as technology readiness levels (TRL). NASA requires the SADA module to meet a TRL of 3.

Table 34: TRL 3 Explanation [19]

TRL	Definition	Hardware Description	Software Description	Exit Criteria
3	Analytical and experimental critical functions and/or characteristic proof of concept	Analytical studies place the technology in an appropriate context and laboratory demonstrations, modeling, and simulation validated analytical predictions	Development of limited functionality to validate critical predictions using non-integrated software components	Documented analytical/experimental results validating predictions of key parameters

This means that JPL requires laboratory experiments on a prototype in conjunction with a paper design for future work. The prototype does not need to be space-ready. This saves costs and

resources. The paper-design is meant to take the information gathered from the prototype experiments and plan for a space-rated design with similar characteristics to the prototype. JPL needs experimental verification that the SADA module with the desired requirements is plausible.

Appendix B: System Evaluation Plan

The two main functions the functional prototype must demonstrate are that the panels rotate within specified rotational speeds and the panels have sun/light tracking capabilities with a pointing accuracy of 10 degrees. The prototype will have the required SADA module geometric dimensions.

To demonstrate the prototype functions, a testing apparatus was constructed:



Figure 68: SADA on Test Apparatus

The center platform has attachment shafts for the prototype to attach to. The prototype has attachment tabs on either side. To attach the prototype, put screws through the attachment tab holes into the shafts. Once attached, the SADA will be on its side. The panel with the light sensors must be on top. To operate the SADA, the AC adapter must be plugged in to an outlet. The light stand position is changeable, but it should be set to the same height as the prototype panel and the light mount should be rotated so the LEDs face the panel.

Once the SADA has been attached and the light stand oriented correctly, rotate the SADA platform to the zero-degree position by matching the zero mark on the center platform to the black line on the larger square platform.



Figure 69: Starting Point

The next step is to activate the SADA. The panels will rotate one full revolution to find the light source, then rotate to face the light. This is a light finding feature that occurs when the SADA is first turned on.

For the light tracking demonstration, rotate the center platform to 20 degrees from the starting point. At this point, the panels should rotate to face the light source. The requirement is that the panels reach within 10 degrees of its initial starting position. During this demonstration, the panels will rotate at 2 RPM to improve visualization of the panel rotation.

The light tracking algorithm also repeats the light finding feature if it loses track of the light. This will be demonstrated by blocking the light source with your hand for a brief moment. After this, remove the obstruction blocking the light source from the panels (i.e. your hand). Once the panels have rotated one full revolution, it should be able to find the light source and rotate to face it again.

Appendix C: Assembly Instructions

Tools/Materials Required:

- a. T5 Screwdriver
- b. Flat-head Screwdriver
- c. Hammer
- d. Right Angle Tweezers
- e. Disposable Wooden Applicators
- f. 150-Grade Sandpaper
- g. Needle File
- h. Thick Aluminum L Bracket
- i. Quick Set Epoxy
- j. Caliper
- k. Soldering Iron
- l. Solder

Chassis Preparation

1. To begin assembly, take the monolithic chassis base and the threaded inserts need to be hammered into the mounting holes. First, take the needle file and make sure to clear and deburr all holes.
2. Using right angled tweezers such as the one shown in Figure 70, grab an insert.



Figure 70: Right Angle Tweezer Used for Soldering Electronics

3. Take a flathead screwdriver and stick the head in the insert which can be seen in Figure 71.

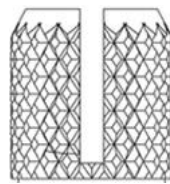


Figure 71: Threaded Inserts

4. Align the insert with hole in the chassis and then press the insert down with the screwdriver to stick it inside slightly.
5. Take the aluminum L bracket and place it over the insert as it sticks out of the hole.

6. Slowly and carefully, hammer the bracket to apply an even force across the insert to go into the chassis hole. Repeat until the top of the insert is flush with the chassis hole. See Figure 72 for before and after images.



Figure 72: Empty Hole (Left) and Hole with Insert (Right)

7. Upon completion of all the chassis holes, the result should be the same as Figure 73.

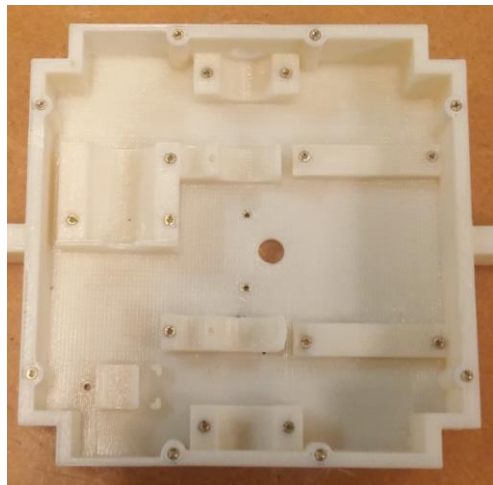


Figure 73: Chassis with All Inserts In

Hinge Preparation

Note: The steps for the mock panel are only for the prototype.

1. The process is similar to chassis preparation, begin by using the needle file to deburr and clear the holes.
2. Using right angled tweezers, grab an insert.
3. Take a flathead screwdriver and stick the head in the insert.
4. Align the insert with a hole and then press the insert down with the screwdriver to stick it inside slightly.

5. Take the aluminum L bracket and place it over the insert as it sticks out of the hole.
6. Slowly and carefully, hammer the bracket to apply an even force across the insert to go into the hole.
7. In total, there will be three holes that need to have inserts on each hinge. The holes can be seen in Figure 74 and Figure 75.
8. Each of the holes will then need a 0-80 set screw.

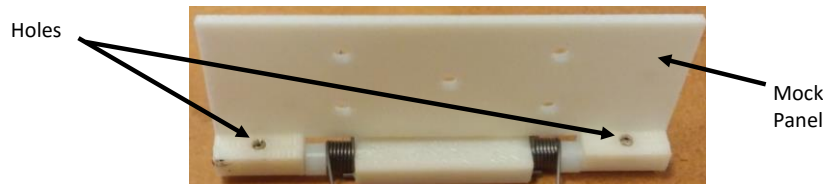


Figure 74: Two Holes on Mock Panel

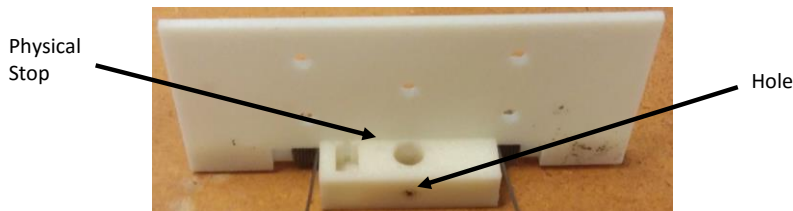


Figure 75: One Hole on Hinge

9. Using the manufacturer's instructions, mix the quick set epoxy using both the resin and hardener.
10. Put a dab of the epoxy on the dowel pin and insert in the dowel hole on hinge using the wooden applicators.
11. Wait the specified amount of time given by the epoxy manufacturer for the adhesive to cure.

Primary Shaft Setup

1. Slide gear with part number 57655K18 (32 teeth) on the pre-cut solid aluminum shaft with part number 9062K24, there will be some resistance since the gear should be press-fitted on the shaft.
2. Next, slide the bearings with part number 6377K49 on each side of the gear.
3. Using the manufacturer's instructions, mix the quick set epoxy using the resin and hardener.
4. Put epoxy on about $\frac{1}{4}$ " of the ends of the solid aluminum shaft using the wooden applicators.
5. Slide the two gears with part number 57655K16 (24 teeth) on both ends of the shaft with the hubs facing inwards of the shaft.
6. Wait the specified amount of time by the epoxy manufacturer for the adhesive to cure.

7. Adjust the center gear to pre-determined location for gear meshing. The result should look like Figure 76.

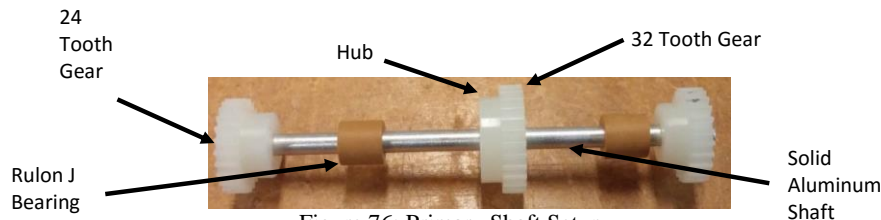


Figure 76: Primary Shaft Setup

Secondary Shafts Setup

1. Slide gear with part number 57655K16 (24 teeth) with the hub flush with the end of the pre-cut hollow steel shaft with part number 50265K31. The result should look like Figure 77.
2. Repeat for a second shaft setup.



Figure 77: Secondary Drive Shafts

Slip Ring Integration

1. Connect a secondary shaft to the rotor of a slip ring. It should fit snuggly with the gear facing the slip ring. Make sure to carefully feed the slip ring wires through the shaft.
2. Slide the bearing with the part number 2685T11 onto the secondary shaft. The result should look like Figure 78.
3. Repeat for the second shaft and slip ring.



Figure 78: Slip Ring Connected to Secondary Shaft

Note: the gear hub should have been flush with the end of the shaft that connects to the rotor of the slip ring.

Mounting Controller/Motor Driver

Note: This can be done at any time.

1. Mount the printed circuit board (PCB) or perfboard on the rails of chassis and secure it using 4x 0-80 screws as shown in Figure 79.

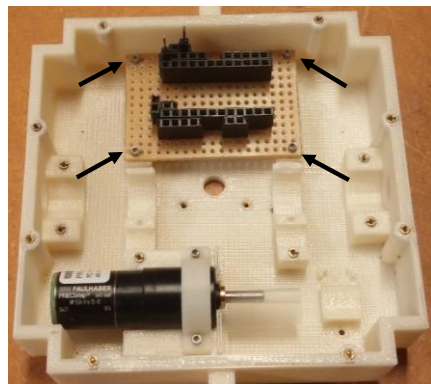


Figure 79: Mounting Points for Controller/Motor Driver

Mounting the Secondary Drive Shafts

1. Using the setup of the secondary shaft, bearing, and slip ring from the slip ring integration section, place the assembly in the corresponding cradles with the secondary shaft through the hole in the side of the chassis.
2. Mount the PTFE bearing brackets using two 0-80 screws. Use Figure 80 as guidance.
3. Repeat for second side.

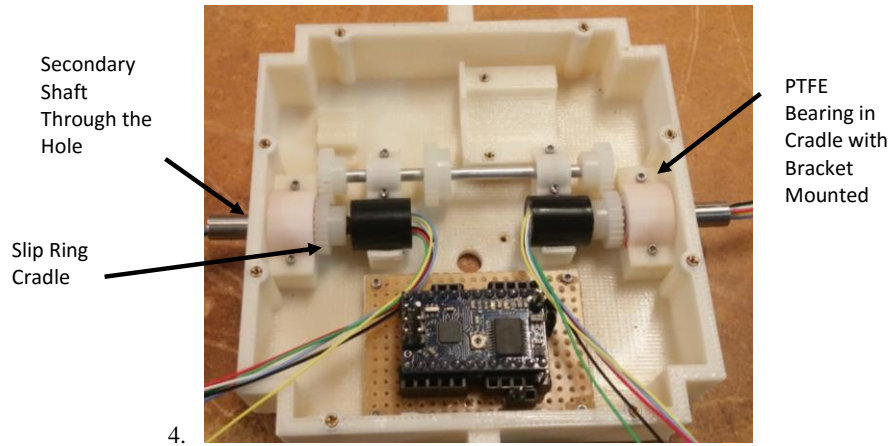


Figure 80: Mounting the Secondary Shafts

Mounting the Primary Drive Shaft

5. Place the primary drive shaft setup with the Rulon J bearings on the cradles.
 6. Place the slip ring bracket over the Rulon J bearing and slip ring.
 7. Make sure to press the side next to the slip rings in the tight space between the cradle and controller rail. File the side of the bracket as needed.
 8. Use two 0-80 screws to mount the bracket, one next to the bearing and the other is under the chassis.
 9. Make sure to rotate the shafts as needed to make sure that the gears from the shafts mesh.
- The final result will look like Figure 82.

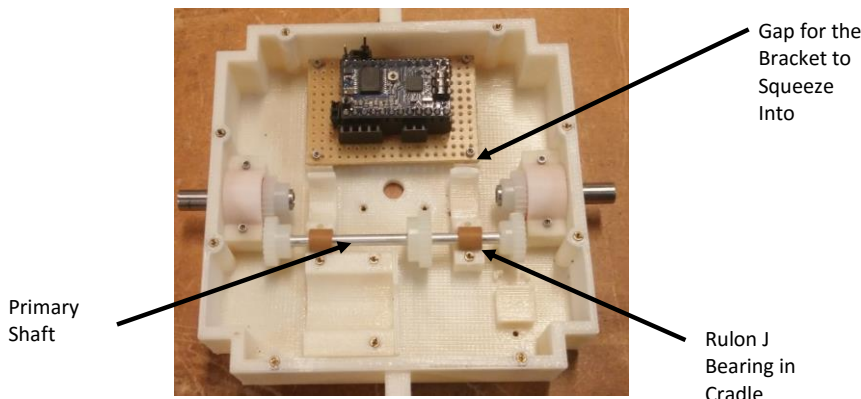


Figure 81: Mounting the Primary Shaft

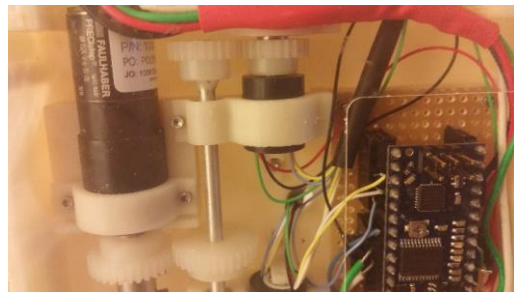


Figure 82: Bracket for Primary Shaft and Slip Ring

Motor Connector

Note: The motor connector is only used for the prototype.

1. Solder four spring loaded contacts which can be seen in Figure 83 on a perfboard in a straight line.
2. Solder wires to each of the individual contacts as close as possible without interfering with the back of the motor.
3. Pick an orientation for the motor to mount. It is preferred to have the contacts in a horizontal line close to the chassis bottom.
4. The next step is to cut two perfboards of the same size (~17 mm by 2 mm). However, use a caliper to measure the height from chassis to the center of the motor contacts. Using this measurement, cut the perfboard in such a manner that when the perfboard is glued to the chassis wall, the contact pins will perfectly align with motor contacts. Adjust measurements as needed. Figure 84 shows the two perfboards prior to epoxying and cutting to final size.



Figure 83: Spring Loaded Contact Pins

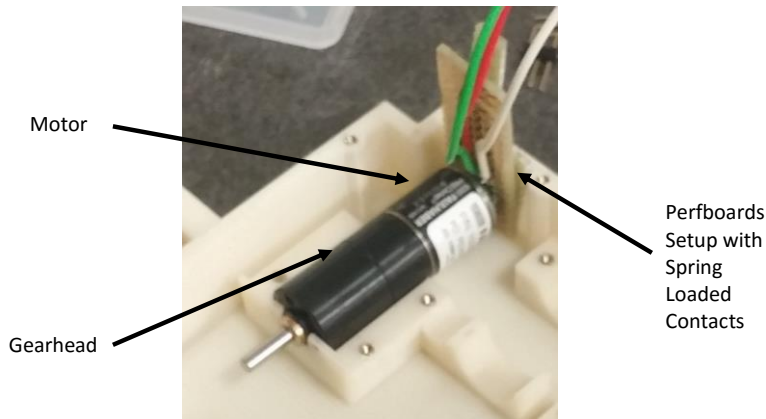


Figure 84: Motor in Cradle with Connector

5. Using the manufacturer's instructions, mix the quick set epoxy using both the resin and the hardener.
6. Using the wooden applicators, apply the epoxy to the backs (side without copper contacts) of the perfboards and compress together.
7. Wait the specified amount of time by the epoxy manufacturer for the adhesive to cure.
8. Using the caliper again, measure the distance that the perfboard needs to be along the chassis wall. Adjust as needed for alignment between the spring contacts and motor contacts.
9. Using the manufacturer's instructions, mix the quick set epoxy using the resin and hardener once again.
10. Using the wooden applicators, apply the epoxy to the side without spring contacts and stick the board in the pre-determined location on the chassis wall. Once in, put the motor in proper alignment and ensure proper contact is made.
11. Wait the specified amount of time by the epoxy manufacturer for the adhesive to cure.

Motor/Gearhead & Encoder Setup/Mounting

1. First remove the motor and press fit the gear with ID number 57655K18 (32 teeth) on the gearhead which is connected to the motor with the hub facing the gearhead. Use Figure 85 as needed.

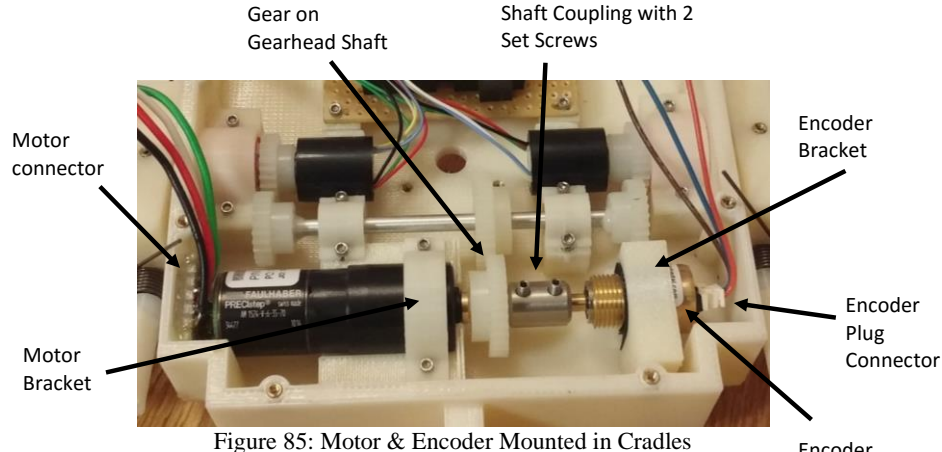


Figure 85: Motor & Encoder Mounted in Cradles

2. Connect the wire connector to the plug on the encoder end.
3. Next, take the shaft coupling and place it halfway on the shaft of the motor and the other half on the encoder.
4. Using the screwdriver for the coupling set screws, tighten the screws down on both shaft.
5. Place the assembly in the motor and encoder cradles. Ensure that the gear on the gearhead shaft meshes with the center gear on the primary drive shaft. Carefully bend the wires on the encoder plug towards the controller.
6. Use two 0-80 screws to mount the motor in the cradle.
7. Next, use one 0-80 screw to mount the encoder bracket from under the chassis.

Wiring

1. For the routing of the wires for the motor and encoder, use some heat shrink tubing on most of the length until it reaches the controller. Also make sure to pass the wire bundles over the bearing brackets for secondary shafts as per Figure 86.
2. For all the wire connections, please refer to the circuit schematic which can be seen in Figure 87.
3. Cut the wires to size and keep the layout as neat as clean as possible.

Note: For space-grade design, some wires will be passing through the hole in the center of the chassis bottom for power and data lines since the on-board controller will be used as well as for the power distribution system.

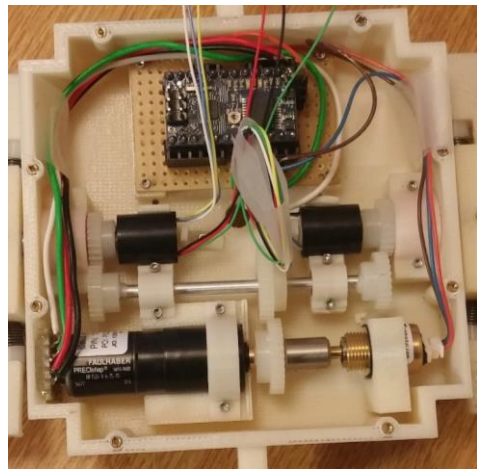


Figure 86: Initial SADA Wiring

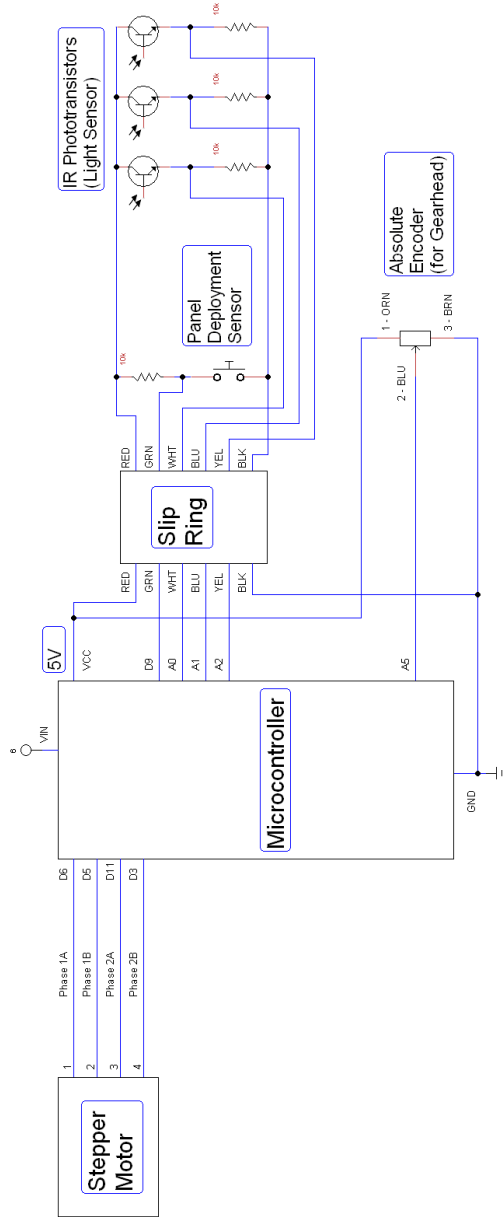


Figure 87: Circuit Schematic

Hinge Assembly

1. Following the preparation of the hinge mechanism, take one of the pre-cut solid aluminum rods with part number 8974K19. Using the orientation that is seen in Figure 88, solder the rod into the mock panel from the left side of the mock panel.

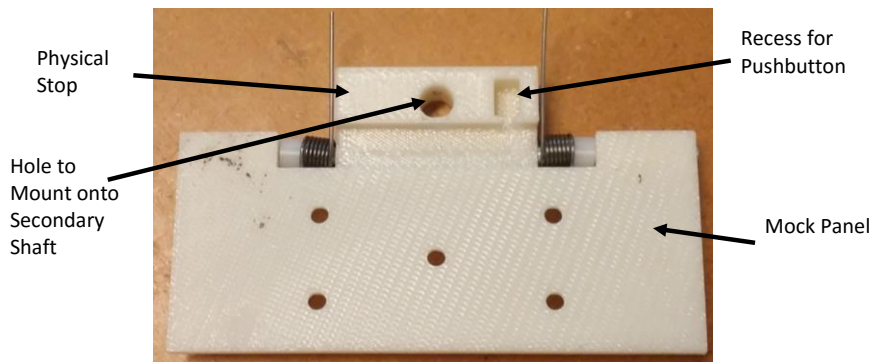


Figure 88: Side View of Hinge Mechanism

2. Once it comes out of first block, insert a nylon spacer (part number 94639A483) on the shaft followed by a right-hand spring (part number 9271K97).
3. Next, feed the rod through the center hinge with the physical stop.
4. Once it leaves the center block, insert a left-hand spring (part number 9271K98) followed by another nylon spacer and through the side of the mock panel.
5. Tighten the two set screws on the mock panel.
6. Take the pushbutton (part number GP11MCBE) and insert it into the recessed fitted hole for it with the leads in the direction coming out of the page.
7. Solder an 18 AWG wire on each of the pushbutton leads.
8. Next, take the mock panel PCB riser as seen in Figure 89. Hammer in the two inserts on the risers.
9. Then mount the board on the panel by using four bolts and nuts.
10. Repeat for second assembly.

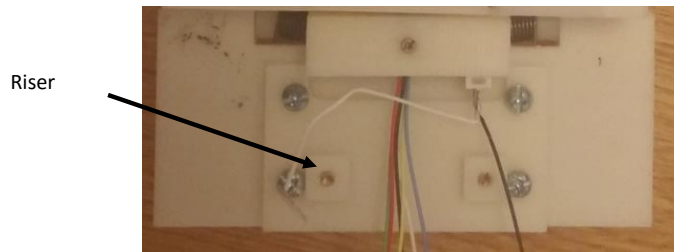


Figure 89: PCB Holder on Mock Panel

IR Phototransistor Sensor Setup

1. Take three of the IR phototransistors and put the leads through the trapezoid holder, all in the same orientation.
2. Using the manufacturer's instructions, mix the quick set epoxy using the resin and hardener.
3. Using the wooden applicators, apply the epoxy to the bottoms of the IR phototransistors so that they get attached to the trapezoid holder.
4. Wait the specified amount of time by the epoxy manufacturer for the adhesive to cure.
5. Once the sensor adhesive has cured, using the manufacturer's instructions, mix the quick set epoxy using the resin and hardener again.
6. Using the wooden applicators, apply the epoxy to the flat bottoms part of the trapezoid piece and attach it to the pre-made perfboard or PCB. Make sure that the legs of the phototransistors are bent and put in the right holes for soldering.
7. Wait the specified amount of time by the epoxy manufacturer for the adhesive to cure.
8. Once complete, solder the remaining components as per Figure 90. The result should look something like Figure 91.

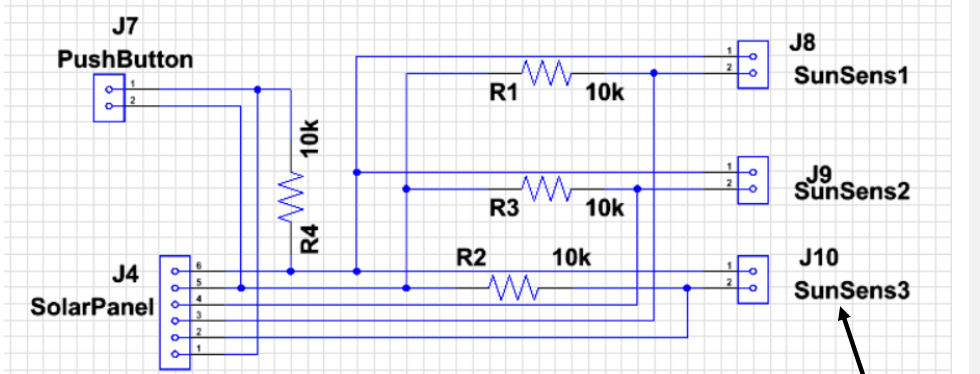


Figure 90: Sensor Schematic

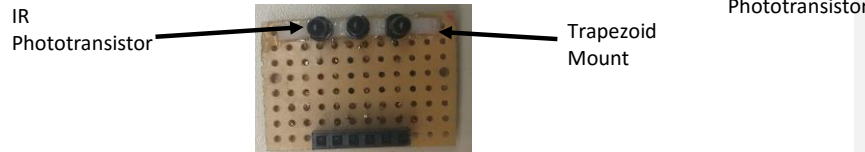


Figure 91: Sensor Result Using a Perfboard

9. Next, mount the sensor to the panel riser using two 0-80 screws as seen in Figure 92.

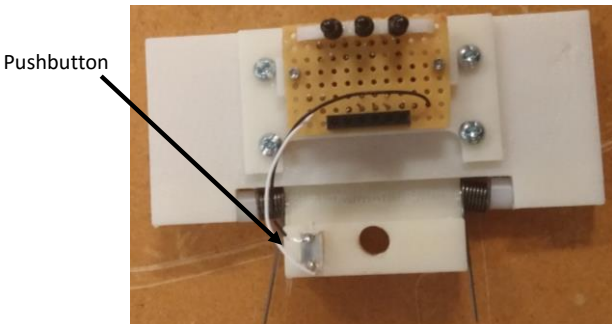


Figure 92: Light Sensor on Mock Panel/Riser

Hinge/Panel Attachment to Chassis

1. Once the hinge and panels are ready, push the hinge assembly onto the secondary shaft that extends out of the chassis. Make sure to keep the side with the physical stop flush with the shaft.
2. Tighten the set screw onto the secondary shaft.
3. Repeat for the other side.

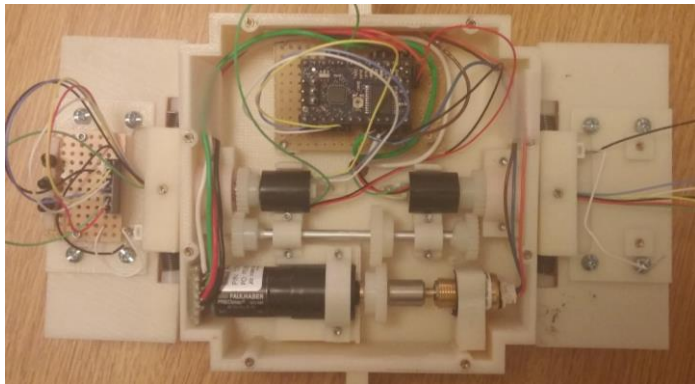


Figure 93: Chassis with Hinge/Panels Connected

Final Steps

1. Make sure to organize the wires so that they cannot get caught on any mechanical component such as gears.
2. Ensure that the hinge and panels do not make contact with the chassis side walls.
3. Mount the L brackets on the sides of the slip rings as shown in Figure 94 so that there is not much play mechanically.

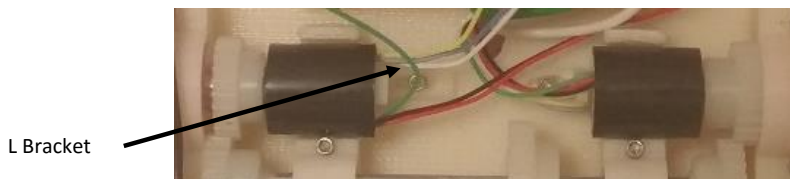


Figure 94: L Brackets for Slip Rings

4. Lastly, load the springs on both hinges in such a manner that they are compressed against the dowel pins that were inserted. Figure 95 shows how the spring legs should be set. Upon the completion of this step, the panels will want to stay deployed at 90 degrees.
5. Once they have been set up, the legs can be cut to size as needed.

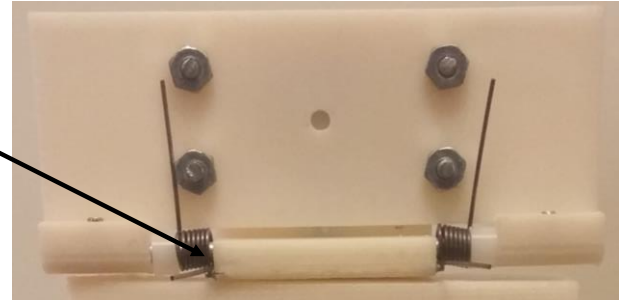


Figure 95: Spring Compression

Appendix D: Expense Report

Table 35: Fabrication of mock chassis

Description	Units	Cost	Date Ordered	Date Received
SADA Chassis mock prism base	1	\$13.50	2/29/16	3/3/16
SADA Chassis mock tuna can cover	1	\$19.90	2/29/16	3/3/16
SADA Chassis mock tuna can top	1	\$3.80	2/29/16	3/3/16
Total Cost		\$ 37.20		

Table 36: Initial Fabrication for Prototype Chassis

Description	Units	Cost	Date Ordered	Date Received
SADA Chassis final base	1	\$41.10	4/21/16	4/25/16
Encoder Bracket	1	\$0.60	4/21/16	4/25/16
Motor Bracket	1	\$0.40	4/21/16	4/25/16
Primary Bearing Bracket	1	\$0.10	4/21/16	4/25/16
Primary Bearing Bracket 2	1	\$0.10	4/21/16	4/25/16
Secondary Bearing Bracket	2	\$0.80	4/21/16	4/25/16
Slip Ring Bracket	2	\$0.20	4/21/16	4/25/16
Total Cost		\$ 43.30		

Table 37: Re-Printing Costs

Description	Units	Cost	Date Ordered	Date Received
Encoder Bracket	1	\$0.90	4/27/16	5/4/16
Primary Bearing Bracket (rev 2)	1	\$0.60	5/4/16	5/11/16
Primary Bearing Bracket 2 (rev 2)	1	\$0.60	5/4/16	5/11/16
Slip Ring Bracket	2	\$0.20	5/4/16	5/11/16
Total Cost		\$ 2.30		

Table 38: Initial Fabrication of Hinge

Description	Units	Cost	Date Ordered	Date Received
Hinge Attachment (rev 2)	2	\$5.40	4/21/16	4/25/16
Mock Panel	2	\$8.80	4/21/16	4/25/16
Total Cost		\$14.20		

Table 39: Hinge Re-Printing Costs

Description	Units	Cost	Date Ordered	Date Received
Hinge Attachment (rev 3)	3	\$8.10	4/27/16	5/4/16
Mock Panel	1	\$4.40	4/27/16	5/4/16
Total Cost		\$12.50		

Table 40: 3D Printed Parts for Testing Apparatus

Description	Units	Cost	Date Ordered	Date Received
Light Mount (rev 3)	2	\$12.00	4/27/16	5/4/16
Sensor Mount	2	\$2.80	4/27/16	5/4/16
Sensor Mount Trapezoid	3	\$0.30	4/27/16	5/4/16
Total Cost		\$ 15.10		

Table 41: Purchased Parts

Description	Part ID	Quantity	Cost	Total
Screw-to-Expand Inserts, for Plastics, Brass, 0-80 Thread Size, Pack of 25	92395A109	1	8.5	8.5
Optically Clear Cast Acrylic Sheet, 1/16" Thick, 6" x 12"	8560K178	1	2.75	2.75
18-8 Stainless Steel Socket Head Cap Screw, 0-80 Thread, 5/32" Length, Pack of 100	92196A053	1	6.74	6.74
18-8 Stainless Steel Socket Head Cap Screw, 0-80 Thread, 1/8" Length, Pack of 100	92196A052	1	5.98	5.98
3 1/8" x 4 1/4" Perfboard	-	1	1.99	1.99
Arduino Stackable Headers	-	1	1.99	1.99
Heat shrink tubing	-	1	1.99	1.99
Baby Orangutan B-328 Controller + USB AVR Programmer Combo	1302	1	31.95	31.95
Contact Probes LOOSE CONTACT Initial Height .137"	0906-0-15-20-76-14-11-0	4	0.49	1.96
MA3 Absolute Encoder, Analog 10-Bit, 1/8" Dia Shaft, Ball Bearing	MA3-A10-125-B	1	45.4	45.4
Cable Assembly, 3 Descrete Wires, MIC3 Connector to No Connector, 1 ft length	CA-MIC3-W3-NC-1	1	6.8	6.8
IR Phototransistors Filtered	LTR-4206E	3	0.123	0.369
10k Ohm Resistors	-	4	-	-
22 AWG Wire	-	-	-	-
Screw Terminals	-	-	-	-
2 PCBs - Sensor and controller	-	1	~35	-
4xAA Battery Pack	-	1	-	-
5V AC Adapter	-	1	-	-
Pushbutton Switches OFF-(ON) SPST PCB	GPI1MCBE	2	5.05	10.1
Unpolished Rod, Multipurpose 6061 Aluminum, 1/8" Diameter, 2 Ft Length	8974K19	1	1.6	1.6
Quick Setting Epoxy	68386	1	7.99	7.99
Metric Type 316 Stainless Steel Dowel Pin, M1 Diameter, 4 mm Length, Pack of 10	93600A030	1	9.01	9.01
Music Wire Torsion Spring, 180 Degree Angle, .249" Spring OD, .028" Wire, Left-Hand, Pack of 6	9271K98	1	7.16	7.16
Music Wire Torsion Spring, 180 Degree Angle, .249" Spring OD, .028" Wire, Right-Hand, Pack of 6	9271K97	1	7.16	7.16
Nylon Unthreaded Spacers, 1/4" OD, 5/32" Length, for Number 6 Screw Size, Pack of 25	94639A483	1	7.75	7.75
0-80 Set screw, 1/16" length	-	6	-	0
3 1/8" x 4 1/4" Perfboard	-	1	1.99	1.99
Ultra-Flexible Positioning Arm	50035A692	1	10.38	10.38
Easy-Position Turntable, 9" Diameter with One Dead Stop	1797K3	1	9.66	9.66
3/8" Female To 5/8" Male Threaded Screw Adapter For Mic Microphone Stand	-	1	4.95	4.95
Mic Stand Jam Nut with Standard 5/8-27 Thread (2-pack)	-	1	9.98	9.98
DC Power Connectors Power Jack/Connector 2.1mm x 5.5mm	CON-SOCJ-2155	1	1	1

Super-bright 5mm IR LED (25 pack) - 940nm	IR333-A	1	7.95	7.95
Unpolished Rod, Multipurpose 6061 Aluminum, 5/8" Diameter, 2 Ft Length	8974K48	1	6.76	6.76
DC Power Connectors Power Jack PCB 2.1mm x 5.5mm	163-179PH-EX	1	1.04	1.04
Zinc-Plated Steel, Number 8-#2 Drive, 1/2" Long Phillips Wood Screw, Pack of 100	90031A194	1	4.5	4.5
8-32 Machine Screws, 1" Long	-	2	0.1	0.2
6-32 Machine Screws, 1" Long	-	2	0.1	0.2
5/16"-18, 1 1/2" Long Bolt	-	1	0.8	0.8
100 Ohm Resistors	-	5	-	-
22 AWG Wire	-	-	-	-
3'x4' Birch Plywood, 3/4" Thick	-	1	-	-
AM1524-V-6-35-70+15A 249:1+MG03	1000008109	1	162	162
Plastic Gear --14 1/2 Degree Pressure Angle, Press-Fit Mount, 48 Pitch, 32 Teeth	57655K18	2	7.06	14.12
Plastic Gear --14 1/2 Degree Pressure Angle, Press-Fit Mount, 48 Pitch, 24 Teeth	57655K16	4	7.71	30.84
Miniature Capsule Slip Ring - 12mm diameter, 6 wires, max 240V @ 2A	SRC012C-6	2	17.5	35
Metric Smooth-Bore Seamless Stainless Steel Tubing, Outer Dia 6mm, Wall 1 mm, Inner Dia 4mm, 0.5 meter Length	50265K31	1	19.96	19.96
Ultra-Low-Friction Dry-Running Sleeve Bearing, Rulon J, Outer Dia 1/4", Inner Dia 0.129", Length 1/4"	6377K49	2	2.23	4.46
Ultra-Low-Friction Dry-Running Sleeve Bearing, PTFE, Outer Dia 12mm, Inner Dia 6mm, Length 10mm	2685T11	2	3.55	7.1
Tight-Tolerance Rods--Precision Ground, Multipurpose 6061 Aluminum, 1/8" Diameter, 1/2 Ft Length	9062K24	1	4.53	4.53
Rigid Shaft Coupling, 303 Stainless Steel, 0.43" Overall Length, Inner Diameter 0.1248", Outer Diameter 0.313"	S5035Y-G5O-1	1	4.92	4.92
		Sum	509.529	

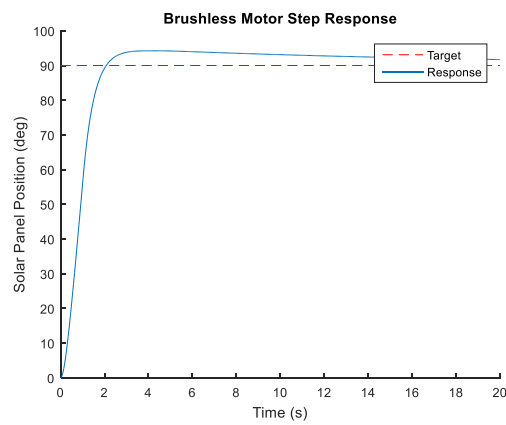
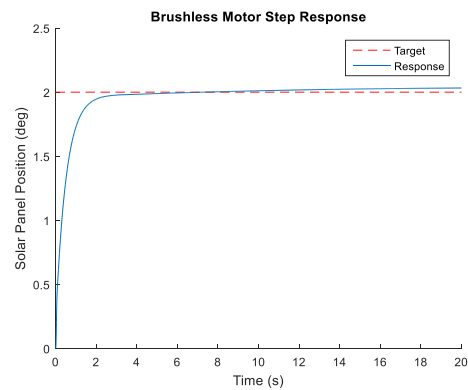
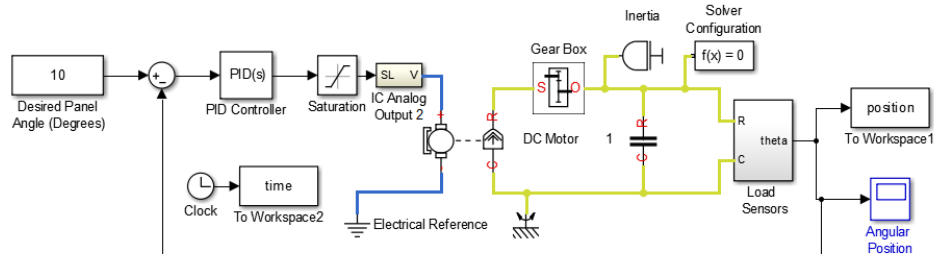
Appendix E: Overshoot Calculations

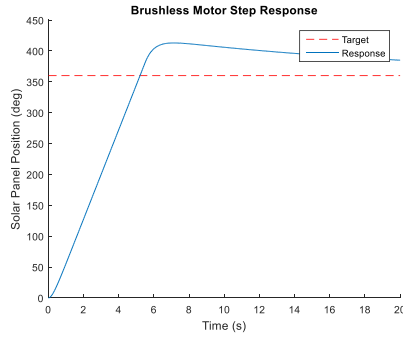
Given the approximate load on the motor, different simulations were made to gauge how well the brushed, brushless, and stepper motors could orient the solar panels. These simulations were constructed using MATLAB in conjunction with Simulink/Simscape.

Brushed/Brushless Motor

The brushless motor model assumed that the motor could be modeled as a brushed DC motor. This was done in order to largely simplify the system and was reasonable since both types of motors act such that speed is proportional to voltage and torque is proportional to current. A simple PID controller was used as this would simplify the feedback system. The maximum supply voltage (saturation voltage) used is 5V because the CubeSat has a 5V power rail. The motor chosen for the simulation was the 0615 brushed DC motor from Micromo. The gear ratio was set to 2000:1 as an estimate for a typical gearhead. Micromo sells a variety of gearheads from 1000:1 to 4000:1.

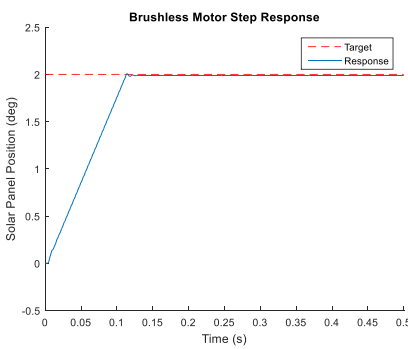
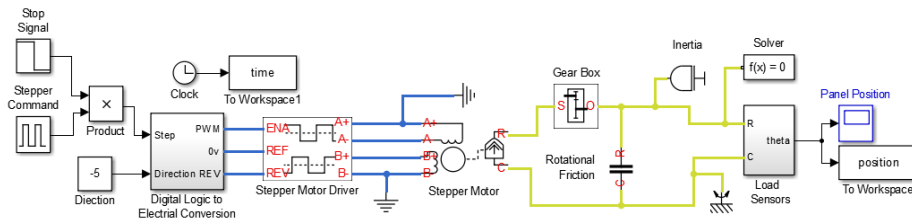
A simple tuning of the PID controller with a step size of 10 (moving the panel 10 degrees) yielded the following results:

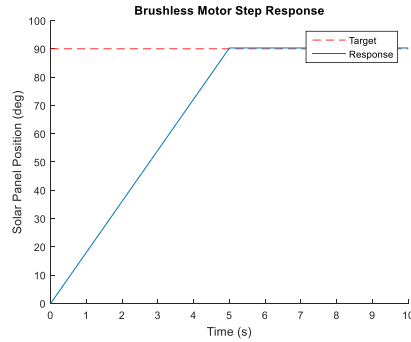




Stepper Motor

The stepper motor overshoot simulation uses an example stepper motor that is run near its maximum speed. Again it uses a 5V maximum power source. The simulation is open-loop because the stepper motor does not require position feedback. The motor is the AM1524 with a 249:1 gear ratio. As can be seen, the overshoot is minimal (about $\frac{1}{2}$ step size of AM1524).





Appendix F: Stepper Motor/Gearhead Analysis

Typical Transient Response

We will calculate the angular displacement and angular velocity of the panels during a single step using the motor step size and settling time. Then, we will calculate the panel angular acceleration, which will allow us to calculate panel torque by multiplying that angular acceleration by panel rotational inertia. Lastly, we will calculate the torque that the motor must exert to meet that panel torque requirement. Our goal will be to find a motor and gearhead combination such that the motor torque rating is greater than or equal to the required panel torque produced by the motor step size, settling time and gearhead reduction ratio.

During a given step, a stepper motor starts from rest, accelerates to a peak angular velocity, then it slows down and stops rotating. A stepper motor has a step size (steps per revolution) rating, an electrical time constant. From this time constant, the settling time can be found. The settling time is the time it takes the stepper motor to its maximum angular speed (half of rotation). The stepper motor will be connected to the panels and produce a certain angular acceleration, and by extension a panel torque, based on its step size and settling time. The stepper motor must have a torque rating that is equal to or exceeds this panel torque or the motor will stall and be unable to turn the panels. Stepper motor failure is most commonly step loss, which includes:

1. Motor fails to start turning. Causes:
 - a. Load is too high
 - b. Frequency of steps is set too high
 - c. One phase may be broken or disconnected. Requires repair or motor replacement.
 - d. Current to the motor is too low
2. Motor does not accelerate up to constant angular velocity (see Figure B1 for velocity plot). Causes:
 - a. Wrong supply voltage or current is too low
 - b. Top speed is set too high.
3. Motor accelerates to its constant angular velocity, but stalls once it does so. Cause:
 - a. Motor torque requirements exceed the specified torque value [20]

The mechanical time constant cannot be determined from the motor data sheet

- Mechanical time constant is the amount of time for a stepper motor to reach 63% of its maximum angular speed [21].
- For stepper motors, the mechanical time constant is NOT given in the data sheet. Based on Figure B3, the mechanical time constant is assumed to be twice the electrical time constant:
 - o Motor starts at zero angular acceleration, reaches peak angular acceleration, then returns to zero, all while the angular speed has reached its peak and must reduce back down to zero to complete the step rotation.

The electrical time constant can be determined from the motor data sheet.

- Electrical time constant is the amount of time for a stepper motor to reach 63% of its rated current/torque, and it is the stepper motor inductance divided by resistance:
 - o $\tau_{electrical} = \frac{Inductance}{Resistance}$ [22].
 - o The settling time is the amount of time it takes a response to get to 98% of its steady state value. This will be approximated as:
 - $T_s = 4 * \tau_m$

Kinematics

The amount of rotation of the motor (Figure C1)

$$\theta_{motor} = \frac{360}{S}$$

The corresponding rotation of the panel is

$$\theta_p = \frac{\theta_m}{R}$$

To find the final angular velocity during the acceleration portion of the step, half of the angular displacement is divided by half of the time of the step (half of the settling time)

$$\omega_{max} = \frac{.5 \theta_p}{.5 T_s}$$

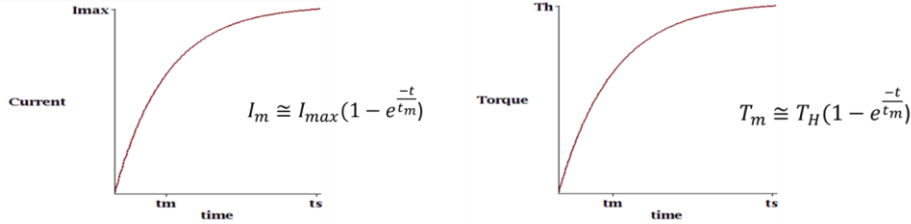
Motor Implementation

Assumptions

- Assume that each step of the motor results in a specified angular change in the panels
- Assume that the torque is proportional to the winding current
- Assume the maximum torque is equal to the holding torque to scale the torque response

Angular Acceleration

-Using the first order transient response of the stepper motor's current provides the following graphs and equations



$$\tau_m = \tau_H \left(1 - e^{\frac{-t}{\tau_m}} \right) = I_e \dot{\omega}_m$$

- Solving for angular acceleration

$$\dot{\omega}_m = \frac{\tau_m(t)}{I_e} = \frac{\tau_H}{I_e} \left(1 - e^{\frac{-t}{\tau_m}} \right)$$

Angular Velocity

- Angular Velocity is the integration of angular acceleration

$$\begin{aligned} \omega_m &= \int \dot{\omega}_m dt = \frac{\tau_H}{I_e} \int \left(1 - e^{\frac{-t}{\tau_m}} \right) dt \\ \omega_m &= \frac{\tau_H}{I_e} \left(t + \tau_m e^{\frac{-t}{\tau_m}} + C \right) \end{aligned}$$

- Since motor is starting from rest, C=0 and thus:

$$\omega_m = \frac{\tau_H}{I_e} \left(t + \tau_m e^{\frac{-t}{\tau_m}} \right)$$

Angular Position

$$\begin{aligned} \theta_m &= \int_0^{t_s} \omega_m dt = \frac{\tau_H}{I_e} \int_0^{t_s} \left(t + \tau_m e^{\frac{-t}{\tau_m}} \right) dt \\ \theta_m &= \frac{\tau_H}{I_e} \left[\frac{1}{2} t^2 - \tau_m^2 e^{\frac{-t}{\tau_m}} \right]_0^{t_s} \\ \theta_m &= \frac{\tau_H}{I_e} \left[\frac{1}{2} (t_s)^2 - \tau_m^2 e^{\frac{-t_s}{\tau_m}} \right] \\ \theta_m &= \frac{\tau_H}{I_e} \left[\frac{1}{2} (4\tau_m)^2 - \tau_m^2 e^{-\frac{(4\tau_m)}{\tau_m}} \right] \\ \theta_m &= R\theta_p = \frac{\tau_H}{I_e} [8\tau_m^2 - \tau_m^2 e^{-4}] \cong 8\tau_m^2 \frac{\tau_H}{I_e} \end{aligned}$$

Motor Inertia

$$\begin{aligned} T_m &= I_e \dot{\omega}_m \\ R &= \frac{\dot{\omega}_m}{\dot{\omega}_p} \\ \tau_p &= I_p \dot{\omega}_p = \eta R \tau_m \end{aligned}$$

$$\tau_m = \frac{I_p}{\eta R} \dot{\omega}_p = \frac{I_p}{\eta R} \left(\frac{\dot{\omega}_m}{R} \right) = \frac{I_p}{\eta R^2} \dot{\omega}_m$$

therefore: $I_e = \frac{I_p}{\eta R^2} + I_m$

Gear reduction

$$\frac{\theta_m}{\theta_p} = R; \quad \theta_m = \frac{R\theta_p\tau_H}{I_e} [8t_m^2 - t_m^2 e^{-4}] \cong 8t_m^2 \frac{R\theta_p\tau_H}{I_e}$$

$$\theta_m = \cong 8t_m^2 \frac{R\theta_p\tau_H}{I_e}$$

Appendix G: Failure Analysis Example Calculations

Introduction

Below are the example calculations of each of the four main types of mechanical failure for the SADA device (excluding the hinge). There are many components in the SADA that are repeated (shafts, gears, bearings). The calculations shown below are intended to show the formulas and thought process behind each of the types of reliability calculation. These calculations will then be expanded to include the rest of the components through the use of a spreadsheet once the formulas of each component are confirmed.

Motor and Gearhead Combination

Table 42 – Extracted Information from AM1524 Motor Data Sheet / Micromo Tech Support

AM1524 Stepper Motor	
Holding Torque (T_H)	6 mNm
Mean Time Before Failure of Motor ($MTBF_m$)	2000 hours

Table 43 – Extracted Information from 15A Gearhead Data Sheet

AM1524 Stepper Motor	
Gear Reduction Ratio (e)	249:1
Gear Efficiency (η)	0.6
Shaft Diameter (d_m)	3 mm
Gearhead Shaft Material	Steel?

The first step in the reliability analysis for the motor was to calculate the hours of use for the motor for one year. Using the fact that the panel would undergo one full rotation during each orbit, the team calculated the amount of times the motor undergoes a full rotation during one LEO orbit.

$$Rot_m = Rot_{panel} * e = 1 \frac{rev}{orbit} * \frac{249}{1} * 2\pi \frac{rad}{rev} = 498\pi \frac{rad}{orbit}$$

Next, the amount of orbits that a CubeSat in LEO would undergo in a year was calculated

$$\# \text{ of } \frac{\text{orbits}}{\text{year}} = \frac{1 \text{ orbit}}{88.290 \text{ min}} * \frac{60 \text{ min}}{1 \text{ hr}} * \frac{24 \text{ hr}}{1 \text{ day}} * \frac{365 \text{ days}}{1 \text{ yr}} = 5959.25840 \frac{\text{orbits}}{\text{year}}$$

The team then proceeded to find the amount of time that the motor would be in use during one orbit in LEO. This was done by dividing the angular distance traveled by the motor in such an orbit by the speed at which the motor would be accomplishing this rotation.

$$t_{orbit} = \frac{Rot_m}{\omega_m} = \frac{498\pi \frac{rad}{orbit}}{300 \frac{rev}{min} * 2\pi \frac{rad}{rev} * \frac{1 min}{60 s}} = 49.8 \cancel{161.573} \frac{s}{orbit}$$

Finally, the motor usage time for one orbit was multiplied by the amount of orbits that the CubeSat would go through in one year to find the equivalent hours of use of the motor per year.

$$\begin{aligned} \text{Hours of use per year} &= t_{orbit} * \# \text{ of } \frac{\text{orbits}}{\text{year}} \\ &= 49.8 \cancel{161.573} \frac{s}{orbit} * 5959.2840 \frac{\text{orbits}}{\text{year}} * \frac{1 hr}{3600 s} \\ \text{Hours of use per year} &= 82.43 \cancel{262.1} \frac{\text{hours}}{\text{year}} \end{aligned}$$

Displayed below in Figure 96 is a plot for the hours of motor use per year for different motor speeds at LEO orbit (200k meter orbit radius). The point used in this example calculation (Motor Speed = 300 RPM) is also marked on the plot.

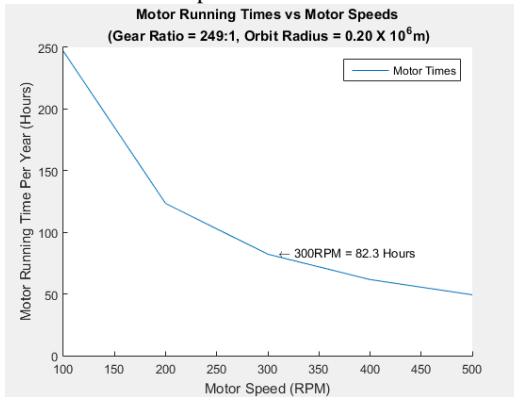


Figure 96 – Plot of Motor Running Times for various Drive Speeds

The values from both the example calculation and from the interpolation point shown in Figure 96 are equivalent. The MTBF of the AM1524 motor was 2000 hours of continuous rotation.

Next, the probability of failure will be calculated by assuming a standard deviation for said MTBF and using statistical analysis to arrive at an estimate.

The team choose to use a standard deviation of 500 hours for the time before failure of the motor. A normal distribution of failures is also assumed.

The z-score of the calculated hours of operation was first obtained:

$$z = \frac{MTBF - \bar{MTBF}}{\sigma} = \frac{80 - 2000}{500} = -3.84$$

Using a probability chart for a normal distribution the probability of failure for the motor/gearhead combination for our device was found to be:

$$\frac{\text{Motor}}{\text{Gearhead}} \text{Reliability} = 1 - \text{Prob of Failure} = 1 - .00006 = .99994$$

Shafts

Number of cycles that motor will perform

$$N_m = 24 \frac{\text{steps}}{\text{cycle}} * \frac{249 \text{ cycles}}{1 \text{ orbit}} * \frac{5840 \text{ orbits}}{1 \text{ year}} = 3.49 \times 10^7 \text{ cycles}$$

Motor Shaft

$$r_m = \frac{d_m}{2} = \frac{.003m}{2} = .0015 m$$

The maximum possible shear stress on the motor was then calculated.

$$\tau_{\text{motor shaft}} = \frac{T_H r_m}{J_m \text{ shaft}} = \frac{T_H r_m}{\frac{\pi}{2} r_m^4} = \frac{(.313 N \cdot m)(.0015 m)}{\frac{\pi}{2} (.0015 m)^4} = 59 \text{ MPa} = 8.6 \times 10^3 \text{ psi}$$

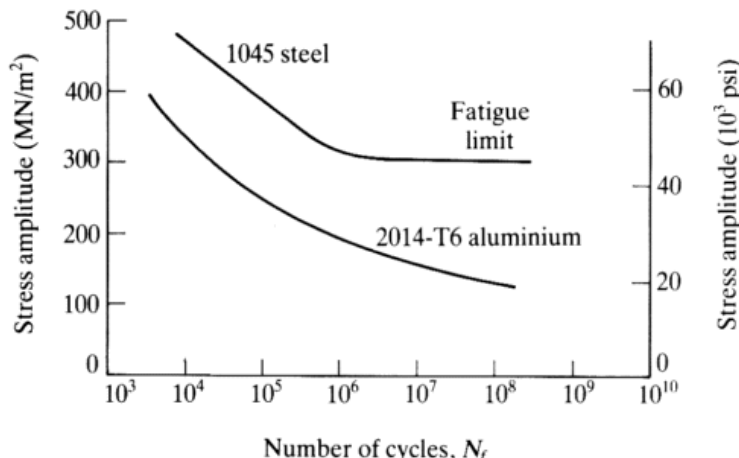


Figure 97 – S-N Curve for 1045 Steel

As can be seen in Figure 97, the 59 MPa shear stress due to torque on the shaft of the motor is well under the fatigue limit of the steel and thus can be theoretically characterized as having a **reliability of 1**.

Gear on Primary Shaft

Speed of Gear (n_1) = 1.205 RPM

$$n_1 = \frac{\omega_m}{e} = \frac{300 \text{ RPM}}{249} = 1.205 \text{ RPM}$$

Diametrical Pitch (P_d) = 48

The pitch diameter is given in the spur gear data sheet

Diameter of Gear (d_1) = 0.017 m

The diameter of the gear is given in the spur gear data sheet as 0.667 inches.

$$d_1 = 0.667 \text{ in} * \frac{1 \text{ m}}{39.3701 \text{ in}} = .017m$$

Radius of gear (r_1) = 8.5 mm

$$r_1 = \frac{d_1}{2} = \frac{.017 \text{ m}}{2} = 8.5 \times 10^{-3} \text{ m}$$

Number of Gear Teeth (N_1) = 32

The number of gear teeth is given in the spur gear data sheet

Tangential Load on Tooth (F_t)

$$F_t = \frac{T_H}{r_1} * \frac{.313 \text{ N} \cdot \text{m}}{8.5 \times 10^{-3} \text{ m}} = 36.82 \text{ N}$$

Face width (b) = 3.18 mm

The face width is given in the spur gear data sheet

$$b = \frac{1}{8} \text{ in} * \frac{1 \text{ m}}{39.3701 \text{ in}} = 3.18 \times 10^{-3} \text{ m}$$

Pitch Line Velocity (V)

$$V = r_1 n_1 = (8.5 \times 10^{-3} \text{ m})(1.205 \text{ RPM}) * \frac{2\pi \text{ rad}}{\text{rev}} * \frac{1 \text{ min}}{60 \text{ s}} = 1.07 \times 10^{-3} \frac{\text{m}}{\text{s}}$$

K_a = Application Factor = 1.0

This is due to our mover being an electric motor and thus having a uniform characteristic.

TABLE 15.6 Application Factor, K_a

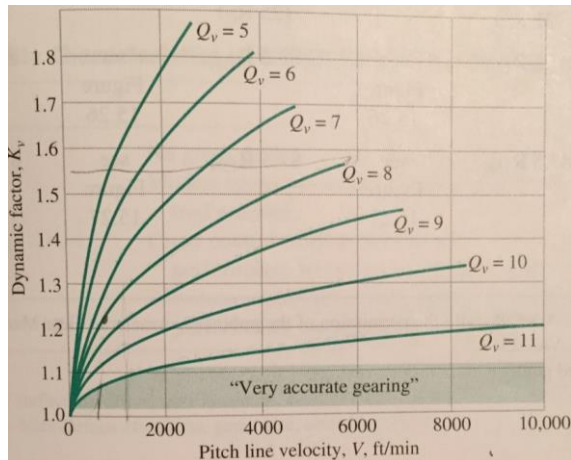
Prime Mover Characteristic	Driven Machine Characteristic		
	Uniform	Moderate Shock	Heavy Shock
Uniform (e.g., electric motor, turbine)	1.00	1.25	1.75 or higher
Light shock (e.g., multicylinder engine)	1.25	1.50	2.00 or higher
Medium shock (e.g., single-cylinder engine)	1.50	1.75	2.25 or higher

Figure 98 – Chart for Application Factor from EMD Text

K_v = Dynamic Factor = 1.05

- A Qv of 5 was chosen as the prototype gears are molded, and thus very low accuracy on the Dudley designation scale.
- Then, with a Qv of 5 and a pitch-line velocity (V) of $1.07 \times 10^{-3} \frac{\text{ft}}{\text{min}}$ a value of 1.05 was chosen from the graph below.

Accuracy Level	Dudley Designation ¹	Approximate Quality Range Q _v Value
Highest possible accuracy. Achieved by special toolroom methods. Used for master gears, unusually critical high-speed gears, or when both highest load capacity and highest reliability are needed.	AA Ultra-high accuracy	14 or 15
High accuracy. Achieved by grinding or shaving with first-rate machine tools, and utilizing skilled operators. Widely used for turbine gearing and aerospace gearing. Sometimes used for critical industrial gears.	A High accuracy	12 or 13
Relatively high accuracy. Achieved by grinding or shaving with emphasis on production rate rather than highest quality. May be achieved by hobbing or shaping with best equipment under favorable conditions. Used for medium-speed industrial gears and critical vehicle gears.	B Medium-high accuracy	10 or 11
Good accuracy. Achieved by hobbing or shaping with first-rate machine tools and skilled operators. May be obtained in high-production grinding or shaving. Typically used for vehicle gears and electric motor industrial gears running at slower speeds.	C Medium accuracy	8 or 9
Nominal accuracy. Can be achieved by hobbing or shaping using older machine tools and less-skilled operators. Typically used for low-speed gears that wear in to yield a reasonable fit. (Lower hardness promotes wear-in.)	D Low accuracy	6 or 7
Minimal accuracy. For gears used at slow speeds and light loads. Teeth may be cast or molded in small sizes. Typically used in toys and gadgets. May be used for low-hardness gears when limited life and lower reliability are acceptable.	E Very low accuracy	4 or 5



K_m = Mounting or Load Distribution Factor = 1.3

- As seen below in Table 15.7, a K_m of 1.3 is chosen due to the face width of the gear of $3.18 \times 10^{-3} \text{ m}$ and the accurate mountings and minimum deflections in our design.

TABLE 15.7 Mounting Factor, K_m

Support Properties and Gear Quality	Face Width, in			
	0 to 2*	6	9	≥ 16
Accurate mountings, small bearing clearances, minimum deflections, precision gears	1.3	1.4	1.5	1.8
Less rigid mountings, more bearing clearance, less accurate gears, contact across full face	1.6	1.7	1.8	2.2
Combinations of mounting properties and gearing precision that produce less than full face contact	2.2 or higher			

K_i = Idler Factor = 1.0 (one-way bending)

J = Geometry Factor = 0.39

- Both the pinion and gear have a 1/1 ratio, each having 32 teeth. In Table 15.9, the closest number of teeth is 35, and that J value is used.

TABLE 15.9 AGMA Geometry Factor J for Bending of 20° Full-Depth Involute Teeth Under HPSTC (used for higher-precision gearing)

Gear Teeth	Pinion Teeth													
	12		14		17		21		26		35		55	
	P ²	G	P	G	P	G	P	G	P	G	P	G	P	G
12	U ³	U												
14	U	U	U	U										
17	U	U	U	U	U	U								
21	U	U	U	U	U	U	0.33	0.33						
26	U	U	U	U	U	U	0.33	0.35	0.35	0.35				
35	U	U	U	U	U	U	0.34	0.37	0.36	0.38	0.39	0.39		
55	U	U	U	U	U	U	0.34	0.40	0.37	0.41	0.40	0.42	0.43	0.43
135	U	U	U	U	U	U	0.35	0.43	0.38	0.44	0.41	0.45	0.45	0.47

Scaled-Up Tooth Bending Stress (σ_b)

$$\sigma_b = \frac{F_t P_d}{b * J} K_a K_v K_m K_i = \frac{(36.82 \text{ N})(48)}{(3.18 \times 10^{-3} \text{ m})(.39)} * (1.0)(1.05)(1.3)(1.0) = 1.95 \text{ MPa}$$

Formula to Solve for Rg

$$S_{tbf} = Y_N R_g S'_{tbf}$$

Reliability Adjustment Factor
Life Adjustment Factor
Tooth Bending Strength per AGMA

- This formula will be used to solve for R_g (reliability factor). $S_{tbf} = \sigma_b$.

Y_N = Life Adjustment Factor = 0.95

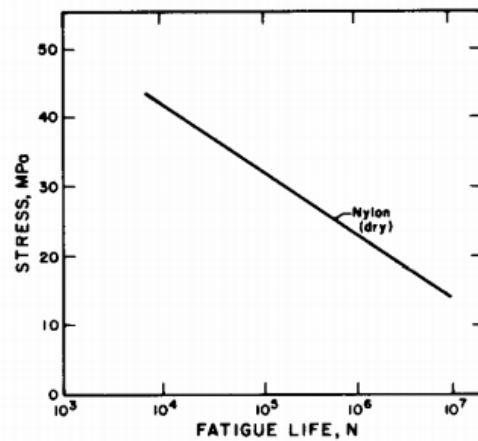
- From the chart, with $N = 3.49 \times 10^7$ cycles a life adjustment factor of 0.95 was chosen

R_g = Reliability Factor = .67

TABLE 15.13 AGMA Reliability Adjustment Factor R_g for Gears ¹	
Desired Reliability, percent	R_g
99.99	0.67
99.9	0.80
99	1.0
90	1.18
50	1.43

S'_{tbf} from S-N Curve

- Extrapolating on the graph for $N = 3.49 \times 10^7$ cycles, a S'_{tbf} of 10 MPa was chosen.



S_{tbf} from 2.5.15

$$S_{tbf} = Y_N R_g S'_{tbf} = (.95)(.67)(10 \text{ MPa}) = 6.365 \text{ MPa}$$

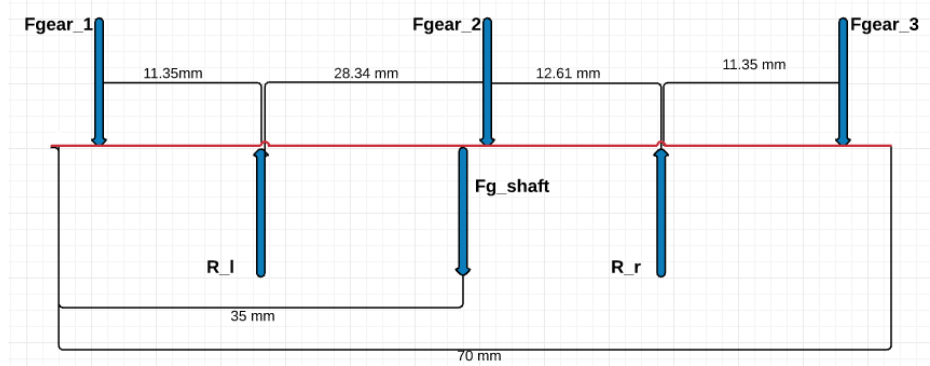
FOS Calculation

$$FOS = \frac{S_{tbf}}{\sigma_b} = \frac{6.365 \text{ MPa}}{1.945 \text{ MPa}} = 3.27$$

- This is a sufficient factor of safety. Thus the reliability of .9999 that was chosen is valid.

Formatted: Font:
 Formatted: Font:
 Formatted: Font:
 Formatted: Font:
 Formatted: Font:
 Formatted: Font:

Primary Shaft Sleeve Bearing



$$m_{gear} = p_{Nylon} V_{gear} = \left(1.15 \frac{g}{cm^3} * \frac{1 \text{ kg}}{1000 \text{ g}} * \frac{(100 \text{ cm})^3}{(1 \text{ m})^3} \right) * \left(586 \text{ mm}^3 * \frac{(1000 \text{ cm})^3}{(1 \text{ m})^3} \right)$$

$$m_{gear} = 6.532 \times 10^{-4} \text{ kg}$$

$$F_{gear} = (m_{gear} * g) = \left(6.532 \times 10^{-4} \text{ kg} * 9.81 \frac{m}{s} \right) = .0064 \text{ N}$$

$$m_{shaft} = p_{Al} V_{shaft} = \left(2.7 \frac{g}{cm^3} * \frac{1 \text{ kg}}{1000 \text{ g}} * \frac{(100 \text{ cm})^3}{(1 \text{ m})^3} \right) * \left(554 \text{ mm}^3 * \frac{(1000 \text{ cm})^3}{(1 \text{ m})^3} \right)$$

$$m_{shaft} = 0.0015 \text{ kg}$$

$$F_{g_shaft} = (m_{shaft} * g) = \left(0.0015 \text{ kg} * 9.81 \frac{m}{s} \right) = .0147 \text{ N}$$

$$\sum M_L = (11.35 \text{ mm})(F_{gear\ 1}) + (28.34 \text{ mm} + 12.61 \text{ mm})(R_R)$$

$$- (35 \text{ mm} - 31.75 \text{ mm})(F_{g_shaft}) - (28.34 \text{ mm})(F_{gear\ 2})$$

$$- (28.34 \text{ mm} + 12.61 \text{ mm} + 11.35 \text{ mm})(F_{gear\ 3}) = 0$$

$$\sum M_L = .07264 - 40.45 * R_R - 0.3 - 0.5161 = 0$$

$$R_R = 18.16 \text{ mN}$$

From force balance in the vertical direction

$$R_L = 15.74 \text{ mN}$$

The pressure on the bearings was then calculated assuming the bearing deforms elastically under load

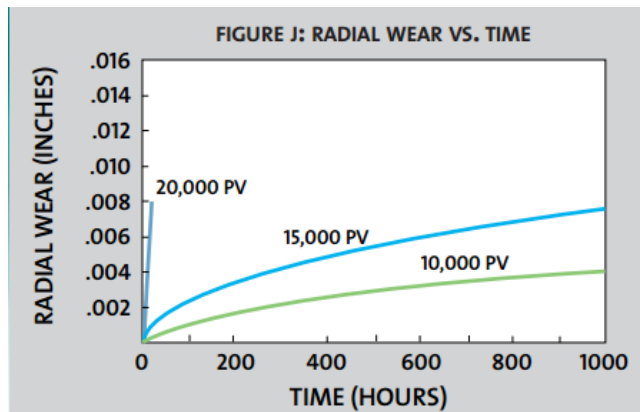
$$P_{left \ bearing} = \frac{4}{\pi} * \frac{R_L}{LD} = \frac{4}{\pi} * \frac{15.74 \ mN}{(6.35 \times 10^{-3} \ m)(3.175 \times 10^{-3} \ m)} * \frac{1 \ N}{1 \ mN} = 994 \ Pa$$

$$P_{right \ bearing} = \frac{4}{\pi} * \frac{R_R}{LD} = \frac{4}{\pi} * \frac{18.16 \ mN}{(6.35 \times 10^{-3} \ m)(3.175 \times 10^{-3} \ m)} * \frac{1 \ N}{1 \ mN} = 1146.8 \ Pa$$

PV or the pressure times the outer most velocity of the bearing was then calculated in order to compared with the manufacturers wear depth chart.

$$PV_L = (994 \ Pa)(2.0 \times 10^{-4} \frac{m}{s}) = .1988 \frac{Pa * m}{s} * \frac{10,000 \ psi * fpm}{.35 \times 10^6 \frac{Pa * m}{s}} = .0057 \ psi * fpm$$

$$PV_R = (994 \ Pa) \left(2.0 \times 10^{-4} \frac{m}{s}\right) = .2294 \frac{Pa * m}{s} * \frac{10,000 \ psi * fpm}{.35 \times 10^6 \frac{Pa * m}{s}} = .0066 \ psi * fpm$$



- The figure above shows the radial depth versus time with various trend lines based on PV values in fpm. As can be seen from the chart, our bearing is under such low pressure and turning so slow that its radial wears depth is not significant for a reasonable amount of hours.
- **The reliability will thus be assumed as 1.**
- This type of calculation was done because of the absence of wear constants for plastics. A metal bearing would thus require to formula $d = kPl$ to be used.

Normal Distribution Probability Chart

STANDARD NORMAL DISTRIBUTION: Table Values Represent AREA to the LEFT of the Z score.

Z	.00	.01	.02	.03	.04	.05	.06	.07	.08	.09
-3.9	.00005	.00005	.00004	.00004	.00004	.00004	.00004	.00004	.00003	.00003
-3.8	.00007	.00007	.00007	.00006	.00006	.00006	.00006	.00005	.00005	.00005
-3.7	.00011	.00010	.00010	.00010	.00009	.00009	.00008	.00008	.00008	.00008
-3.6	.00016	.00015	.00015	.00014	.00014	.00013	.00013	.00012	.00012	.00011
-3.5	.00023	.00022	.00022	.00021	.00020	.00019	.00019	.00018	.00017	.00017
-3.4	.00034	.00032	.00031	.00030	.00029	.00028	.00027	.00026	.00025	.00024
-3.3	.00048	.00047	.00045	.00043	.00042	.00040	.00039	.00038	.00036	.00035
-3.2	.00069	.00066	.00064	.00062	.00060	.00058	.00056	.00054	.00052	.00050
-3.1	.00097	.00094	.00090	.00087	.00084	.00082	.00079	.00076	.00074	.00071
-3.0	.00135	.00131	.00126	.00122	.00118	.00114	.00111	.00107	.00104	.00100
-2.9	.00187	.00181	.00175	.00169	.00164	.00159	.00154	.00149	.00144	.00139
-2.8	.00256	.00248	.00240	.00233	.00226	.00219	.00212	.00205	.00199	.00193
-2.7	.00347	.00336	.00326	.00317	.00307	.00298	.00289	.00280	.00272	.00264
-2.6	.00466	.00453	.00440	.00427	.00415	.00402	.00391	.00379	.00368	.00357
-2.5	.00621	.00604	.00587	.00570	.00554	.00539	.00523	.00508	.00494	.00480
-2.4	.00820	.00798	.00776	.00755	.00734	.00714	.00695	.00676	.00657	.00639
-2.3	.01072	.01044	.01017	.00990	.00964	.00939	.00914	.00889	.00866	.00842
-2.2	.01390	.01355	.01321	.01287	.01255	.01222	.01191	.01160	.01130	.01101
-2.1	.01786	.01743	.01700	.01659	.01618	.01578	.01539	.01500	.01463	.01426
-2.0	.02275	.02222	.02169	.02118	.02068	.02018	.01970	.01923	.01876	.01831
-1.9	.02872	.02807	.02743	.02680	.02619	.02559	.02500	.02442	.02385	.02330
-1.8	.03593	.03515	.03438	.03362	.03288	.03216	.03144	.03074	.03005	.02938
-1.7	.04457	.04363	.04272	.04182	.04093	.04006	.03920	.03836	.03754	.03673
-1.6	.05480	.05370	.05262	.05155	.05050	.04947	.04846	.04746	.04648	.04551
-1.5	.06681	.06552	.06426	.06301	.06178	.06057	.05938	.05821	.05705	.05592
-1.4	.08076	.07927	.07780	.07636	.07493	.07353	.07215	.07078	.06944	.06811
-1.3	.09680	.09510	.09342	.09176	.09012	.08851	.08691	.08534	.08379	.08226
-1.2	.11507	.11314	.11123	.10935	.10749	.10565	.10383	.10204	.10027	.09853
-1.1	.13567	.13350	.13136	.12924	.12714	.12507	.12302	.12100	.11900	.11702
-1.0	.15866	.15625	.15386	.15151	.14917	.14686	.14457	.14231	.14007	.13786
-0.9	.18406	.18141	.17879	.17619	.17361	.17106	.16853	.16602	.16354	.16109
-0.8	.21186	.20897	.20611	.20327	.20045	.19766	.19489	.19215	.18943	.18673
-0.7	.24196	.23885	.23576	.23270	.22965	.22663	.22363	.22065	.21770	.21476
-0.6	.27425	.27093	.26763	.26435	.26109	.25785	.25463	.25143	.24825	.24510
-0.5	.30854	.30503	.30153	.29806	.29460	.29116	.28774	.28434	.28096	.27760
-0.4	.34458	.34090	.33724	.33360	.32997	.32636	.32276	.31918	.31561	.31207
-0.3	.38209	.37828	.37448	.37070	.36693	.36317	.35942	.35569	.35197	.34827
-0.2	.42074	.41683	.41294	.40905	.40517	.40129	.39743	.39358	.38974	.38591
-0.1	.46017	.45620	.45224	.44828	.44433	.44038	.43644	.43251	.42858	.42465
-0.0	.50000	.49601	.49202	.48803	.48405	.48006	.47608	.47210	.46812	.46414

Spur Gear Datasheet

Plastic Gear—14-1/2 Degree Pressure Angle

Press-Fit Mount, 48 Pitch, 32 Teeth



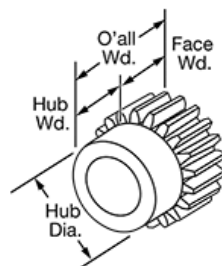
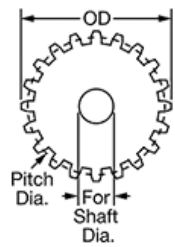
Each

In stock

\$7.06 Each

ADD TO ORDER

57655K18



Pressure Angle 14 1/2°

Pitch 48

Number of Teeth 32

Pitch Diameter 0.667"

OD 0.7"

Face Width 1/8"

Overall Width 0.375"

Fabrication Molded

Color White

Material Nylon

Bore Type Plain

Mount Type Press Fit

For Shaft Diameter 1/8"

Hub
Diameter 0.5"
Width 0.25"

A light duty alternative to metal, these gears have a 14 1/2° pressure angle that maximizes contact between

Appendix H: Shaft Loadings and Minimum Shaft Diameter Calculation

Table 42: Required Inputs for Calculations

Inputs									
Torque	Pitch dia A	Pitch dia C	Pitch dia E	Su 2	Sf 2	Su 1	Sf 1	G 2	G 1
mNm	in	in	in	PSI	PSI	PSI	PSI	PSI	PSI
158	0.333	0.333	0.333	200000	61236	200000	61236	11000000	11000000
158	0.375000203	0.3750002	0.3750002	200000	61236	200000	61236	11000000	11000000
158	0.416929359	0.41692936	0.41692936	200000	61236	200000	61236	11000000	11000000
158	0.50000027	0.50000027	0.50000027	200000	61236	200000	61236	11000000	11000000
158	0.550000297	0.5500003	0.5500003	200000	61236	200000	61236	11000000	11000000
158	0.583071181	0.58307118	0.58307118	200000	61236	200000	61236	11000000	11000000
158	0.666929494	0.66692949	0.66692949	200000	61236	200000	61236	11000000	11000000
158	0.750000405	0.75000041	0.75000041	200000	61236	200000	61236	11000000	11000000
158	0.833071316	0.83307132	0.83307132	200000	61236	200000	61236	11000000	11000000
158	0.333	0.333	0.333	45000	5266	45000	5266	3770000	3770000
158	0.375000203	0.3750002	0.3750002	45000	5266	45000	5266	3770000	3770000
158	0.416929359	0.41692936	0.41692936	45000	5266	45000	5266	3770000	3770000
158	0.50000027	0.50000027	0.50000027	45000	5266	45000	5266	3770000	3770000
158	0.550000297	0.5500003	0.5500003	45000	5266	45000	5266	3770000	3770000
158	0.583071181	0.58307118	0.58307118	45000	5266	45000	5266	3770000	3770000
158	0.666929494	0.66692949	0.66692949	45000	5266	45000	5266	3770000	3770000
158	0.750000405	0.75000041	0.75000041	45000	5266	45000	5266	3770000	3770000
158	0.833071316	0.83307132	0.83307132	45000	5266	45000	5266	3770000	3770000
158	0.333	0.333	0.333	83000	9185	83000	9185	3900000	3900000
158	0.375000203	0.3750002	0.3750002	83000	9185	83000	9185	3900000	3900000
158	0.416929359	0.41692936	0.41692936	83000	9185	83000	9185	3900000	3900000
158	0.50000027	0.50000027	0.50000027	83000	9185	83000	9185	3900000	3900000
158	0.550000297	0.5500003	0.5500003	83000	9185	83000	9185	3900000	3900000
158	0.583071181	0.58307118	0.58307118	83000	9185	83000	9185	3900000	3900000
158	0.666929494	0.66692949	0.66692949	83000	9185	83000	9185	3900000	3900000
158	0.750000405	0.75000041	0.75000041	83000	9185	83000	9185	3900000	3900000
158	0.833071316	0.83307132	0.83307132	83000	9185	83000	9185	3900000	3900000
158	0.333	0.333	0.333	90000	17350	90000	17350	11200000	11200000
158	0.375000203	0.3750002	0.3750002	90000	17350	90000	17350	11200000	11200000
158	0.416929359	0.41692936	0.41692936	90000	17350	90000	17350	11200000	11200000
158	0.50000027	0.50000027	0.50000027	90000	17350	90000	17350	11200000	11200000
158	0.550000297	0.5500003	0.5500003	90000	17350	90000	17350	11200000	11200000
158	0.583071181	0.58307118	0.58307118	90000	17350	90000	17350	11200000	11200000
158	0.666929494	0.66692949	0.66692949	90000	17350	90000	17350	11200000	11200000
158	0.750000405	0.75000041	0.75000041	90000	17350	90000	17350	11200000	11200000
158	0.833071316	0.83307132	0.83307132	90000	17350	90000	17350	11200000	11200000
158	0.333	0.333	0.333	75000	16834	75000	16834	12500000	12500000

158	0.375000203	0.3750002	0.3750002	75000	16834	75000	16834	12500000	12500000
158	0.416929359	0.41692936	0.41692936	75000	16834	75000	16834	12500000	12500000
158	0.50000027	0.50000027	0.50000027	75000	16834	75000	16834	12500000	12500000
158	0.550000297	0.5500003	0.5500003	75000	16834	75000	16834	12500000	12500000
158	0.583071181	0.58307118	0.58307118	75000	16834	75000	16834	12500000	12500000
158	0.666929494	0.66692949	0.66692949	75000	16834	75000	16834	12500000	12500000
158	0.750000405	0.75000041	0.75000041	75000	16834	75000	16834	12500000	12500000
158	0.833071316	0.83307132	0.83307132	75000	16834	75000	16834	12500000	12500000

Table 43: Forces Generated by Gears

Faz	Fax	Fcz	Fcx	Fez	Fex
Ibf	Ibf	Ibf	Ibf	Ibf	Ibf
0.003361	0.000842	0.003361	0.000842	0.003361	0.000842
0.002985	0.000747	0.002985	0.000747	0.002985	0.000747
0.002684	0.000672	0.002684	0.000672	0.002684	0.000672
0.002238	0.00056	0.002238	0.00056	0.002238	0.00056
0.002035	0.000509	0.002035	0.000509	0.002035	0.000509
0.001919	0.000481	0.001919	0.000481	0.001919	0.000481
0.001678	0.00042	0.001678	0.00042	0.001678	0.00042
0.001492	0.000374	0.001492	0.000374	0.001492	0.000374
0.001343	0.000336	0.001343	0.000336	0.001343	0.000336
0.003361	0.000842	0.003361	0.000842	0.003361	0.000842
0.002985	0.000747	0.002985	0.000747	0.002985	0.000747
0.002684	0.000672	0.002684	0.000672	0.002684	0.000672
0.002238	0.00056	0.002238	0.00056	0.002238	0.00056
0.002035	0.000509	0.002035	0.000509	0.002035	0.000509
0.001919	0.000481	0.001919	0.000481	0.001919	0.000481
0.001678	0.00042	0.001678	0.00042	0.001678	0.00042
0.001492	0.000374	0.001492	0.000374	0.001492	0.000374
0.001343	0.000336	0.001343	0.000336	0.001343	0.000336
0.003361	0.000842	0.003361	0.000842	0.003361	0.000842
0.002985	0.000747	0.002985	0.000747	0.002985	0.000747
0.002684	0.000672	0.002684	0.000672	0.002684	0.000672
0.002238	0.00056	0.002238	0.00056	0.002238	0.00056
0.002035	0.000509	0.002035	0.000509	0.002035	0.000509
0.001919	0.000481	0.001919	0.000481	0.001919	0.000481
0.001678	0.00042	0.001678	0.00042	0.001678	0.00042
0.001492	0.000374	0.001492	0.000374	0.001492	0.000374
0.001343	0.000336	0.001343	0.000336	0.001343	0.000336
0.003361	0.000842	0.003361	0.000842	0.003361	0.000842
0.002985	0.000747	0.002985	0.000747	0.002985	0.000747

0.002684	0.000672	0.002684	0.000672	0.002684	0.000672
0.002238	0.00056	0.002238	0.00056	0.002238	0.00056
0.002035	0.000509	0.002035	0.000509	0.002035	0.000509
0.001919	0.000481	0.001919	0.000481	0.001919	0.000481
0.001678	0.00042	0.001678	0.00042	0.001678	0.00042
0.001492	0.000374	0.001492	0.000374	0.001492	0.000374
0.001343	0.000336	0.001343	0.000336	0.001343	0.000336
0.003361	0.000842	0.003361	0.000842	0.003361	0.000842
0.002985	0.000747	0.002985	0.000747	0.002985	0.000747
0.002684	0.000672	0.002684	0.000672	0.002684	0.000672
0.002238	0.00056	0.002238	0.00056	0.002238	0.00056
0.002035	0.000509	0.002035	0.000509	0.002035	0.000509
0.001919	0.000481	0.001919	0.000481	0.001919	0.000481
0.001678	0.00042	0.001678	0.00042	0.001678	0.00042
0.001492	0.000374	0.001492	0.000374	0.001492	0.000374
0.001343	0.000336	0.001343	0.000336	0.001343	0.000336

Table 44: Calculated Reaction Forces on Bearings

R1x	R1z	R2x	R2z
lbf	lbf	lbf	lbf
0.001262	0.005041	0.000421	0.00168
0.001121	0.004477	0.000374	0.001492
0.001008	0.004027	0.000336	0.001342
0.000841	0.003358	0.00028	0.001119
0.000764	0.003052	0.000255	0.001017
0.000721	0.002879	0.00024	0.00096
0.00063	0.002517	0.00021	0.000839
0.00056	0.002238	0.000187	0.000746
0.000505	0.002015	0.000168	0.000672
0.001262	0.005041	0.000421	0.00168
0.001121	0.004477	0.000374	0.001492
0.001008	0.004027	0.000336	0.001342
0.000841	0.003358	0.00028	0.001119
0.000764	0.003052	0.000255	0.001017
0.000721	0.002879	0.00024	0.00096
0.00063	0.002517	0.00021	0.000839
0.00056	0.002238	0.000187	0.000746
0.000505	0.002015	0.000168	0.000672
0.001262	0.005041	0.000421	0.00168
0.001121	0.004477	0.000374	0.001492
0.001008	0.004027	0.000336	0.001342

0.000841	0.003358	0.00028	0.001119
0.000764	0.003052	0.000255	0.001017
0.000721	0.002879	0.00024	0.00096
0.00063	0.002517	0.00021	0.000839
0.00056	0.002238	0.000187	0.000746
0.000505	0.002015	0.000168	0.000672
0.001262	0.005041	0.000421	0.00168
0.001121	0.004477	0.000374	0.001492
0.001008	0.004027	0.000336	0.001342
0.000841	0.003358	0.00028	0.001119
0.000764	0.003052	0.000255	0.001017
0.000721	0.002879	0.00024	0.00096
0.00063	0.002517	0.00021	0.000839
0.00056	0.002238	0.000187	0.000746
0.000505	0.002015	0.000168	0.000672
0.001262	0.005041	0.000421	0.00168
0.001121	0.004477	0.000374	0.001492
0.001008	0.004027	0.000336	0.001342
0.000841	0.003358	0.00028	0.001119
0.000764	0.003052	0.000255	0.001017
0.000721	0.002879	0.00024	0.00096
0.00063	0.002517	0.00021	0.000839
0.00056	0.002238	0.000187	0.000746
0.000505	0.002015	0.000168	0.000672

Table 45: Calculated Moments and Minimum Diameter at Point A

Max	Maz	Ma	Diameter A
lbf-in	lbf-in	lbf-in	inch
0.000248	0.000992	0.001023032	0.007256083
0.000221	0.000881	0.000908452	0.006993287
0.000198	0.000793	0.000817092	0.006768635
0.000165	0.000661	0.000681339	0.006404367
0.00015	0.000601	0.000619399	0.006223469
0.000142	0.000567	0.000584268	0.00611601
0.000124	0.000496	0.000510803	0.005878201
0.00011	0.000441	0.000454226	0.005681006
9.93E-05	0.000397	0.000408932	0.005512657
0.000248	0.000992	0.001023032	0.016217395
0.000221	0.000881	0.000908452	0.015604655
0.000198	0.000793	0.000817092	0.015079156
0.000165	0.000661	0.000681339	0.014223102

0.00015	0.000601	0.000619399	0.013795824
0.000142	0.000567	0.000584268	0.013541225
0.000124	0.000496	0.000510803	0.01297544
0.00011	0.000441	0.000454226	0.012503478
9.93E-05	0.000397	0.000408932	0.012098206
0.000248	0.000992	0.001023032	0.013466225
0.000221	0.000881	0.000908452	0.012956691
0.000198	0.000793	0.000817092	0.012519655
0.000165	0.000661	0.000681339	0.011807591
0.00015	0.000601	0.000619399	0.011452118
0.000142	0.000567	0.000584268	0.011240282
0.000124	0.000496	0.000510803	0.010769455
0.00011	0.000441	0.000454226	0.01037662
9.93E-05	0.000397	0.000408932	0.010039221
0.000248	0.000992	0.001023032	0.010958857
0.000221	0.000881	0.000908452	0.010551846
0.000198	0.000793	0.000817092	0.010203249
0.000165	0.000661	0.000681339	0.009636462
0.00015	0.000601	0.000619399	0.009354157
0.000142	0.000567	0.000584268	0.009186158
0.000124	0.000496	0.000510803	0.008813468
0.00011	0.000441	0.000454226	0.008503357
9.93E-05	0.000397	0.000408932	0.008237717
0.000248	0.000992	0.001023032	0.011094913
0.000221	0.000881	0.000908452	0.010685759
0.000198	0.000793	0.000817092	0.010335518
0.000165	0.000661	0.000681339	0.009766501
0.00015	0.000601	0.000619399	0.009483325
0.000142	0.000567	0.000584268	0.009314894
0.000124	0.000496	0.000510803	0.008941508
0.00011	0.000441	0.000454226	0.008631129
9.93E-05	0.000397	0.000408932	0.008365517

Table 46: Calculated Moments and Minimum Shaft Diameters at Point C

Mc _x	Mc _z	Mc	Diameter C
lbf-in	lbf-in	lbf-in	inch
0.002029233	-0.02436672	0.024451074	0.020460736
0.001801958	-0.02163764	0.021712542	0.01966881
0.001620741	-0.01946162	0.019528986	0.018988337
0.001351468	-0.01622823	0.016284406	0.017876738
0.001228608	-0.01475294	0.014804006	0.017320214
0.001158923	-0.01391617	0.013964346	0.016987979

0.001013202	-0.01216638	0.012208498	0.016247768
0.000900979	-0.01081882	0.010856271	0.015628006
0.000811136	-0.00974001	0.009773722	0.01509386
0.002029233	-0.02436672	0.024451074	0.046327475
0.001801958	-0.02163764	0.021712542	0.044531058
0.001620741	-0.01946162	0.019528986	0.04298723
0.001351468	-0.01622823	0.016284406	0.040464735
0.001228608	-0.01475294	0.014804006	0.039201538
0.001158923	-0.01391617	0.013964346	0.03844732
0.001013202	-0.01216638	0.012208498	0.0367666
0.000900979	-0.01081882	0.010856271	0.035358953
0.000811136	-0.00974001	0.009773722	0.034145407
0.002029233	-0.02436672	0.024451074	0.038485504
0.001801958	-0.02163764	0.021712542	0.036993078
0.001620741	-0.01946162	0.019528986	0.035710492
0.001351468	-0.01622823	0.016284406	0.033614829
0.001228608	-0.01475294	0.014804006	0.032565369
0.001158923	-0.01391617	0.013964346	0.031938765
0.001013202	-0.01216638	0.012208498	0.030542412
0.000900979	-0.01081882	0.010856271	0.029372919
0.000811136	-0.00974001	0.009773722	0.028364677
0.002029233	-0.02436672	0.024451074	0.031141231
0.001801958	-0.02163764	0.021712542	0.02993458
0.001620741	-0.01946162	0.019528986	0.028897656
0.001351468	-0.01622823	0.016284406	0.027203549
0.001228608	-0.01475294	0.014804006	0.026355268
0.001158923	-0.01391617	0.013964346	0.025848815
0.001013202	-0.01216638	0.012208498	0.024720312
0.000900979	-0.01081882	0.010856271	0.023775275
0.000811136	-0.00974001	0.009773722	0.022960645
0.002029233	-0.02436672	0.024451074	0.031459346
0.001801958	-0.02163764	0.021712542	0.030240748
0.001620741	-0.01946162	0.019528986	0.029193582
0.001351468	-0.01622823	0.016284406	0.027482806
0.001228608	-0.01475294	0.014804006	0.026626213
0.001158923	-0.01391617	0.013964346	0.02611481
0.001013202	-0.01216638	0.012208498	0.024975317
0.000900979	-0.01081882	0.010856271	0.024021123
0.000811136	-0.00974001	0.009773722	0.023198641

Table 47: Calculated Moments and Minimum Shaft Diameter at Point E

Mex	Mez	Me	Diameter E
-----	-----	----	------------

lbf-in	lbf-in	lbf-in	inch
0	0	0	0.002911553
7.36E-05	0.000294	0.000303	0.005071788
6.62E-05	0.000264	0.000272	0.00493001
0.000386	0.001542	0.00159	0.008339625
-0.00018	-0.00073	0.000757	0.006613175
-0.00017	-0.00069	0.000714	0.006496779
-0.00055	-0.0022	0.002268	0.009348124
0.000257	0.001028	0.00106	0.00733664
0.000232	0.000926	0.000954	0.007100502
0.00058	0.002316	0.002387	0.021404113
0.000515	0.002056	0.00212	0.020582854
0.000463	0.001849	0.001907	0.019877667
0.000386	0.001542	0.00159	0.018726867
0.000351	0.001402	0.001445	0.018151359
0.000331	0.001322	0.001363	0.017808029
0.000289	0.001156	0.001192	0.017043819
0.000257	0.001028	0.00106	0.016404841
0.000232	0.000926	0.000954	0.015854881
0.00058	0.002316	0.002387	0.017777735
0.000515	0.002056	0.00212	0.017095186
0.000463	0.001849	0.001907	0.016509074
0.000386	0.001542	0.00159	0.015552524
0.000351	0.001402	0.001445	0.015074121
0.000331	0.001322	0.001363	0.014788706
0.000289	0.001156	0.001192	0.014153366
0.000257	0.001028	0.00106	0.013622087
0.000232	0.000926	0.000954	0.013164777
0.00058	0.002316	0.002387	0.014419016
0.000515	0.002056	0.00212	0.013869906
0.000463	0.001849	0.001907	0.013398686
0.000386	0.001542	0.00159	0.012630363
0.000351	0.001402	0.001445	0.012246495
0.000331	0.001322	0.001363	0.012017625
0.000289	0.001156	0.001192	0.011508595
0.000257	0.001028	0.00106	0.011083472
0.000232	0.000926	0.000954	0.010717992
0.00058	0.002316	0.002387	0.014579441
0.000515	0.002056	0.00212	0.014025953
0.000463	0.001849	0.001907	0.013551092
0.000386	0.001542	0.00159	0.01277711

0.000351	0.001402	0.001445	0.012390565
0.000331	0.001322	0.001363	0.012160155
0.000289	0.001156	0.001192	0.011647867
0.000257	0.001028	0.00106	0.011220226
0.000232	0.000926	0.000954	0.010852753

Appendix I: Calculated Dynamic Load Rating

Table 48: Calculated Basic Dynamic Load Rating for Primary Shaft

Primary Shaft		
Pe	Cd at LEO	Cd at GEO
lbf	lbf	lbf
0.005197	0.000354	0.001419
0.004615	0.000314	0.00126
0.004151	0.000283	0.001133
0.003461	0.000236	0.000945
0.003147	0.000214	0.000859
0.002968	0.000202	0.000811
0.002595	0.000177	0.000709
0.002307	0.000157	0.00063
0.002077	0.000142	0.000567
0.005197	0.000354	0.001419
0.004615	0.000314	0.00126
0.004151	0.000283	0.001133
0.003461	0.000236	0.000945
0.003147	0.000214	0.000859
0.002968	0.000202	0.000811
0.002595	0.000177	0.000709
0.002307	0.000157	0.00063
0.002077	0.000142	0.000567
0.005197	0.000354	0.001419
0.004615	0.000314	0.00126
0.004151	0.000283	0.001133
0.003461	0.000236	0.000945
0.003147	0.000214	0.000859
0.002968	0.000202	0.000811
0.002595	0.000177	0.000709
0.002307	0.000157	0.00063
0.002077	0.000142	0.000567
0.005197	0.000354	0.001419

0.004615	0.000314	0.00126
0.004151	0.000283	0.001133
0.003461	0.000236	0.000945
0.003147	0.000214	0.000859
0.002968	0.000202	0.000811
0.002595	0.000177	0.000709
0.002307	0.000157	0.00063
0.002077	0.000142	0.000567
0.005197	0.000354	0.001419
0.004615	0.000314	0.00126
0.004151	0.000283	0.001133
0.003461	0.000236	0.000945
0.003147	0.000214	0.000859
0.002968	0.000202	0.000811
0.002595	0.000177	0.000709
0.002307	0.000157	0.00063
0.002077	0.000142	0.000567

Table 49: Calculated Basic Dynamic Load Rating for Secondary Shaft

Secondary Shaft		
Pe	Cd at LEO	Cd at GEO
lbf	lbf	lbf
0.001732	0.000118	0.000473
0.001538	0.000105	0.00042
0.001384	9.43E-05	0.000378
0.001154	7.86E-05	0.000315
0.001049	7.15E-05	0.000286
0.000989	6.74E-05	0.00027
0.000865	5.89E-05	0.000236
0.000769	5.24E-05	0.00021
0.000692	4.72E-05	0.000189
0.001732	0.000118	0.000473
0.001538	0.000105	0.00042
0.001384	9.43E-05	0.000378
0.001154	7.86E-05	0.000315
0.001049	7.15E-05	0.000286
0.000989	6.74E-05	0.00027
0.000865	5.89E-05	0.000236
0.000769	5.24E-05	0.00021
0.000692	4.72E-05	0.000189

0.001732	0.000118	0.000473
0.001538	0.000105	0.00042
0.001384	9.43E-05	0.000378
0.001154	7.86E-05	0.000315
0.001049	7.15E-05	0.000286
0.000989	6.74E-05	0.00027
0.000865	5.89E-05	0.000236
0.000769	5.24E-05	0.00021
0.000692	4.72E-05	0.000189
0.001732	0.000118	0.000473
0.001538	0.000105	0.00042
0.001384	9.43E-05	0.000378
0.001154	7.86E-05	0.000315
0.001049	7.15E-05	0.000286
0.000989	6.74E-05	0.00027
0.000865	5.89E-05	0.000236
0.000769	5.24E-05	0.00021
0.000692	4.72E-05	0.000189
0.001732	0.000118	0.000473
0.001538	0.000105	0.00042
0.001384	9.43E-05	0.000378
0.001154	7.86E-05	0.000315
0.001049	7.15E-05	0.000286
0.000989	6.74E-05	0.00027
0.000865	5.89E-05	0.000236
0.000769	5.24E-05	0.00021
0.000692	4.72E-05	0.000189

Appendix J: Software

Code for Prototype Demonstration

```
/*NASA/JPL CubeSat SADA (2)
RPI Capstone Project: Spring 2016
* 5/15/2016
* Code used for CubeSat (2) final prototype
* This code processes readings on the sensors, pushbutton, and
encoder, and uses them to drive the SADA motor according to the
prototype algorithm
* To be used with Arduino library
*/
#include <Stepper.h>
```

```

//15 degrees per step
const int stepsPerRevolution = 24;

//Define pin connections
Stepper myStepper(stepsPerRevolution, 5, 6, 3, 11);
int sensor3 = A2;
int sensor2 = A0;
int sensor1 = A1;
int encoder = A5;
int pushButton = 1;

//If lightFound is false, a 360 degree check is needed
bool lightFound = false;

int encoderValue = 0;

void setup() {
  pinMode(pushButton, INPUT);

  myStepper.setSpeed(500);
  Serial.begin(9600);
}

//Function to locate light upon startup, and when light source
is lost
//Does a 360 scan, finds the max light source, and rotates
panels towards light source
void findLight(){
  int maxSensorValue = 0;
  int maxEncoder = 0;
  int maxStep = 0;
  int encoderValue = analogRead(encoder);
  int sensor2Value = analogRead(sensor2);

  //Use step values to keep track of position, read encoder to
  check for error
  Serial.println("360 Check");
  for(int i = 0; i < 600; i++){
    myStepper.step(10);
    encoderValue = analogRead(encoder);
    sensor2Value = analogRead(sensor2);

    //If new maximum light source found, log its brightness,
    step number, and encoder value
    if(sensor2Value > maxSensorValue){
      maxSensorValue = sensor2Value;
    }
  }
}

```

```

        maxEncoder = encoderValue;
        maxStep = i;
    }
}

Serial.println("Moving...");
//Complete 360 degrees traveled, go to place with max light
//Rotate in direction with shortest path
if(maxStep > 300){
    for(int i = 0; i < 600-maxStep; i++){
        myStepper.step(-10);
    }
}
else{
    for(int i = 0; i < maxStep; i++){
        myStepper.step(10);
    }
}

Serial.print("Max encoder position: ");
Serial.print(maxEncoder);
Serial.print(" Current encoder position: ");
Serial.println(analogRead(encoder));
lightFound = true;
}

void loop() {
    int sensor1Value = analogRead(sensor1);
    int sensor2Value = analogRead(sensor2);
    int sensor3Value = analogRead(sensor3);
    int encoderValue = analogRead(encoder);
    int pushButtonValue = digitalRead(pushButton);
    //Do not do rotate panels until panels are deployed
    //Uncomment if-else block if this functionality is desired
    //if(pushButtonValue == 0)
    //{
        //Position lost, prepare to do 360 check again
        if(sensor1Value < 100 && sensor2Value < 100 && sensor3Value
        < 100){
            lightFound = false;
        }
        if(!lightFound){
            findLight();
            sensor1Value = analogRead(sensor1);
            sensor2Value = analogRead(sensor2);
            sensor3Value = analogRead(sensor3);
        }
    }
}

```

```

encoderValue = analogRead(encoder);
pushButtonValue = digitalRead(pushButton);
}

//if sensor 1 is brightest value, rotate on -Y axis
if(sensor1Value >= sensor2Value && sensor1Value >=
sensor3Value)
    myStepper.step(10);
//if sensor 3 is brightest value, rotate on Y axis
else if(sensor3Value >= sensor2Value && sensor3Value >=
sensor1Value)
    myStepper.step(-10);

//Print values for debugging
Serial.print("Sensor1: ");
Serial.print(sensor1Value);
Serial.print(" Sensor2: ");
Serial.print(sensor2Value);
Serial.print(" Sensor3: ");
Serial.print(sensor3Value);
Serial.print(" Encoder: ");
Serial.print(encoderValue);
Serial.print(" Deployed: ");
Serial.println(pushButtonValue);

//}
//else
// Serial.println("Panels not deployed");
}

```

MATLAB Code for Sensor Analysis

```

%NASA/JPL CubeSat SADA (2) RPI Capstone Project: Spring 2016
%5/15/2016
%Code used for LTR-4206E analysis
%This code plots the information listed on the LTR-4206E datasheet

%Define sensor ranges for 20 degree offset
thetal = -50 : 2.5 : 10;
theta2 = -30 : 2.5 : 30;
theta3 = -10 : 2.5 : 50;

%Values taken from LTR-4206E datasheet
sensitivity = [0.05, 0.06, 0.07, 0.08, 0.1, 0.15, 0.2, 0.35, 0.53, ...
    0.68, 0.87, 0.97, 1, 0.97, 0.87, 0.68, 0.53, 0.35, 0.2, 0.15, 0.1, ...
    0.08, 0.07, 0.06, 0.05];

%Plot first figure
plot(theta1,sensitivity,'color','r'); hold on;
plot(theta2,sensitivity,'color','g'); hold on;
plot(theta3,sensitivity,'color','b');

%Figure Labels

```

```

title('Sensitivity with 20 Degree Offset');
xlabel('Angle from Centerline (Degrees)');
ylabel('Normalized Sensitivity');

%Define sensor ranges for 15 degree offset
theta4 = -45 : 2.5 : 15;
theta5 = -30 : 2.5 : 30;
theta6 = -15 : 2.5 : 45;

%Plot second figure
figure();
plot(theta4,sensitivity,'color','r'); hold on;
plot(theta5,sensitivity,'color','g'); hold on;
plot(theta6,sensitivity,'color','b');

%Figure Labels
title('Sensitivity with 15 Degree Offset');
xlabel('Angle from Centerline (Degrees)');
ylabel('Normalized Sensitivity');

Orbit Period Calculation Code
function [ time ] = orbitPeriod( orbitHeight )
%orbitPeriod calculates how long it takes an object
%to rotate around the earth at a given height.

%Formula Source:
%http://www.dummies.com/how-to/content/how-to-calculate-the-period-and-orbiting-radius-of.html

%INPUT: Height of orbit above earth (meters)
%OUTPUT: Time to rotate the earth (hours)

eM = 5.972 * 10^(24); %Earth mass in kilograms
eR = 6.371 * 10^(6); %Radius of earth in meters
G = 6.67 * 10^(-11); %Gravitational Constant. m^3 kg^-1 s^-2

% T (seconds) = 2pi * sqrt(Radius^3 / (Gravity Constant * Mass Earth))
time = 2*pi * sqrt((orbitHeight + eR).^3)/(G*eM) ;
time = time/3600; %Convert the output time to hours

end

Orbit Time in Shadow Code
% Control Algorithm Corner Cases
clc; clf; clear; close all;

eM = 5.972 * 10^(24); %Earth mass in kilograms
eR = 6.371 * 10^(6); %Radius of earth in meters
d2s = 149.6 * 10^(9); %Distance = 149.6 billion meters

G = 6.67 * 10^(-11); %Gravitational Constant. m^3 kg^-1 s^-2

```

```

%Orbit radii for GEO and LEO as found at:
%http://www.slideshare.net/kamranahmed7186/satellite-communication-a-
tutorial-28226854
rLEO = 200*10^(3); %Height of orbit above earth for LEO (m)
rGEO = 36000*10^(3); %Height of orbit above earth for GEO(m)

%Verification of working formula
T_LEO = orbitPeriod(rLEO); %Outputs 01.4730 hours (expected ~1.5 hours)
T_GEO = orbitPeriod(rGEO); %Outputs 24.1189 hours (expected ~24 hours)

radii = (linspace(rLEO,rGEO))'; %Make a list of radii from LEO to GEO
orbitTime = orbitPeriod(radii); %Make a list of the orbit times theta1 =
asin(eR./(eR+radii)); %Find positive angle assuming parallel sun rays

%Time in shadow = Shadow Angle / Full Circle * Orbit Period
%Shadow angle = 2 X Theta1
shadowTime = orbitTime.* (2*theta1/(2*pi)); %Find the time in the shadow

%-----
% Plot Figures
%-----
figure(1), hold on
p2 = plot(radii,shadowTime, 'b');
hold off
title('Radius of Orbit vs Time in Shadow');
xlabel('Orbit Radius (m)');
ylabel('Time in Shadow (hr)');

figure(2)
p3 = plot(radii,shadowTime./orbitTime * 100);
title('Radius of Orbit vs Percent Time in Shadow');
xlabel('Orbit Radius (m)');
ylabel('Percent of Orbit Spent in Shade (%)');

```

Full Orbit Control Simulation Code

```

% Control Algorithm Simulations:
% Assumptions:
% 1) Nadir Circular Orbits
% 2) Assumes sun's rays are parallel according to the following source:
%
http://earthguide.ucsd.edu/eoc/special\_topics/teach/sp\_climate\_change/p\_sunlight\_parallel.html
% 3) Motor movement is linear when rotating

clc; clf; clear; close all;

%% -----
% Background Stats/Variables
%-----
earthMass = 5.972 * 10^(24); %Earth mass in kilograms
earthRadius = 6.371 * 10^(6); %Radius of earth in meters

```

```

d2s = 149.6 * 10^(9); %Distance = 149.6 billion meters

G = 6.67 * 10^(-11); %Gravitational Constant. m^3 kg^-1 s^-2

%Orbit radii for GEO and LEO as found at:
%http://www.slideshare.net/kamranahmed7186/satellite-communication-a-
tutorial-28226854
rLEO = 2000*10^(3); %Height of orbit above earth for LEO (m)
rGEO = 36000*10^(3); %Height of orbit above earth for GEO(m)

%% -----
% Simulation Variables
%-----
%----- Orbit Variables -----
orbitHeight = 2000*10^(3); %Radius of orbit (meters)
orbitTime = 3600*1.5;
startPos = 0.0; %Starting position (degrees)

%----- Feedback Variables -----
encGain = 5; %Encoder maximum voltage
sunSensAng = 45; %Sun sensor Angle for 3 sensor system (Degrees)
sunSensGain = 5; %Sun sensor maximum voltage reading
maxPower = 96; %solar panel power (Watts)
panelEff_Low = .8; %solar panel efficiency (Decimal represent percentage)

%----- Motor/Electric Variables -----
voltageCon = 6; %Motor driving voltage

phaseR = 1; %Phase resistance (Ohms)
phaseI = 1; %Phase inductance (Henries)
Kt = 1; %Torque constant (Nm/A)
detentTor = 1; %Detent Torque (Nm)
stepSize = 24; %Step Size # steps / rotation
stepAng = 360/stepSize; %(Degrees per step)

rotorInertia = 1; %Motor Inertia (kg*m^2)
rotorDamp = 1; %Motor Damping (N*m/(rad/s))
rotorInitPos = 1; %Initial Postion of rotor (degrees)
backlash = 4; %Backlash (degrees)

%----- Motor Load Variables -----
gearRatio = 249; %Step down gear ratio from motor
loadInertia = 1; %Load inertia kg*m^2
coulombFrict = 1; %Coulomb Friction of load N*m
breakFrict = coulombFrict; %Breakaway Friction of load N*m
viscousFrict = 1; %Viscous Friction of load N*m/(rad/s)

%% -----
% Running the Simulation
%-----
deltaT = .01; %Time increment for simulation (seconds)
endTime = 150; %Final time (in seconds) for simulation
startPanAng = 0.0; %Starting position for panel relative to cubesat

```

```

panAngNow = startPanAng;
t = [0:deltaT:endTime];
arrLen = endTime/deltaT + 1;
satX = zeros(1,arrLen); %Angle of CubeSat
satY = zeros(1,arrLen); %Angle of CubeSat
satAng = zeros(1,arrLen); %Angle of CubeSat
panAng = zeros(1,arrLen); %Angle of Panels
netAng = zeros(1,arrLen); %Net angle of panels to sun
powerMot = zeros(1,arrLen); %Power draw of motor
powerPan= zeros(1,arrLen); %Power generated by panels
LightIntensity = true; %Is cubeSat in light
stepping = false; %if panels are rotating (motor is stepping)
delayed = false; %if control algorithm calls for a time delay
delayTime = 0.0; %duration that control algorithm requires delay
sunSens = zeros(3); %vector for sun sensor readings
encSens = 0.0; %Encoder reading
steps = 0.0; % the number of steps the control wants to move
stepPerSec = 300; %speed of motor rotation
timePerStep = 1/(stepPerSec); %speed of motor rotation

for m = 1:1:arrLen;
    %% Satellite Position
    satAng(m) = (360/orbitTime)*t(m) + startPos; %position of satellite
    X = cos(satAng(m)*pi/180)*(orbitHeight + earthRadius); %X coordinate
    Y = sin(satAng(m)*pi/180)*(orbitHeight + earthRadius); %Y coordinate
    satX(m) = X; satY(m) = Y; %Save the variables for plotting

    %Determine if the sun is visible from the CubeSat
    if (X > 0 || abs(Y) > earthRadius)
        LightIntensity = 1.0;
    else
        LightIntensity = 0.0;
    end

    %% Panel Position
    if (stepping)
        %If stepping and not done stepping
        %Then the instantaneous power is 1.4W and move the panels
        if (t(m) < switchTime )
            powerMot(m) = 1.4;
            deltaP = sign(steps)*(stepAng/gearRatio)*stepPerSec*deltaT;
            panAngNow = panAngNow + deltaP;
        %Else (panels should be done rotating to position)
        %so motor movement (stepping) stops
        else
            stepping = false;
        end
    end
    panAng(m)=panAngNow; %save panel position for plotting

    %% Power Calculation
    netAng(m) = satAng(m)+panAng(m); %find net angle solar panels to sun
    cosAng = cos(netAng(m)*pi/180);
    %If the net angle has the panels facing the sun, calculate power
    if (cosAng > 0)

```

```

powerPan(m) = cosAng*maxPower*LightIntensity;
%else the solar panels are not getting any power
else
    powerPan(m) = 0.0;
end

%% Sun Sensor Calculation
%For each sensor 45 degree apart...
for iter = 1:1:3
    %find the angle of the sensor relative to sun
    tempAng = netAng(m)+(iter-2)*45;
    tempAng = cos(tempAng*pi/180);
    %If the angle is between -90 and 90, it can detect sun
    if (tempAng > 0)
        sunSens(iter) = tempAng*sunSensGain*LightIntensity;
    %Else the sun sensor does not pick up any reading
    else
        sunSens(iter) = 0.0;
    end
end

%% Encoder Calculation
encSens = (mod(panAngNow,360)/360)*encGain;

%% Motor Controller Main Loop
% If the motor is not stepping and not creating a delay
% Then execute code to find
if (~stepping && ~delayed)
    % If the angle is >1 degree (5*cos(1) = 4.9992)
    % Then step to make the angle -1 degrees
    if (sunSens(2) < 4.9992 && sunSens(1) > sunSens(3))
        stepping = true; %Motor is moving
        steps = -33; %Number of steps required to travel
        switchTime = t(m)+abs(steps)*timePerStep; %when program knows to
stop stepping
    % If the angle is <-1 degree (5*cos(1) = 4.9992)
    % Then step to make the angle 1 degrees
    elseif (sunSens(2) < 4.9992 && sunSens(1) > sunSens(3))
        stepping = true; %Motor is moving
        steps = 33; %Number of steps required to travel
        switchTime = t(m)+abs(steps)*timePerStep; %when program knows to
stop stepping
    %Need to Find Sun!!!!!
    elseif (sunSens(2) < .5)
        %Rotate X amount -> run typical stepping algorithm
        stepping = true;
        steps = -1000;
        switchTime = t(m)+abs(steps)*timePerStep;

        %Wait Y Amount -> Set delayTime to switchTime + delay amount
        delayTime = switchTime+200;
        delayed = true;
    end
%ElseIf the control asks for a delay, wait until delay is over
elseif (delayed)
    if (t(m) < delayTime )

```

```

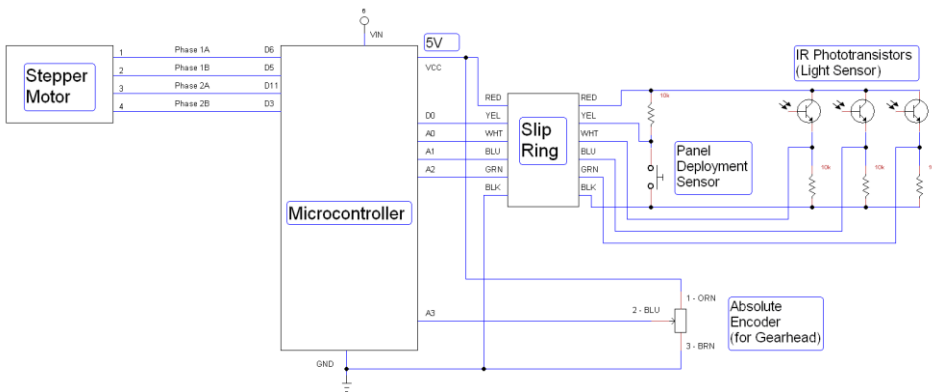
        delayed = true;
    else
        delayed = false;
    end
end

%% Plotting Position
figure(1), hold on
plot(t,netAng);
plot(t,panAng);
plot(t,satAng);
legend('Net','Pan','Sat');
title('Satellite Angles');
xlabel('Time (s)');
ylabel('Position (Degrees)');
hold off;

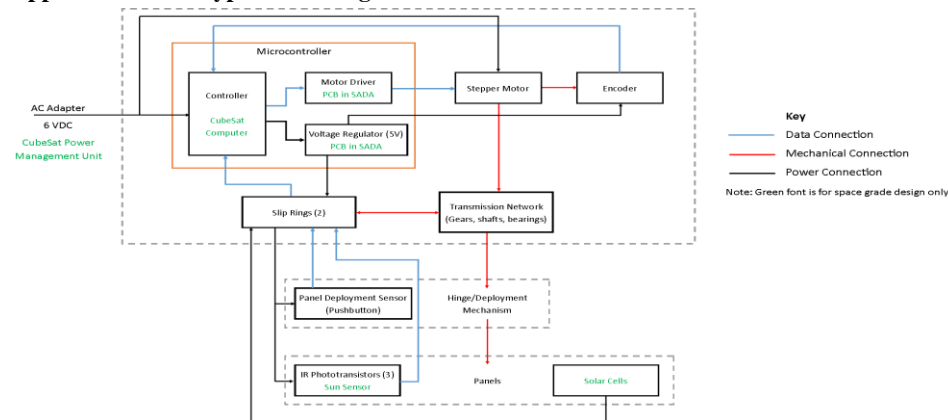
%% Plotting Power
figure(2), hold on;
%plot(t,powerPan);
plot(t,powerMot);
%plot(t,satAng);
xlabel('Time (s)');
ylabel('Motor Power (W)');
title('Motor Power for LEO Orbit at 300 step/s');
hold off;

```

Appendix K: Full Prototype Schematic



Appendix L: Prototype Block Diagram



Appendix M: Hinge and Deployment

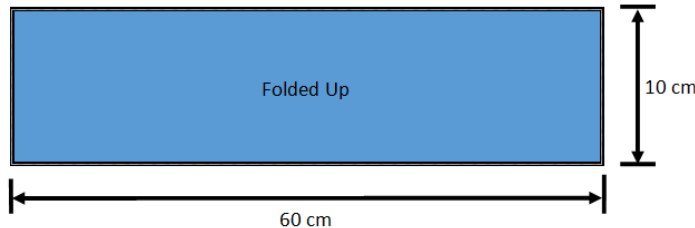


Figure 8: Folded Panel Dimensions (Top View)

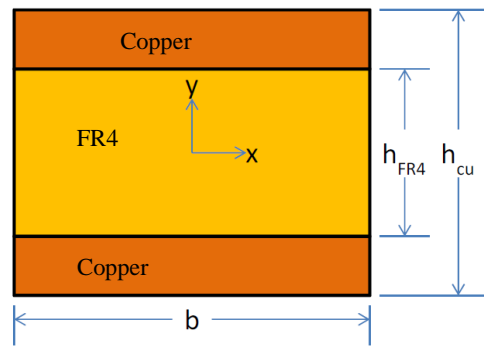


Figure 99: Cross Sectional View of the Panel for Pumpkin

$$b = 10 \text{ cm}$$

$$L = 60 \text{ cm}$$

Thickness = $t = 6 \text{ mm}$ (3 Panels Folded)

Mass = $m = 1.5 \text{ kg}$

$$h_{cu} = 0.0016 \text{ m}$$

$$h_{FR4} = 0.0015 \text{ m}$$

$$E_{copper} = 120 \text{ GPa}$$

$$E_{FR4} = 21 \text{ GPa}$$

$$\sigma_y \text{ copper} = 70 \text{ MPa}$$

Rotational Inertia Equation

$$I_{rotation} = \frac{1}{3} m L^2$$

$$I_{rotation} = \frac{1}{3} (1.5 \text{ kg})(0.6 \text{ m})^2 = 0.18 \text{ kg} * \text{m}^2$$

Bending Moment of Inertia

$$I_{bending} = \frac{b * t^3}{12}$$

$$I_{bending} = \frac{10 \text{ cm} * (6 \text{ mm})^3}{12} = 1.8 * 10^{-9} \text{ m}^4$$

Bending Stiffness

$$H = E_{cu} * I_{bending}$$

$$H = 120 \text{ GPa} * (1.8 * 10^{-9} \text{ m}^4) = 216 \text{ Nm}^2$$

Yield Stress Equation to find Max Moment

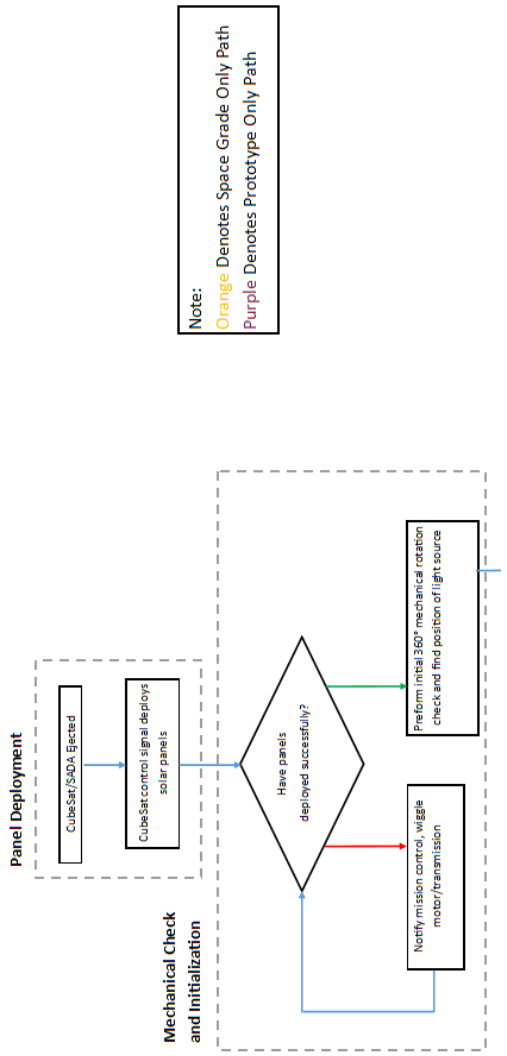
$$\sigma_y = E * M * \frac{y}{H}$$

$$\sigma_{y copper} = 70 \text{ MPa} = 120 \text{ GPa} * M * \frac{0.0016 \text{ m}}{2} * \frac{1}{216 \text{ Nm}^2}$$

$$M = 157.5 \text{ Nm}$$

Appendix N: Control Algorithm Flowchart

(Part 1 of 2)



(Part 2 of 2)

